Jostein Malmo

Chitosan-based nanocarriers for gene- and siRNA-delivery

Thesis for the degree of Philosophiae Doctor

Trondheim, September 2012

Norwegian University of Science and Technology
Faculty of Natural Sciences and Technology
Department of Biotechnology

NTNU – Trondheim
Norwegian University of
Science and Technology

NTNU
Norwegian University of Science and Technology

Thesis for the degree of Philosophiae Doctor

Faculty of Natural Sciences and Technology
Department of Biotechnology

ISBN 978-82-471-3746-8 (printed ver.)
ISBN 978-82-471-3748-2 (electronic ver.)
ISSN 1503-8181

Doctoral theses at NTNU, 2012:223

Printed by NTNU-trykk

Acknowledgements

This work has been carried out at the Department of Biotechnology at the Norwegian University of Science and Technology (NTNU) in the period 2009-2012. Financial support has been provided by the Faculty of Natural Sciences and Technology (NTNU).

First, I would like to thank Sabina P Strand for being an excellent and very helpful supervisor during these years. I would also like to thank Professor Kjell M Vårum for guidance and for sharing his expertise on chitosan. Axel Sandvig is thanked for initiating the collaboration project, for performing animal experiments, and his enthusiasm in this work. Ioanna Sandvig is thanked for performing the animal experiments and for help with sample analysis.

Further, I would like to thank Professor Catharina de L. Davies for giving me the opportunity to use the equipment and facilities available at the Department of Physics (NTNU). Kristin G Sæterbø is especially thanked for all the help and advice regarding the experimental work.

I would like to thank my colleagues at the Department of Biotechnology for making these years both fun and rewarding.

Former master students involved in this project are also thanked: Elen Møller, Morten Dille, Hanne Sørgård, Hanne Auganes and Christian Wold.

I would also like to thank the Norwegian Biochemical Society, the Federation of European Biochemical Societies (FEBS) and the Faculty of Natural Sciences and Technology for travel grants.

Finally, I would like to thank family and friends for their supporting and for taking interest in my work. I would especially like to thank Karen N Seglem for being helpful and for repeatedly reminding me what is important in life.

Jostein Malmo
Trondheim, June 2012

Table of contents

Summary

Gene therapy is promising for the treatment of many currently incurable diseases by delivering or silencing specific genes with pDNA or siRNA, respectively. Clinical trials have mostly been conducted with viral or relatively toxic nonviral nucleic acid delivery systems. The biopolymer chitosan have the recent years gained interest in nucleic acid delivery. However, chitosan lacks the efficiency of many alternative viral-, lipid- and polymer-based delivery systems. Hence, this study was initiated to characterize chitosan molecular properties favoring efficient delivery of pDNA and siRNA in mammalian cells. Chitosans were optimized by investigating a range of chain lengths (MW/DP), chain architectures, degrees of *N*-acetylation (F_A) and concentration in the formulations (N/P). Promising siRNA-chitosan nanoparticles were investigated for their potential to increase the drug delivery in a blood-brain barrier (BBB) model by silencing the drug efflux pump P-glycoprotein (P-gp).

Self-branching of fully de-*N*-acetylated chitosans was investigated as a strategy to optimize the delivery efficiency of pDNA-chitosan nanoparticles. Self-branched (SB) and self-branched trisaccharide-substituted chitosan oligomers (SBTCO) of different MW (molecular weight) were synthesized, characterized and compared to their linear counterparts with respect to delivery efficiency, cellular uptake, formulation stability and cytotoxicity. While the linear unmodified chitosans failed to mediate efficient pDNA delivery in HeLa cells, the self-branching resulted in high transgene expression at the optimal combinations of MW and N/P. The most efficient nanoparticles formed with SBTCO exhibited a higher colloidal stability of formulation, efficient internalization without excessive cell surface binding and low cytotoxicity.

To identify fundamental chitosan molecular properties for efficient gene silencing, siRNA-chitosan nanoparticles were prepared from chitosans of various DP (degree of polymerization), chain architectures and F_A at N/P 10-60. Structure-activity relationships were determined by the cellular uptake of siRNA and the knockdown efficiency. Additionally, the nanoparticle cytotoxicity was evaluated on the basis of cellular metabolic activity and membrane integrity. The results show that the most efficient gene silencing was achieved using fully de-*N*-acetylated chitosans with number average degree of polymerization (DP_n)>50 and N/P>10. These chitosans mediated efficient siRNA delivery at low siRNA concentrations and potent long-term silencing with minimal cytotoxicity.

The BBB limits the availability of drugs to therapeutic targets in the central nervous system. The barrier is maintained by membrane bound efflux pumps efficiently transporting specific xenobiotics back into the blood. The efflux pump P-gp is expressed at high levels in brain endothelial cells and has several drug substrates. Consequently, siRNA mediated silencing of the P-gp gene is a feasible strategy to improve the brain drug delivery. Herein, siRNA-chitosan nanoparticles selected on basis of the structure-activity optimization were investigated for potential silencing of P-gp in a BBB model cell line. The results show that the transfection of rat brain endothelial cells mediated effective knockdown of P-gp with subsequent decrease in P-gp substrate efflux. This increased the cellular delivery and efficacy of the model drug doxorubicin.

Abbreviations

Alexa-647	Alexa Fluor 647
AAM	2-acetamido-2-deoxy-D-glucopyranosyl-β-(1-4)-2-acetamido-2-deoxy-D-glucopyranosyl-β-(1-4)-2,5-anhydro-D-mannofuranose
AJ	Adherence junctions
BBB	Blood-brain barrier
CD	Cyclodextrin
bp	Base pairs
CLSM	Confocal laser scanning microscopy
CNS	Central nervous system
DLS	Dynamic light scattering
DP	Degree of polymerization
DP_n	Number average DP
ds	Double stranded
ECM	Extracellular matrix
EGFP	Enhanced green fluorescent protein
F_A	Degree of *N*-acetylation
FC	Flow cytometry
GAPDH	Glyceraldehyde-3-phosphate dehydrogenase
GFP	Green fluorescent protein
GlcNAc	*N*-acetyl-D-glucosamine
GlcN	D-glucosamine
HMW	High molecular weight
LIN	Linear
MW	Molecular weight
M_n	Number average MW
M_w	Weight average MW
N/P	Amino/phosphate ratio
NT	Non-targeting
PDI	Polydispersity index
PDMAEMA	Poly[2-(dimethylamino)ethyl methacrylate]
pDNA	Plasmid DNA
PEG	Polyethylene glycol
PEI	Polyethylenimine
PEST	Penicillin and streptomycin
P-gp	P-glycoprotein
pK_a	Acid dissociation constant
PLL	Poly-l-lysine
qRT-PCR	Quantitative real-time RT-PCR
R123	Rhodamine 123
RNAi	RNA-interference
RT-PCR	Reverse transcriptase-polymerase chain reaction
SB	Self-branched
SBTCO	Self-branched trisaccharide substituted chitosan oligomer
shRNA	Short hairpin RNA
siRNA	Small interfering RNA
T	Targeting
TB	Trypan blue
TJ	Tight junctions

List of papers

Paper I

Malmo J, Vårum KM, Strand SP. Effect of chitosan chain architecture on gene delivery: comparison of self-branched and linear chitosans. *Biomacromolecules* 2011;**12**:721-729.

Paper II

Malmo J, Sørgård H, Vårum KM, Strand SP. siRNA delivery with chitosan nanoparticles: molecular properties favoring efficient gene silencing. *Journal of controlled release* 2012;**158**:261-268.

Paper III

Malmo J, Sandvig A, Vårum KM, Strand SP. Nanoparticle mediated P-glycoprotein silencing for improved drug delivery across the blood-brain barrier: a siRNA-chitosan approach. Submitted manuscript.

1. Introduction

Gene therapy is the concept of transferring genetic material in the form of nucleic acids into somatic cells, tissues or whole organs for treating or at least amending disease. Instead of the conventional drug-based therapeutic approach to treat clinical symptoms, gene therapy offers a possibility to correct the underlying cause of the disease. The success of gene therapy relies on efficient nucleic acid delivery to the target cells[1]. However, the lack of efficient and safe delivery systems is currently a major bottleneck in the development of this technology[2]. The delivery systems can be divided as viral- or nonviral, where those based on viruses are most efficient but suffer from issues related to their production and safety of use[2]. The nonviral delivery systems are most commonly based on various polymers, lipids, liposomes or peptides[3]. In polymer-based nucleic acid delivery systems, cationic polymers are employed to form nanoparticles of characteristics suitable for cellular internalization[2,4].

As a general introduction, this section starts by covering the basic aspects of gene therapy. Next follows an introduction to the biopolymer chitosan and an overview of polymeric nonviral delivery vehicles. Furthermore, an overview of the biological barriers that the nanoparticles must successfully overcome in nucleic acid delivery is presented. Finally, the blood-brain barrier is covered due to its relevance in the last part of this study.

1.1 Gene therapy

The cellular delivery of nucleic acids is a relatively old technology emerging from genetic engineering experiments with recombinant DNA in the 1970s[5]. These experiments illustrated the possibility of transferring functional genes between different species[5]. The first approved clinical trial aiming to introduce genes in humans started in 1990[6] and the promising results emerging from this investigation encouraged further research[7]. Another relevant hallmark is the publishing of the human genome sequence in 2001[8]. This formed a foundation for the possibility to characterize and indentify genes involved in diseases, giving an additional motivation for gene therapy research. Combined with the rapidly declining cost and improved output of genomic sequencing[9], gene therapy can very well be the breakthrough for personalized medicine.

However, as of 2011 and 1,643 approved clinical trials later[10], only two commercial cancer gene therapy products (Gendicine and Oncorine) are available. The efficacy and safety of these viral-based gene medicines is a topic of debate[11,12] and currently they are only approved for use in China[13,14]. To overcome the issues preventing this technology to reach the clinic, gene therapy is a field of intensive research effort worldwide. The enormous interest can be explained by the vast opportunities in treating severe congenital and acquired genetic disorders of which many are currently incurable.

The genetic manipulations facilitated by nucleic acid delivery is normally performed with plasmid DNA (pDNA) for replacing defective genes or short RNA sequences such as small interfering RNA (siRNA) for blocking the expression of harmful genes.

1.1.1 pDNA delivery

The pDNA introduced into cells carries the gene of interest linked to a promoter and enhancer ensuring efficient expression[15]. pDNA delivery has many applications besides gene therapy; e.g. as an experimental tool[16,17], it can be utilized for industrial production of proteins[18] and is promising for the development of a new generation vaccines[19]. Several therapeutic targets for pDNA delivery have been addressed in gene therapy, and some examples from animal models and clinical studies are given in Table 1-1.

Table 1-1: Selected studies addressing pDNA delivery in animal models and clinical trials.

***In vivo* animal models**					
Targeted disease	**Delivered gene**	**Delivery system**	**Route of administration**	**Animal model**	**Ref.**
Glaucoma	BDNF + TrkB	Adeno-associated virus	Intraocular	Rat	20
Huntington	BDNF + GDNF	Adeno-associated virus	Intracranial	Rat	21
Hemophilia	Factor VIII	Chitosan (polymer)	Oral	Mouse	22
Vaccine	Derp2	Chitosan (polymer)	Oral	Mouse	23
Colon cancer	Apc	Lipofectamine (lipid)	Oral	Mouse	24

***In vivo* clinical studies**					
Targeted disease	**Delivered gene**	**Delivery system**	**Route of administration**	**Clinical phase**	**Ref.**
Parkinson	GAD	Adeno-associated virus	Intracranial	II*	25
Cystic fibrosis	CFTR	DOTAP (liposome)	Intranasal	I	26
Bladder cancer	Diphtheria toxin	PEI (polymer)	Intravesical	I/II	27
Cystic fibrosis	CFTR	PEG-PLL (polymer-peptide)	Intranasal	II	28
SCID	ADA	Retrovirus	*Ex vivo*	I/II	6

ADA: Adenosine deaminase, Apc: Adenomatous polyposis coli, BDNF: Brain-derived neurotrophic factor, CFTR: Cystic fibrosis transmembrane conductance regulator, Derp2: Encodes the major house dust mite allergen, GAD: Glutamic acid decarboxylase, GDNF: Glial cell-derived neurotrophic factor, Intravesical: Delivery directly into the bladder (see Figure 1-6 for an overview of the most common administration routes in humans), PEG: Polyethylene glycol, PEI: Polyethylenimine, PLL: Poly-l-lysine, SCID: Severe combined immunodeficiency, TrkB: Tropomyosin-related kinase B. *Study is terminated.

Expression of the delivered gene depends on successful transport of the pDNA into the cellular nucleus where the gene must be processed by the cellular transcription machinery. Once transcribed into mRNA, the gene is transported to the cytoplasm and binds freely-floating ribosomes possibly directed to the surface of the rough endoplasmic reticulum (ER). The ribosomes then translate the mRNA into proteins. If the protein is synthesized in the ER, it either remains or is transported to the Golgi network for further post-translational modifications crucial for protein functionality. From the Golgi network, the protein is delivered to its final destination, either integrated into the plasma membrane or secreted extracellularly. If the protein is synthesized in the cytoplasm it usually ends up fully functional here or, if carrying appropriate signaling peptides, is transported into cellular organelles such as the nucleus or the mitochondria.[29]

1.1.2 siRNA delivery

RNA-interference (RNAi) is an important regulatory mechanism in cells, involved in the regulation of endogenous gene expression by inducing degradation of mRNA[30]. RNAi is suggested to be an evolutionary conserved mechanism as defense against viruses and a means to shut off transposon migration[30,31]. The interest in RNAi was triggered by Nobel Prize winning experiments in the late 1990s, demonstrating that introduction of double-stranded (ds) RNA mediated specific silencing of genes in eukaryotic cells[32]. A few years later, gene silencing induced by synthetic small interfering RNA (siRNA) was demonstrated in mammalian cells *in vitro*[33]. In 2003, the first successful therapeutic *in vivo* siRNA delivery experiment was performed in mice[34], followed by the first clinical study initiated in 2004[35].

RNAi represents a new and potent strategy for post-transcriptional silencing of specific genes that can be mediated by delivery of synthetic double-stranded siRNA. RNAi has become a well established tool for gene function analysis[36] and has shown promising therapeutic results[37-46]. Several therapeutic targets for siRNA delivery have been addressed in clinical trials to overcome diseases by gene silencing. Some examples are given in Table 1-2.

Table 1-2: Selected studies addressing siRNA delivery and gene silencing in animal models and clinical trials.

***In vivo* animal models**					
Targeted disease	**Silenced gene**	**Delivery system**	**Route of administration**	**Animal model**	**Ref.**
Rheumatoid arthritis	TNF-α	Chitosan (polymer)	Intraperitoneal	Mouse	37
Gut inflammation	Cyclin D1	Liposome-based	Intravenous	Mouse	44
Cancer	VEGF R2	PEI-PEG-RGD (polymer)	Subcutaneous	Mouse	45
Influenza	Viral capsid	PEI (polymer)	Retroorbital	Mouse	46
High cholesterol	ApoB	PLL (peptide)	Intravenous	Mouse	38

***In vivo* clinical studies**					
Targeted disease	**Silenced gene**	**Delivery system**	**Route of administration**	**Clinical phase**	**Ref.**
Cancer	RRM2	CDP-PEG-Tf (polymer)	Intravenous	I	39
Hepatitis B	4 viral genes	Lipid-based	Intravenous	I*	41
AMD	VEGF	Modified naked siRNA	Intraocular	II*	42
PC	K6a	Naked siRNA	Topical	I	43
RSV	Viral capsid	Naked siRNA	Intranasal	II	40

AMD: Age-related macular degeneration, ApoB: Apolipoprotein B, CDP: Cyclodextrin based polymer, K6a: Keratin 6a, PLL: Poly-l-lysine, Tf: Transferrin, RRM2: Ribonucleotide reductase M2, RSV: Respiratory syncytial virus, PC: Pachyonychia congenita, VEGF R2: Vascular endothelial growth factor receptor 2. *Study is terminated.

There are several pathways of RNAi culminating in gene silencing[30,47,48]. An overview of the gene silencing mechanisms is shown in Figure 1-1.

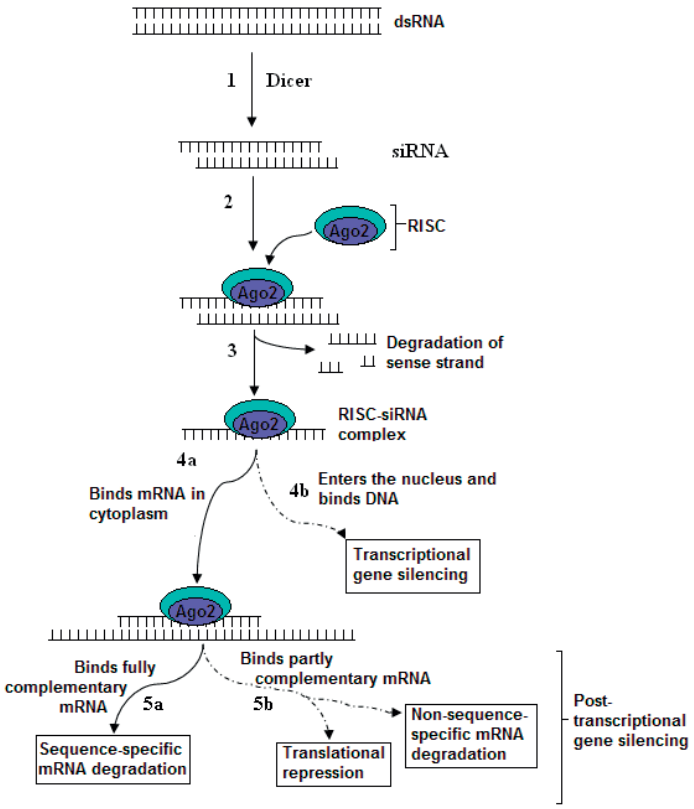

Figure 1-1: The mechanisms and possible pathways culminating in RNAi. The numbers refer to the details in the text. Adapted from Becker et al.[29].

RNAi can be artificially induced either by delivering dsRNA (e.g. siRNA) into the cytoplasm, or by nuclear delivery of plasmids expressing small hairpin RNA (shRNA) which after synthesis is exported to the cytoplasm by the protein exportin 5 for further processing into siRNA[49]. When a cell internalize long dsRNA or express shRNA and release it into the cytoplasm, the RNaseIII-type enzyme Dicer cleaves it into siRNA fragments (Step 1 in Figure 1-1) of approximately 21 base pairs (bp)[50]. However, when delivering siRNA to cells for gene silencing, this step will not be necessary since the nucleotides already are of appropriate size. Delivering siRNA instead of shRNA or longer dsRNA is beneficial for avoiding the need of nucleic acid delivery to the nucleus or possible activation of the immune receptors sensitive to dsRNA longer than 30 bp[51], respectively. In the next step (Step 2 in Figure 1-1), the siRNA is loaded into the RNA-induced silencing complex (RISC)[52]. Ago2, an enzyme component of RISC, cleaves and discards one of the siRNA strands (sense strand) while the other (antisense strand) is retained (Step 3 in Figure 1-1)[52]. If the RNA is perfect or near perfectly complementary to the target mRNA, it will follow the post-transcriptional gene silencing pathway (Step 4a in Figure 1-1)[47]. The RISC-associated siRNA strand then binds complementary mRNA sequences, and the endonuclease region of RISC cleaves the target mRNA at the

site between nucleotide 10 and 11 complementary to the antisense strand relative to the 5′-end (Step 5a in Figure 1-1)[52]. The target mRNA is then released and further degraded by intracellular nucleases[53]. After cleavage and release, the processive siRNA-RISC complex is capable of binding new complementary mRNA in a catalytic fashion[48]. This ultimately results in gene silencing due to the depletion of mRNA available for protein synthesis. If the RNA is not fully complementary to the target mRNA (Step 5b in Figure 1-1) it will mediate translational repression either by binding but not degrading the target mRNA, or by non-specific degradation[47].

Transcriptional gene silencing (Step 4b in Figure 1-1) only occurs if the siRNA is complementary to promoter regions and delivered to the nucleus[54]. This triggers chromatin remodeling and histone modifications, binding of siRNA to the genomic DNA and inhibition of the gene expression[55].

The endogenous gene regulatory function of RNAi is ensured by microRNAs[56]. They are derived from non-coding hairpin RNA transcribed by the genome, most often imperfectly paired with their targeting mRNA[56]. The microRNAs will not be further discussed in this thesis.

1.2 Chitosan

1.2.1 Molecular properties

The polysaccharide chitosan is a cationic linear copolymer of β-1,4 glycosidic bond linked *N*-acetyl-D-glucosamine (GlcNAc; A-unit) and D-glucosamine (GlcN; D-unit). The distribution of the two building sugar units in homogeneously deacetylated chitosans has been shown to be according to a random distribution[57,58]. Chitosans are derived from water insoluble chitin. The molecular structures of chitin and chitosan are shown in Figure 1-2.

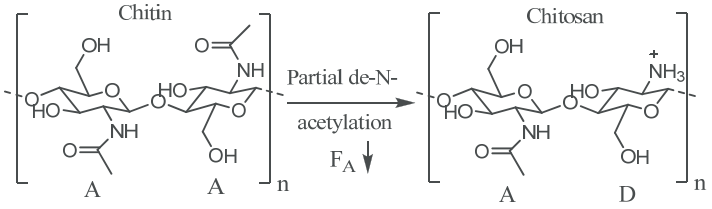

Figure 1-2: The molecular structures of chitin and chitosan.

The sugar units are in the $^4C_1$ conformation and the β-1,4 linkage gives the chitin and chitosan molecules an extended chain conformation where neighboring units are rotated 180º relative to each other in a similar way as in the cellulose chain. Chitosans can be considered as a family of polymers having a fraction of *N*-acetylated glucosamine units (F_A) lower than approximately 0.7. There is no generally accepted definition that can easily distinguish chitosan and chitin. Chitins and chitosans can vary widely in chain lengths, usually expressed as the molecular weight (MW) or the chain length (degree of polymerization, DP). As these polysaccharides normally are polydisperse, the MW of a sample is an average of the whole distribution of molecular weights. The two most common averages are the number-average (M_n) and weight-average (M_w):

$$M_n = \frac{\sum_i N_i M_i}{\sum_i N_i} \qquad \text{Eq. 1}$$

$$M_w = \frac{\sum_i w_i M_i}{\sum_i w_i} = \frac{\sum_i N_i M_i^2}{\sum_i N_i M_i} \qquad \text{Eq. 2}$$

where N_i is the number of molecules with molecular weight M_i and w_i is the weight of the molecules with molecular weight M_i. In a polydisperse sample $M_w > M_n$, while in a monodisperse sample $M_w = M_n$. The polydispersity index (PDI) is defined as follows:

$$PDI = \frac{M_w}{M_n} \qquad \text{Eq. 3}$$

For a randomly degraded polymer where the undegraded molecules are very long compared to the degraded molecules, the PDI will be 2. PDI lower than 2 suggests that a fractionation occurred during the production process. On the other hand, a PDI higher than 2 possibly indicates a mixing of samples with different molecular weights. A convenient method to determine the MW and size distribution of chitins and chitosans is size exclusion chromatography (SEC) combined with detectors determining the concentration and MW of the fractionated samples. When the molecular weights are measured, the chitosan DP is determined by dividing the polymer MW by the proportional weight of the GlcN and GlcNAc monomers.

Chitin occurs mainly in the exo-skeleton of crustaceans and insects and is one of the most abundant biopolymers in nature[59]. Chitosan, in contrast, is much less abundant and occurs as a component in the cell wall of certain fungi[60-62]. The main commercial source of chitosan is from shellfish waste, where chitin is isolated by chemical extractions, before chitosan is obtained by alkaline de-*N*-acetylation[59]. Acidic de-*N*-acetylation results in severe degradation of the chain and is therefore not feasible[63]. The chitosan chain is quite stiff and extended due to the rigid $^4C_1$ sugar units, restricted rotation around glycosidic bonds, but also charge repulsion from protonated amines[64]. Nevertheless, the chitosan chain is much less stiff than the double-stranded DNA molecule[59]. The solubility of chitosan at neutral pH-values increases at higher F_A values, e.g. high molecular weight (HMW) chitosans with a degree of acetylation of around 50% (F_A 0.5) is fully soluble even at pH 9, while fully de-*N*-acetylated HMW chitosans are completely insoluble at neutral pH[65]. Thus, fully de-*N*-acetylated chitosans need to have quite short chain lengths to be soluble at physiological pH[63]. Chitosan is a weak polybase with an intrinsic pK_a of approximately 6.5[66], making the molecule only slightly positively charged at pH values around 7.2-7.4.

The interest in chitosans has been increasing over the last decade, owing to their interesting biological properties, availability, excellent safety profile, biodegradability and ease of modification. Chitosan is used in a number of biomedical applications, e.g. in nucleic acid delivery, drug delivery[67-70], as a drug absorption enhancer[71], immunoadjuvant[72] and in wound dressings[73].

1.2.2 Self-branching and substitution of linear chitosans

Several approaches for structural manipulations of chitosan have been developed at the Dept. of Biotechnology (NTNU) the recent years[74-76]. This includes the production of fully de-*N*-acetylated chitosan oligomers of conventional linear structure (LIN)[75] and the preparation of chitosans with self-branched molecular architectures (SB)[74]. In addition, LIN and SB derivatives substituted with the trisaccharide 2-acetamido-2-deoxy-D-glucopyranosyl-β-(1-4)-2-acetamido-2-deoxy-D-glucopyranosyl-β-(1-4)-2,5-anhydro-D-mannofuranose (AAM)[76] have resulted in trimer substituted (TCO)[76] and self-branched trimer substituted chitosan oligomers (SBTCO)[77], respectively. The syntheses of the different chitosan molecular architectures are illustrated in Figure 1-3.

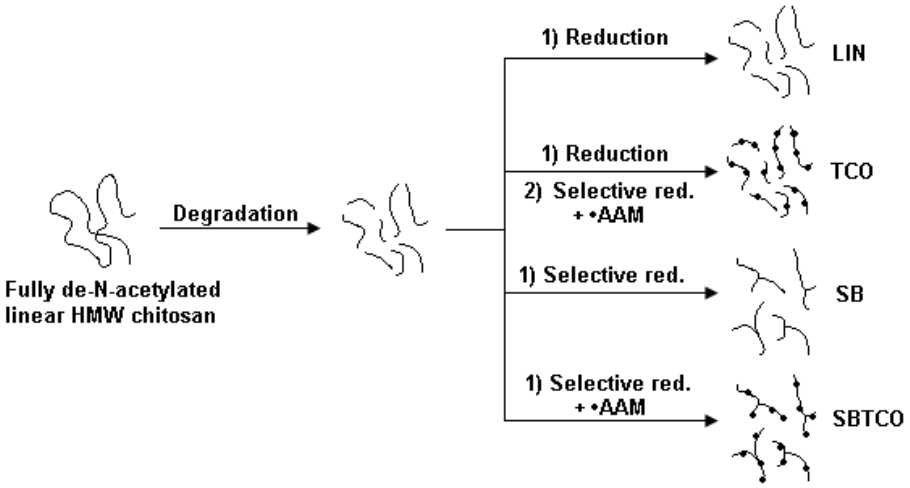

Figure 1-3: Overview of structure manipulations and synthesis of chitosans for nucleic acid delivery.

Briefly, the LIN chitosans are prepared by nitrous acid depolymerization and reduction of a HMW fully de-*N*-acetylated chitosan[75]. SB chitosans are prepared by omitting the reduction step after depolymerization, and incubated under selective reduction conditions[74]. The TCO and SBTCO are obtained by reductive *N*-alkylation with AAM of LIN and SB, respectively[75].

1.3 Polymer based nonviral nucleic acid delivery

Naked nucleic acids are unable to penetrate intact cellular membranes[78]. In addition, nucleotides are prone to degradation by ubiquitous nucleases[78]. Hence, pDNA and siRNA cannot efficiently be transported into cells without the aid of suitable carriers. The ideal delivery vehicle for gene therapy is considered to be applied non-invasively. It enters only the target cells at specific tissues where it mediates the desired gene regulation for a defined length of time, and importantly, without toxic effects[79].

Gene therapy was originally performed by viral delivery of nucleic acids, utilizing the ability of viruses to efficiently infect cells[80]. Viral mediated gene delivery and silencing are both normally dependent on the nucleic acids to reach the nucleus since viral RNAi is mediated by the expression of shRNA. The most commonly used viral delivery systems have been based on retroviruses and adenoviruses[81]. The adenovirus efficiently delivers nucleic acids to the nucleus but has high inflammatory potential and often mediates short duration of transgene expression[81]. The retrovirus on the other hand integrates its genome into the host genome ensuring stable expression, but this might also induce oncogenesis[81]. Despite delivering nucleic acids very efficiently, the size of viral capsids limits the length of the nucleotide sequences that can be transported. In addition, large scale production of viruses is difficult and targeting them to specific cell types can be challenging[82]. As a consequence, nonviral nucleic acid delivery systems based on e.g. cationic polymers have gained interest.

Cationic polymers spontaneously assemble with DNA/siRNA to form nanoparticles when mixed with nucleic acids[83-86]. This is facilitated by compaction of the nucleic acids via electrostatic interactions between the cationic polymer and the anionic phosphate groups in the nucleotide backbone. The polycation mediated collapse and compaction of the nucleic acid structure is considered to be a two step process[86]. First, the negative charge on the nucleic acid is neutralized by the interacting cations from the polymer, causing reduced charge repulsion and decreasing the nucleotide stiffness. Secondly, the resulting release of counterions from the polymer and nucleic acids increase the overall entropy and drives the complex formation. The resulting nanoparticles can adopt several different morphologies such as toroids[87], spheroids[84,88,89] and rods[84,87,89] typically with diameters of 50-100 nm. This is a significant reduction in size compared to the up to micrometer large native pDNA molecules, often several kbp long[90]. However, the 21 bp siRNA molecule is only 2 nm in diameter and 7 nm long, so the nanoparticle formation with siRNA probably differs from the process compacting pDNA[90] and is expected to rather involve interparticle-assembly involving many siRNA molecules. Furthermore, nanoparticle assembly with the shorter nucleotides will require cationic polymers of different properties due to the lower number of anionic charges per molecule compared to pDNA.

Unfortunately, the polymer based nonviral delivery systems of today have lower delivery efficiencies than the viral systems, limiting their current use *in vivo*[91]. This emphasizes the need to characterize and understand the polymer molecular properties favoring efficient nucleic acid delivery for further optimization.

1.3.1 Chitosan based nanoparticles

Chitosan was reported as a gene delivery vehicle for the first time in 1995 by Mumper et al.[92]. This group was also the first to demonstrate *in vivo* transfection with pDNA-chitosan nanoparticles[83]. Numerous studies have proven chitosan to be a promising nucleic acid delivery vehicle[93], and its use has been increasing the recent years.

Chitosans ability to form nanoparticles with nucleic acids relies on the positive charge given by the protonated amino groups of GlcN units, allowing interactions with the anionic phosphate groups of nucleotides. The cationic character of chitosan also to a large extent determines its aqueous solubility[65,77,94]. Consequently, the degree of de-*N*-acetylation (F_A) has major effects on the chitosans nucleic acid delivery efficiency as it affects the charge density of the molecule. Moreover, the chitosan length (MW/DP) also determines the interactions between the carrier and the nucleic acids. Together with the amino/phosphate (i.e. chitosan GlcN/nucleic acid) ratio (N/P), these fundamental properties of the nucleic acid-chitosan nanoparticles are important in balancing condensation, protection[84,87] and intracellular release[84,95-97], to ensure efficient nucleic acid delivery. The different properties will be presented in more detail in the following paragraphs. Since the short siRNA molecules allow for less charge interactions compared to the longer pDNA, the required properties for the chitosan carrier molecule in these applications differ[90,98].

*1.3.1.1 Effect of the degree of de-*N*-acetylation*

The degree of de-*N*-acetylation largely influences the chitosan charge density and solubility[65], but also its degradability[63,99-101]. Previous studies have discovered a positive correlation between low F_A and efficient nucleic acid delivery[84,102]. Kiang et al.[102] discovered that chitosans of lower F_A mediated better transgene expression in a range of different cell lines. Furthermore, F_A<0.35 has been shown necessary to mediate stable complexes able to transfect cells[103]. It has also been shown that increasing the F_A results in increased particle size and lower net charge, followed by decreased gene delivery[104]. Similarly, chitosan mediated siRNA delivery have shown more efficient gene silencing at lower F_A[84]. Possible explanations can be that charge dense chitosans interact more efficient with the nucleic acids during the assembly, resulting in more condensed and stable nanoparticles, well protected from nucleases. In addition, the net positive charge of nanoparticles assembled at lower F_A is higher[104], promoting interactions with the negatively charged cell surface. Since the number of charges per molecule of siRNA nucleotides is low compared to pDNA, the F_A is possibly an even more important chitosan molecular parameter in gene silencing applications.

1.3.1.2 Effect of the chain length

The length of the chitosan chain influences nanoparticle size and stability[77,95,105], cellular internalization[97,106] and determines the ability to release nucleic acids after complex formation[97,106]. A decrease in pDNA-chitosan particle size is observed when decreasing the MW of chitosan[83]. However, if the chitosan MW is too low the particle size will increase, indicating poor ability for nucleic acid condensation[104]. This correlates well with the observation that shorter chitosans are less efficient in protecting pDNA due to reduced particle stability[107]. In addition, chain entanglement is less involved in the

complex formation if the chitosan is short[102]. On the other hand, too high MW is known to result in very stable nanoparticles unable to release pDNA intracellularly, which leads to low transfection efficiency[106]. This illustrates the need to balance the nanoparticles ability to form particles of a size internalizable by cells and to protect but also release the nucleic acids. For siRNA delivery, there have been studies showing that higher MW chitosans have better gene silencing capability than shorter chitosan oligomers[84]. This is probably linked to the inability of the small siRNA molecules to form stable discrete complexes with short chitosans due to low availability of electrostatic interactions[84].

1.3.1.3 Effect of the N/P

The N/P is also found important to balance the nanoparticle stability[77,97,102,105,108-111], and this parameter affects the particle net surface charge[102,108-110]. Neutral particles tend to aggregate, while positively charged particles repel each other[112]. In addition, positively charged particles bind more efficiently to the anionic cell surfaces[104]. There is also evidence that positive charge helps nanoparticles reach the nucleus by binding to microtubules, molecular motor proteins and move along the cytoskeletal network[113]. It has been suggested that higher N/P values results in higher chitosan concentrations in the nanoparticles, possibly increasing the osmotic pressure in the endosomes and facilitating release to the cytoplasm[98]. This view is strengthened by another study suggesting that the free chitosan in solution promotes lysosomal escape after uptake[114]. Nevertheless, the N/P must be optimized since too low ratios give unstable particles, while too high N/P results in very stable particles that cannot dissociate. In general, pDNA delivery seems to depend on lower N/P values compared to siRNA delivery[84,97].

Several studies have shown that different combinations of F_A and MW need different N/P values for optimal pDNA delivery[95,102,103]. Since chitosan solutions are polydisperse, an increase in N/P can therefore compensate for a low MW by providing more high MW chitosans. While pDNA delivery seems very dependent on optimization for intracellular release[97], the assembly of nanoparticles for siRNA delivery appears less prone to result in too stable particles, and the delivery is successful even at high N/P and MW[84]. This is probably explained by easier dissociation of the small nucleotides compared to the several kbp long pDNA with numerous chitosan interactions.

1.3.1.4 Effect of self-branching and substitution

Generic chitosans usually mediate poor nucleic acid delivery[84,102]. This is probably a consequence of the low charge density of chitosan near physiological pH values, which is manifested in the poor physical and colloidal stabilities of the nanoparticles. The optimization of F_A, chain length and N/P is not always sufficient to achieve efficient nucleic acid delivery with chitosan, and some cell lines have proved difficult to transfect with pDNA and linear chitosan[77,102,115]. In order to improve the nucleic acid delivery efficiency with chitosans, molecular modifications are necessary.

Trimer substitution of linear chitosans with AAM has been shown to improve the colloidal stability of nanoparticles, resulting in increased gene delivery compared to unsubstituted chitosans[77,97,116]. Substitution with short oligosaccharide chains may also be used as a tool to control the unpacking of nanoparticles[97]. Self-branching has been

employed as another tailoring tool, and the self-branching of AAM-substituted chitosan oligomers have been shown to enhance the pDNA delivery efficiency[77].

1.3.1.5 Effect of serum and cell type

Another major factor affecting the nucleic acid delivery efficiency is the presence of serum[77,102,117,118]. In general, serum promotes interparticle aggregation due to negatively charged proteins[119] in addition to nucleic acid degradation by nucleases[120]. But low serum content during transfection have actually been shown to increase the efficiency, probably due to increased cell activity[121]. The delivery efficiency is also very dependent on the cell type involved[77,102,115,116]. This is possibly caused by variations in endocytic activity, rate of cell division and growth, side-effects from the nanoparticles and enzymatic composition of the endosomes.

1.3.1.6 Effect of pH

The major disadvantage of chitosan in nucleic acid delivery is its poor solubility at physiological pH values that results from deprotonation of the primary amino groups of GlcN as a consequence of its pK_a-value of 6.5. This makes the charge density of chitosan very pH dependent around physiological pH-values. Several studies have shown that optimal gene delivery is obtained between pH 6.5 and 7.0, and the efficiency rapidly declines at higher pH due to the release of pDNA from the chitosans[77,95,121]. In addition, the interactions between chitosan and siRNA have been shown to decrease at increasing pH, where the interactions were negligible at neutral or high pH[122].

1.3.2 Other chitosan based delivery systems

Many approaches have been undertaken in order to increase the performance of nucleic acid-chitosan nanoparticles. Some interesting strategies investigated in the literature are presented in this section.

1.3.2.1 Conjugation with receptor ligands

Targeting of chitosan based nanoparticles for improved nucleic acid delivery has been carried out by conjugations with a number of receptor specific ligands. Galactose ligands have been used to target lectin receptors on hepatocytes[115,123,124]. The asialoglycoprotein receptors, expressed at high levels on hepatocytes[125], recognize galactose and could prove useful in gene therapy for treating liver diseases. Transferrin receptors are responsible for the iron uptake in mammalian cells and are expressed at high levels in most cancer cells[126]. Thus, transferrin ligands have been conjugated to chitosan and were shown to increase the pDNA delivery efficiency in e.g. HEK293 and HeLa cells[127]. Several cells of the immune system express high levels of mannose receptors[128], and mannose ligands have successfully targeted and improved the gene delivery to macrophages using chitosan delivery vehicles[129]. In addition, gene delivery using chitosans with folate ligands have improved the transfection efficiency[130,131]. Folate receptors are overexpressed in many human cancers but is absent in most normal tissues[132], so folate ligands appears to be a potential utility for targeted nucleic acid delivery. To improve siRNA delivery, chitosans have been conjugated with RGD peptides targeting integrins *in vitro* and *in vivo* tumor vasculature[133].

1.3.2.2 Hydrophilic modifications

Hydrophilic chitosan derivatives have been made to increase the solubility and decrease the pH sensitivity of nucleic acid-chitosan nanoparticles. To increase the charge density at physiological pH values, chitosan have been quaternized by trimethylation of the amino groups of GlcN[134-137]. However, a high charge density will also lead to excessive unspecific binding and increased interactions with negatively charged extracellular or cellular components, such as endogenous intracellular proteins. Hence, the quaternization of chitosan has been shown to increase their toxicity[135]. Furthermore, increasing the charge density of chitosan leads to stronger interactions with the nucleic acids and may prevent intracellular dissociation due to high nanoparticle stability, as previously described. Chitosan nanoparticle stabilization has also been performed with polyethylene glycol (PEG) for improved *in vitro* and *in vivo* nucleic acid delivery[138-142]. The PEGylation increases the chitosan solubility at physiological pH. Furthermore, it reduces the sequestration by the opsonizing immune cells and prevents aggregation with serum proteins, thereby elongating the plasma circulation time of nanoparticles.

1.3.2.3 Hydrophobic modifications

Hydrophobic modifications of polymeric nucleic acid carriers can increase the adsorption on cell surfaces and cell uptake[143]. Introducing hydrophobic units is also thought to assist dissociation of the nanoparticles and facilitate nucleic acid release due to a decreased occurrence of ionic interactions[98]. The hydrophobic modification of glycol chitosan with 5β-cholanic acid has been performed to enhance the uptake and delivery of plasmids, and was shown to improve the transfection efficiency *in vitro* and *in vivo*[144]. Deoxycholic acid-modified chitosans have also been developed with the aim to increase cell membrane-carrier interactions and destabilization of the cell membranes for enhanced endosomal release[145]. The modification with deoxycholic acid was shown to improve the transfection efficiency in the presence of serum, and enhanced the nanoparticle condensation and protection of pDNA from nucleases[145]. Another strategy to improve the release of nanoparticles from endosomes has been to modify chitosan with stearic acid[146]. This approach resulted in efficient protection of pDNA from nuclease degradation and no interference with transfection efficiency was detected in the presence of serum[146].

1.3.2.4 pH-sensitive modifications

Improving the endosomal escape of chitosan based nanoparticles has been approached by developing pH-sensitive chitosan carriers. This is an interesting strategy, as inefficient release of nanoparticles from the endosomes due to the low buffering capacity of conventional chitosans is considered to be one of the primary causes of their poor transfection efficiency. The grafting of chitosan with polyethylenimine (PEI) has been performed to combine the buffering capacity of PEI to promote endosomal release with the biocompatibility of chitosan[147-149]. Further, urocanic acid-grafting of chitosan has been performed for a similar purpose[150]. The proposed mechanism is that the excellent buffer capacity of urocanic acid or PEI will lead to osmotic swelling and rupture of endosomes as the pH decrease. This is explained by the resulting accumulation of chloride counterions after proton influx and protonation of the polymer, and the following water influx and endosomal swelling. This is often referred to as the proton sponge effect[151]. Another pH-sensitive approach has been to introduce thiol groups in chitosan,

that are able to form reversible disulfide bonds[152]. The purpose of this modification has been to facilitate the intracellular dissociation of the nanoparticles, as the reductive environment and decrease in endosomal pH should result in breaking of the disulfide bonds and consequently nanoparticle dissociation. This strategy resulted in increased release of pDNA from the chitosan nanoparticles with improved transfection efficiency as compared to unmodified chitosan controls[152].

1.3.2.5 Co-assembly with negatively charged polymers

Several negatively charged polymers have been incorporated without covalent modification in chitosan nucleic acid nanoparticles to increase the water solubility or facilitate intracellular dissociation. One example is the inclusion of negatively charged poly(γ-glutamic acid) into chitosan-siRNA nanoparticles[153]. This resulted in enhanced uptake and intracellular dissociation, with more rapid onset in addition to increased and prolonged duration of knockdown compared to conventional chitosan-siRNA nanoparticles[153]. Another approach was to include the water soluble vitamin thiamine pyrophosphate to increase the solubility of the siRNA-chitosan nanoparticles[108]. This resulted in improved knockdown efficiencies at physiological pH and higher N/P values compared to the conventional nanoparticles with chitosan only[108].

1.3.3 Other polymer based delivery systems

1.3.3.1 Polyethylenimine

Polyethylenimine (PEI) is arguably the most commonly used polycation in nucleic acid delivery and several commercial transfection reagents based on this polycation are available. The molecular structure of PEI has been subject to numerous manipulations to improve its physiochemical and biological properties and exists both as linear and branched structures as shown in Figure 1-4.

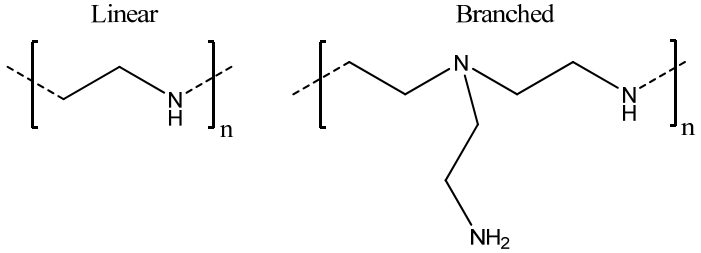

Figure 1-4: The chemical structure of linear and branched polyethylenimine (PEI).

PEI is a very efficient nucleic acid delivery vehicle, probably due to its excellent buffering capacity[151]. The buffering capacity is a result of the high density of amino groups and the relatively low pK_a value[151]. The proton sponge hypothesis explains that PEI, and possibly other polycations, together with its pDNA cargo is efficiently released from the endosomes[151]. Similar as for chitosan the transfection efficiency of PEI depends on the size of the polymer. The transfection efficiency has been shown to increase with increasing size for pDNA delivery[154]. However, the toxicity is also shown to increase for larger polymer sizes[155,156]. The degree of branching has also been shown to affect the performance of PEI and it has been shown that linear PEI is less efficient in condensing

pDNA compared to branched structures[157]. However, results comparing the transfection efficiency of linear and branched PEI *in vitro* and *in vivo* have been conflicting[158]. PEI has also been subject to a number of modifications for improved performance aimed for *in vivo* delivery of nucleic acids. Some examples are PEGylation, inclusion of disulfide linkages, grafting with less toxic polymers such as chitosan and conjugation with RGD peptides or other ligands such as mannose and galactose[3]. Successful delivery of siRNA resulting in knockdown has also been performed with PEI[159,160].

1.3.3.2 Poly-l-lysine

Poly-l-lysine (PLL) is a cationic polypeptide used extensively for *in vitro* delivery of pDNA[161]. The molecular structure of PLL is shown in Figure 1-5.

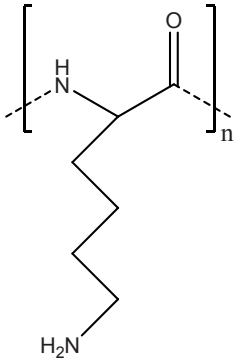

Figure 1-5: The molecular structure of poly-l-lysine (PLL).

PLL effectively condenses nucleic acids, but the excessive net-positive charge can facilitate interactions with serum proteins and complicate their use for *in vivo* delivery. The pK_a value of approximately 10 ensures that PLL is fully protonated at physiological pH[162], and thus the polymer has no buffering capacity to aid in endosomal escape. However, modifications such as conjugation with histidine groups with pK_a 6 provides buffering capacity and can possibly facilitate the delivery of nucleic acids by also reducing the electrostatic binding between PLL and the nucleic acid[163]. Indeed, this modification has been shown to promote efficient delivery of both pDNA and siRNA[164]. To ensure effective condensation of PLL and nucleic acids, a minimum PLL chain length must be exceeded[165]. However, the longer the PLL, the more toxic the resulting nanoparticles become[166]. Furthermore, the use of high molecular weight PLL results in aggregation and precipitation[167]. Similar as for chitosan and PEI, the modification of PLL such as PEGylation for improved colloidal stability and ligand conjugations with e.g. galactose and transferrin have been performed to improve *in vivo* performance[3].

1.3.3.3 Polymethacrylate and cyclodextrin

In addition to the widely investigated PEI and PLL polymers, two other examples of commonly used polymers for nucleic acid delivery are poly[2-(dimethylamino) ethyl methacrylate] (PDMAEMA) and cyclodextrin (CD). PDMAEMA shows efficient transfection efficiency due to its ability to destabilize endosomes and easily dissociate in the cytoplasm[168]. However, PDMAEMA suffers from cytotoxic effects[169] in addition to

aggregation if injected into the blood[170]. Interestingly, the efficient release of PDMAEMA nanoparticles from endosomes appears not to be explainable by the proton sponge hypothesis, indicating that also other mechanisms are responsible for the endosomal release of nanoparticles based on cationic polymers[171]. CD has a transfection efficiency comparable to PEI[172] and the cytotoxic properties of this polymer can be reduced by modification of the molecular structure[3]. Similar as for most cationic polymers, CD nanoparticles aggregates at ionic strengths comparable to *in vivo* conditions[3]. However, modifications improving the colloidal stability are possible, and a multicomponent CD based siRNA delivery system have successfully been applied to inhibit tumor growth in mice[173].

1.3.4 Other nonviral delivery systems

Several nucleic acid delivery systems based on other components rather than cationic polymers have been developed. Some examples of such delivery system are presented in Table 1-3.

Table 1-3: An overview of nonpolymeric nonviral delivery systems.

Delivery system	Type of delivery	Advantages	Disadvantages	Ref.
Lipoplexes	Lipid-nucleic acid complexes	Relatively efficient transfection	Cytotoxicity, immunological reactions, rapid loss in the blood	174
Liposomes	Nanoparticles	Efficient transfection, less toxic than lipoplexes	Cytotoxicity	175
Gene gun or electroporation	Ballistic/physical delivery with or without nanoparticles	Suitable for topological or muscle delivery of nucleic acids, e.g. for gene vaccination	Limited areas of application	176,177
Dendrimers	Nanoparticles	Efficient cellular uptake and endosomal release	Moderate cytotoxicity	3,178
Quantum dots	Nanoparticles	Low toxicity, efficient gene delivery	Inefficient siRNA delivery	3
Gold nanoparticles	Nanoparticles	Can improve the transfection efficiency of polymers	Need to be conjugated with other molecules to mediate transfection, cytotoxic	3

1.4 Barriers for cellular delivery of nanoparticles

The first step in nucleic acid delivery is to assemble stable nanoparticles of appropriate size. For successful delivery the particles need to overcome several extra- and intracellular barriers. In addition, they must dissociate intracellularly to mediate RNAi or gene expression. Nanoparticles may be introduced to target cells in therapeutic applications *ex vivo*[179] or *in vivo*[180]. *Ex vivo* delivery is performed by harvesting the target cells from the patient and adding the nanoparticles *in vitro* before the cells are implanted back. *In vivo* administration of nanoparticles in humans as shown in Figure 1-6, commonly occurs at local sites such as topical, intranasal, intraocular and oral, or systemically by intravenous injection into the blood stream. In animal experiments intraperitoneal and intratumoral delivery, and delivery into the central nervous system is commonly performed[181].

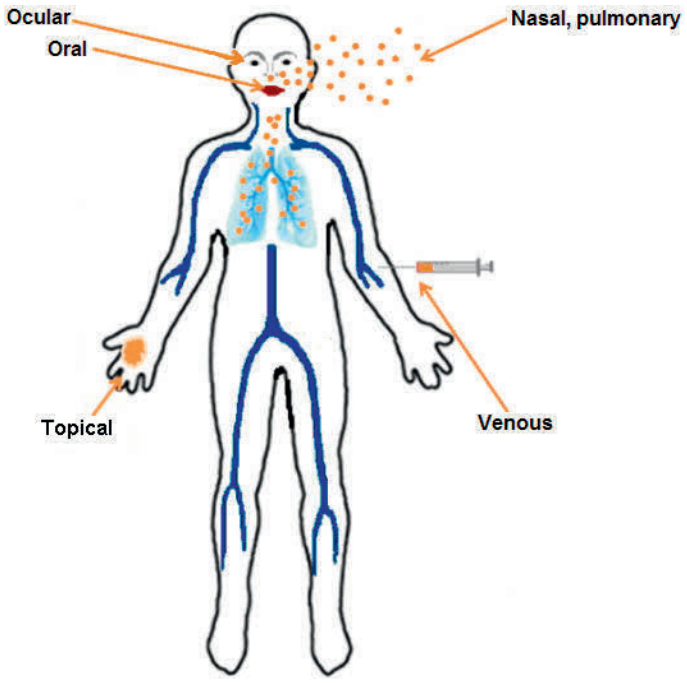

Figure 1-6: The most common routes of nanoparticle administration in humans. Adapted from Yildirimer et al.[182].

Several anatomical barriers limit the availability to the target cells. The extracellular barriers encountered by the nanoparticles depend on the route of administration. For example, ocular and topical deliveries circumvent the blood circulation and thus the need for the nanoparticles to migrate across endothelial cells and extracellular matrix. Similar, intranasal delivery can be an efficient method to reach target cells in the lungs and this has previously been shown to be an efficient delivery route for chitosan nanoparticles[110]. However, several barriers are independent on the means of administration, e.g. those

encountered at the target cell surface and intracellular. In this section, the barriers encountered by intravenously administered nanoparticles are covered.

As illustrated in Figure 1-7 (Step 1), immediately after systemic administration the first extracellular barriers are encountered.

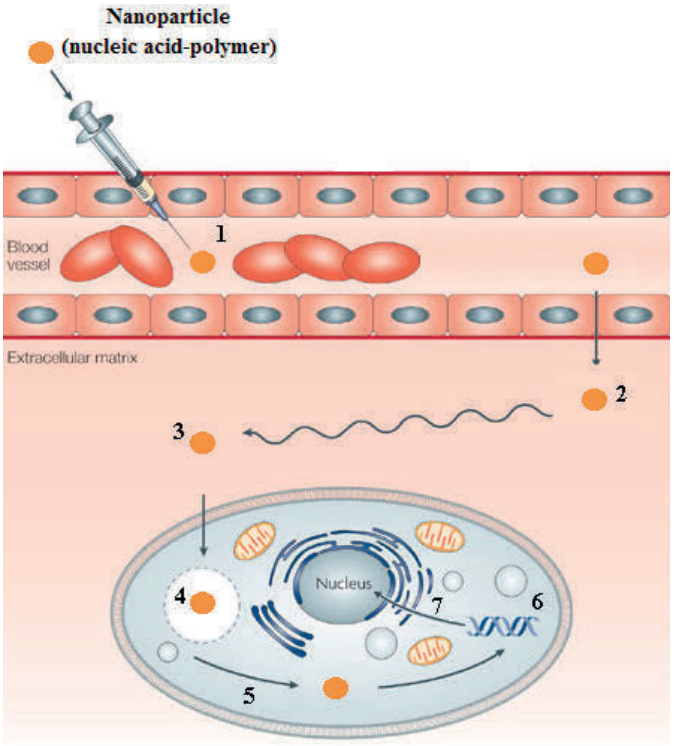

Figure 1-7: Barriers encountered after systemic administration of nanoparticles for gene therapy. The numbers refer to the detail in the text. Adapted from Whitehead et al.[180].

Nucleic acids are prone to degradation by nucleases located in the blood, extracellular matrix (ECM) and intracellular[82,90,180]. In addition, phagocytes and macrophages in the blood, ECM[180] or in tissues[82] can efficiently remove injected nanoparticles. The nanoparticles can potentially stimulate the immune system resulting in activation of the complement system and clearance[183]. Intravenously administered nanoparticles can also be sequestered and lost by electrostatic interactions with serum proteins[119,120], which facilitates capture and clearance by phagocytosis[184]. Naked nucleic acids are rapidly cleared from the circulation and siRNA molecules are assumed to be freely excreted through the kidneys due to the small molecular size[91]. As a consequence, naked unmodified pDNA and siRNA have a half-life of less than 5 minutes in serum after systemic administration[185,120].

To enter the ECM, intravenously administered nanoparticles must first penetrate the endothelium (Step 2 in Figure 1-7). This can be achieved by the enhanced permeability and retention effect in tumors, but is more challenging in intact microvasculature[90,180]. As discussed earlier, directing the nanoparticles to target tissues or cells can be mediated by conjugating them with receptor specific ligands. Once inside the ECM, the nanoparticles need to avoid resident macrophages and interactions with matrix components that prevent them from reaching the target cell[180]. The ECM largely consists of collagen proteins, glycosaminoglycans and proteoglycans[186]. Together, the ECM components form an overall negatively charged matrix, potentially immobilizing the transport or disrupting the positively charged nanoparticles[186].

After the nanoparticles successfully escapes the ECM and reach the target cell (Step 3 in Figure 1-7), they will bind to the cell via electrostatic interactions between the cationic particle and the anionic cell surface leading to non-specific adsorptive endocytosis, e.g. endocytosis, phagocytosis or pinocytosis[187]. Alternatively, a targeting approach mediated by ligands targeting cellular receptors results in clathrin mediated endocytosis[187]. Naked nucleic acids are unable to cross cellular plasma membranes by themselves due to the negative charge repulsion from the phosphodiester backbone and the anionic cell surface. In addition, the passive transport across the lipid bilayer is size restricted[91].

After the nanoparticles have been internalized (Step 4 in Figure 1-7) their intracellular processing pathway depends on the mode of uptake[187]. However, independent on the uptake mechanism, the nanoparticles normally end up in endosomes where a gradual decrease in pH occurs with a possible subsequent fusion with lysosomes containing degrading enzymes[188]. Hence, the nucleic acids need to escape the endo/lysosomes and reach the cytoplasm, either as intact nanoparticles or in naked form after dissociation (Step 5 in Figure 1-7). Since lysosomes contain nucleases, the nucleic acids must be protected or escape the endosomes before they develop into lysosomes.

When the nanoparticles have dissociated and siRNA is released into the cytoplasm the transport ends as the target mRNA resides in this cellular compartment (Step 6 in Figure 1-7). pDNA on the other hand needs to reach the nucleus for transcription (Step 7 in Figure 1-7). Naked pDNA has a very low diffusion rate in the cytoplasm[189,190], and as mentioned earlier, the nuclear delivery of pDNA seems to depend on transport of the cationic nanoparticles along the microtubules[113].

The nuclear import of pDNA is assumed to mainly occur during mitosis for dividing cells[191]. Hence, the import is more challenging in non-dividing cells as the pDNA in this case needs to gain indirect access to the nucleus by active transport[90]. This can be mediated by nuclear localization signal peptide sequences in transcription factors that associates with the pDNA in the cytoplasm and directs internalization with the nuclear transport system[90].

1.5 The blood-brain barrier

The blood-brain barrier (BBB) is a specialized anatomical and physiological barrier constituting a major hurdle for the delivery of systemically injected drugs to the central nervous system (CNS). Thus, strategies to overcome this challenge are needed to improve the treatment of CNS related diseases. In the current study, chitosan-siRNA nanoparticles were investigated as a tool to overcome the limitations in brain drug delivery, and the BBB is therefore discussed in this section.

Neurons in the CNS maintain vital functions in humans and animals by synaptic communication using chemical and electrical signals[192]. To ensure reliable signaling, a stable local ionic microenvironment at the synapses and axons is critical, with no fluctuation of neurotransmitters from the peripheral nervous system. In addition, neurons are very sensitive to inflammation and have low toxic threshold for many substances, even endogenous metabolites[192,193]. Replacement of dead neurons is an inefficient, limited and slow process, so preventing loss of neuronal cells is important[194]. Thus, to ensure a stable microenvironment and protect neurons from microbes and toxins, the CNS has an extraordinary barrier for defence[192,195].

The BBB is defined by the endothelial cells lining the capillaries[196], recognized by their restricted transcytosis due to low pinocytotic activity[197,198]. The paracellular diffusion barrier of the BBB is formed by complex tight junctions sealing the transport pathway between the endothelial cells[199]. Consequently, the barrier is only permeable by transcellular passive diffusion across the brain endothelial cells of lipophilic molecules with a size less than 400 Da, which includes virtually all commonly used CNS drugs[200]. However, specific transporters at the endothelial cell membranes ensure supply of important compounds such as nutrients, hormones and antibodies by active receptor-mediated or non-specific adsorptive transcytosis[201]. Importantly, gases such as O_2 and CO_2 diffuse freely across the BBB[192].

Despite the ability to freely diffuse across the BBB, even small lipophilic molecules enter the brain at very low rate[192]. This is explained by the presence of cellular efflux pumps forming a defensive transcellular diffusion barrier[192,202]. The efflux pumps maintain the BBB by efficient excretion of specific lipophilic xenobiotics diffused into or taken up by the endothelial cells[192,202]. Thus, many drugs are transported across the BBB at low efficiency[196]. This is a pharmacokinetic challenge and currently limits the treatment of e.g. schizophrenia[203], depression[204], brain tumors[205], HIV[206] and epilepsy[207]. The best characterized BBB efflux pump is P-glycoprotein (P-gp), which is also involved in several other physiological barriers[208-212] and is often responsible for cancer cell multidrug resistance[213-216].

1.5.1 Anatomy of the blood-brain barrier

The cellular elements of the BBB are mainly the endothelial cells, astrocyte end-feet and pericytes[192]. In addition, the brain capillary endothelial cells are surrounded by a thick basement membrane of laminins, type IV collagen and heparan sulfate proteoglycans[217]. An overview of the BBB is given in Figure 1-8.

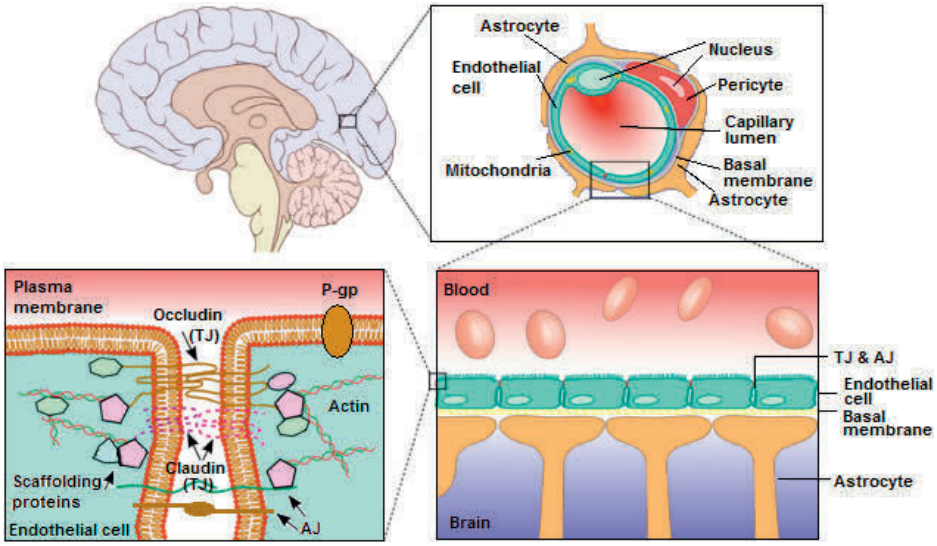

Figure 1-8: Schematic illustration of the cells and proteins involved in the blood-brain barrier. Adapted from reference 218.

The BBB endothelial cells are connected with specialized tight junctional complexes (TJ) in addition to conventional cell-cell adherens junctions (AJ)[192,201]. The TJ is formed by several transmembrane proteins efficiently sealing off paracellular transport. The main contributors of the TJ are claudin proteins and occludins, and several cytoplasmic scaffolding proteins connecting the transmembrane proteins to the intracellular actin cytoskeleton. The AJ provides structural integrity and attachment between the endothelial cells and are necessary for the formation of TJ. However, the barrier to paracellular diffusion appears to be largely due to the TJ, making the brain parenchyma inaccessible for polar- and macromolecules without active transport[201]. The brain endothelial cells are recognized by their high density of mitochondria[219]. This provides the metabolic work capacity needed by the efflux pumps to maintain the ionic gradient across the BBB.

Astrocytic end-feet ensheath over 99% of the microvessels surfaces[220] and maintain the BBB endothelial cell phenotype with TJ and asymmetric (polarized) organization, with an apical (in contact with blood) and basolateral (brain tissue) side[201,221]. Astrocytes are also thought to be regulators of the water permeability in the brain[201], and is able to change blood vessel diameter in both directions[220]. Together with the pericytes, astrocytes are believed important for the BBB respond to changes in the microenvironment via complex signaling cascades[222]. Astrocytes also express several types of efflux transport proteins including P-gp[196], possibly mediating xenobiotic efflux to the blood via the endothelial cells.

The pericytes are embedded in the basement membrane surrounding the endothelial cells. They are shown to be involved in the formation of the TJ, reduction of the pinocytosis activity, polarization of astrocyte end-feet and the deposition of astrocyte derived basement membrane[223]. In addition, pericyte-endothelial cell interactions are important

during the BBB development[224]. Similar as the astrocytes, the pericytes can regulate blood flow by changing the blood vessel diameter[222]. As undifferentiated stem cells, the pericytes function as supporters of the endothelial cells[222]. However, they can differentiate into smooth muscle cells, fibroblasts or macrophages if needed[222].

1.5.2 P-glycoprotein

Passively diffusing lipophilic molecules are actively effluxed from the brain and its capillaries by members of the ABC (ATP-binding cassette) transporter family[196]. The ABC transporters are a superfamily of proteins with 48 members grouped into seven sub-families[225]. The ABC transporters of greatest significance in the BBB are P-gp, the multidrug resistance proteins (MRPs) and the breast cancer resistance proteins (BCRP)[226]. This section will only cover P-gp, due to its relevance in the last part of this study. In addition to the presence in the endothelial cells of the BBB, P-gp is also expressed in tissues such as the lungs, kidneys, testes and intestines[208-212]. P-gp is expressed at the apical side of the endothelial cell membranes[196] where it transports substrates from the BBB to the blood. As mentioned earlier, P-gp is also expressed at the astrocytic end-feet[196]. The molecular structure of P-gp is schematically illustrated in Figure 1-9.

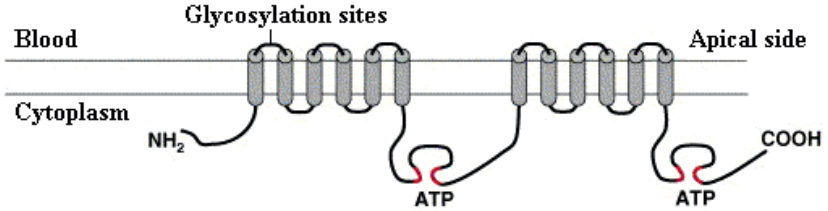

Figure 1-9: A schematic illustration of the P-gp protein structure. Adapted from Löscher et al.[196].

P-gp is a 170 kDa protein of 1,280 amino acids divided in four domains[227]. Two of the domains are cytoplasmic and have nucleotide binding domains providing energy for the substrate efflux transport. These domains are preceded by a polytopic membrane spanning domain composed of six transmembrane helices. The first extracellular loop has three glycosylation sites. In humans, there are two types of P-gp encoded by the *MDR1* and *MDR2* gene, whereas only the *MDR1* encoded variant is involved in BBB drug efflux[196]. In rodents, two P-gp variants are encoded for by the genes *mdr1a* and *mdr1b*. The substrate specificity is partly overlapping, but their efflux efficiency and tissue distribution differs[228,229]. In rat brain capillaries, only *mdr1a* is expressed, whereas only *mdr1b* is expressed in the brain parenchyma[212,230].

The exact mechanism of P-gp mediated drug efflux is still unknown. Of the suggested models providing an explanation for the efflux mechanism, the so-called flippase model is currently favored[231]. This model suggests that the P-gp substrates gain access to the core of the transmembrane domains after interacting with the plasma membrane. At the cytoplasmic membrane surface, the P-gp protein flips the drug to the outer leaflet where the substrate diffuses out of the cellular membrane. The P-gp substrates are primarily cationic, lipophilic planar molecules and the flippase model provides an explanation for

why P-gp can have such broad spectrum of substrate drugs, since the only requirement is membrane association on the inner plasma membrane leaflet. It also provides an explanation for why molecules of higher lipophilicity are more easily removed from a P-gp expressing cell.

Several structurally diverse drugs are P-gp substrates, limiting their efficacy in therapy. Some examples of drugs and associated brain diseases where therapy is limited by P-gp efflux are given in Table 1-4.

Table 1-4: P-gp substrate drugs involved in the treatment of brain diseases[196,201].

Drug	Class	Disease
Daunorubicin Doxorubicin	Athracycline	Brain tumors
Vincristine Vinblastine	Vinca alkaloid	
Paclitaxel Docetaxel	Taxane	
Phenobarbital	Barbiturate	Epilepsy
Phenytoin	Hydantoin derivative	
Indinavir Saquinavir	Protease inhibitor	Brain HIV
Erythromycin	Macrolide antibiotic	Brain infection
Actinomycin D	Polypeptide antibiotic	
Doxepin	Tricyclic antidepressant	Depression
Olanzapine	Antipsychotic agent	Schizophrenia

Previous work on strategies to avoid P-gp mediated drug efflux at the BBB includes the use of specific inhibitors[232] such as verapamil and cyclosporin A[233] and altering the gene regulation with e.g. cytokines[234] or using lipid mediated drug transport to increase the cellular uptake[235]. In addition, repeated injections of naked siRNA in mice *in vivo* has recently been shown to significantly reduce the expression of P-gp in brain endothelial cells[236].

2. Aims

The overall aim of this study has been to characterize chitosan molecular properties favoring efficient pDNA and siRNA delivery in mammalian cells. Furthermore, siRNA-chitosan nanoparticles were investigated for their potential to improve drug delivery across the BBB by silencing the efflux pump P-gp.

This study has resulted in three papers that form the basis of this thesis. The papers are attached. The following specific aims have been addressed:

i) Optimize and investigate the effect of self-branching chitosans for improved nanoparticle mediated pDNA delivery and transgene expression in HeLa cells (Paper I).

ii) Characterize the chitosan molecular properties favoring efficient siRNA delivery and silencing of genes in mammalian cells (Paper II).

iii) Silence P-gp expression in a BBB model using siRNA-chitosan nanoparticles to improve the delivery of P-gp substrate drugs to the brain (Paper III).

3. Summary of papers

3.1 Paper I

Alterations of chitosan molecular properties have in numerous studies shown to affect the gene delivery efficiency. In this paper, the self-branching of fully de-*N*-acetylated chitosans was investigated as a strategy to optimize the delivery properties of pDNA-chitosan nanoparticles without compromising the safety profile. SB and SBTCO chitosans with a weight average molecular weight (M_w) of 11−71 kDa were synthesized, characterized and compared with their linear counterparts with respect to gene delivery efficiency, cellular uptake, formulation stability and cytotoxicity. While the linear unmodified chitosans failed to transfect HeLa cells, the self-branching resulted in high transfection efficiencies. The most efficient chitosan, a SBTCO with a M_w of 30 kDa, yielded higher gene expression than the tested commercial transfection reagents. Nanoparticles formed with SBTCO chitosans exhibited a higher colloidal stability of formulation, efficient internalization without excessive cell surface binding and low cytotoxicity.

3.2 Paper II

Most siRNA delivery studies have been performed with conventional partially *N*-acetylated chitosans relying on high N/P and siRNA doses for efficient gene silencing. In this study, the purpose was to identify fundamental chitosan molecular properties favoring siRNA delivery and efficient gene silencing in mammalian cells. siRNA-chitosan nanoparticles of N/P 10-60 were prepared from well-defined chitosans of various F_A, chain lengths and chain architectures. Structure-activity relationships were determined by the cellular uptake of siRNA and the knockdown efficiency at mRNA and protein levels. Additionally, the nanoparticle cytotoxicity was evaluated on the basis of cellular metabolic activity and membrane integrity. The results show that the most efficient gene silencing was achieved using fully de-*N*-acetylated chitosans with number average degree of polymerization (DP_n)>50 (M_w>16 kDa). These chitosans mediated efficient siRNA delivery at low siRNA concentrations and potent long-term silencing of both exogenous and endogenous target genes, with minimal cytotoxicity.

3.3 Paper III

The BBB, composed of tightly organized endothelial cells, limits the availability of drugs to therapeutic targets in the CNS. The barrier is maintained by membrane bound efflux pumps efficiently transporting specific xenobiotics back into the blood. The efflux pump P-gp, expressed at high levels in brain endothelial cells, has several drug substrates. Hence, siRNA mediated silencing of the P-gp gene is a possible strategy to improve the delivery of drugs to the brain. In this study, siRNA-chitosan nanoparticles selected on basis of the results in Paper II were investigated for the potential in silencing P-gp in a BBB model. The results show that the transfection of rat brain endothelial cells mediated effective knockdown of P-gp with subsequent decrease in P-gp substrate efflux. This resulted in increased cellular delivery and efficacy of the model drug doxorubicin.

4. Experimental procedures

This part summarizes the experimental procedures used in this study. For further details, the reader is referred to the attached papers.

4.1 Cell culture

The HeLa (human cervical cancer) cells were a gift from Prof. Marit Otterlei (Dept. of Cancer Research and Molecular Medicine, NTNU). The cells were grown in DMEM (Gibco, Invitrogen) supplemented with 1 mM non-essential amino acids (Gibco, Invitrogen), 10% FBS (Gibco, Invitrogen) and 1 mM L-glutamine (Sigma). The transduced H1299 cell line (human lung carcinoma) stably expressing destabilized EGFP (Enhanced Green Fluorescent Protein) was a gift from Prof. Jørgen Kjems (Dept. of Molecular Biology, Aarhus University, Denmark). The cells were grown in RPMI 1640 medium (Sigma) supplemented with 1 mM non-essential amino acids (Gibco, Invitrogen), 10% FBS (Gibco, Invitrogen) and 500 µg/mL G418 selection antibiotic (Sigma). MCF-7 (human breast cancer) cells were provided by Kristin G. Sæterbø (Dept. Physics, NTNU) and were grown in MEM (Gibco, Invitrogen) with 1 mM non-essential amino acids, 1 mM sodium pyruvate (Gibco, Invitrogen) and 10% FBS. The HUVEC (human umbilical vein endothelial) cells were supplied by Lonza and were grown in EBM-2 (Lonza) with full supplements (EGM-2 BulletKit, Lonza). The immortalized rat endothelial cell line RBE4 was kindly provided by Prof. Tore Syversen (Dept. of Neuroscience, NTNU). The cells were grown in alpha MEM supplemented with 10% FBS, 300 µg/mL G418 selection antibiotic and 1 ng/mL basic fibroblast growth factor (Invitrogen). The RBE4 cells were grown on surfaces coated with rat tail type I collagen (BD Biosciences). When seeding cells for experiments, the growth medium was supplemented with 100 U/mL of penicillin and streptomycin (PEST, Sigma). The cells were cultured at 37ºC in a humidified atmosphere with 5% CO_2.

4.2 Transfection reagents

4.2.1 Chitosans

Chitosans were prepared by nitrous acid depolymerization of fully de-*N*-acetylated chitosan (F_A<0.002, M_w 146 kDa) as previously described[75]. To produce the linear oligomers, depolymerized chitosan was conventionally reduced by $NaBH_4$, dialyzed and lyophilized. Self-branched chitosans were prepared directly after depolymerization by omitting the reduction step and incubating the chitosan solution under selective reduction conditions ($NaCNBH_3$) for 48 h. The details of the synthesis may be found elsewhere[74]. The glycosylation of chitosans using the trimer 2-acetamido-2-deoxy-D-glucopyranosyl-β-(1-4)-2-acetamido-2-deoxy-D-glucopyranosyl-β-(1-4)-2,5-anhydro-D-mannofuranose (AAM) was carried out as previously described[76]. For confocal microscopy, the chitosans were labeled with an Alexa Fluor 488 succinimidyl ester (Molecular Probes) using a molar ratio of 1 dye per 200 GlcN units.

To determine the degree of substitution, the substituted chitosan samples were characterized by ^{1}H NMR (Avance DPX 400, Bruker). The weight (M_w) and number (M_n) averages of molecular weight and molecular weight distribution were determined by

size-exclusion chromatography (SEC) with a refractive index detector (RI, Dawn Optilab 903, Wyatt Technology) and a multiangle laser light scattering detector (MALLS, Dawn DSP, Wyatt Technology). All samples were dissolved in Milli-Q (MQ) deionized water (5-7 mg/mL) and filtered through a 0.22 μm syringe filter (Millipore). A TSK 3000 PWXL column (Tosoh Bioscience) was used, and the sample was eluted with 0.2 M ammonium acetate (pH 4.5) at a low flow rate of 0.5 mL/min.

The four different structure types of chitosan oligomers are denoted as linear (LIN), self-branched (SB), trisaccharide-substituted (TCO) and self-branched trisaccharide-substituted (SBTCO). The number used in the notation is the measured M_w (Paper I) or the DP_n (Paper II and III).

4.2.2 Commercial

The lipid-based transfection reagents Lipofectamine 2000 and RNAiMAX were purchased from Invitrogen. Exgen 500, a linear PEI (M_w 22 kDa) based transfection reagent, was purchased from Fermentas. The reagents were used as described in the manufacturer's protocol.

4.3 Nanoparticle assembly

Formulations with different N/P values were prepared by a self-assembly method while keeping the amount of pDNA or siRNA constant. A solution of nucleic acids was diluted with the necessary amount of sterile nuclease free water (5 Prime). Subsequently, the required amount of chitosan was added from a sterile filtered solution during vortex mixing. The assembled nanoparticles were incubated for 30 min at room temperature before transfection. siRNA was normally delivered at 50 or 100 nM, corresponding to 2.5 or 5.0 pmol per well in a 96 well plate, respectively. While the siRNA was delivered to the cells at different concentrations, the pDNA was always delivered at a concentration of 6.65 μg/mL, corresponding to 0.33 μg per well.

4.4 Nanoparticle characterization

4.4.1 Dynamic light scattering

Nanoparticle size determination was performed using dynamic light scattering (DLS) on a Zetasizer Nano ZS (Malvern Instruments). Measurements were performed at a 173º angle and a temperature of 25ºC when analyzing samples in MQ water. Aggregation kinetics were measured by diluting the samples with an equal volume of hypertonic Opti-MEM and the analysis was performed at 37ºC. The undiluted nucleic acid-chitosan nanoparticles were measured at a pDNA/siRNA concentration of 13.3 μg/mL. Each sample was analyzed in triplicate over a time span of 30 min. The nanoparticle size was expressed as the z-average hydrodynamic diameter obtained by a cumulative analysis of the correlation function using the viscosity and refractive index of water in the calculations.

4.4.2 Nanoparticle tracking analysis
The nanoparticle concentrations were determined using nanoparticle tracking analysis (NTA) on a NanoSight LM10 (NanoSight). Measurements were performed in MQ water at room temperature using the viscosity of water in the calculations. The siRNA-chitosan nanoparticles were measured at a siRNA concentration of 6.65 µg/mL. Video capture parameters such as the shutter value and recording gain and the analysis parameter detection threshold were set manually. The capture duration was set to 60 s and the temperature was recorded with a digital thermometer. The sizes measured by NTA were similar as those obtained by DLS; sizes of approximately 40-100 nm were observed for the siRNA-chitosan nanoparticles.

4.5 Transfection
Cells were seeded in well plates (Corning) 24 h prior to experiments in densities with approximately 90% (pDNA experiments) or 50-75% confluency (siRNA experiments) on the day of transfection. The nanoparticles assembled in water were diluted with an equal volume of Opti-MEM (Gibco, Invitrogen), supplemented with 270 mM mannitol (Sigma) and 20 mM HEPES (Sigma) for adjustment of the osmolarity to 300 mOsm/kg and the pH to 7.2. The formulations were not supplemented with FBS or antibiotics. The pH value and reduced serum content during transfection was chosen to ensure optimal nanoparticle stability while maintaining a physiological environment with limited extent of particle aggregation and without deleterious effects on the treated cells. Prior to adding the nanoparticles, the cells were washed and briefly incubated with Hank's balanced salt solution (HBSS, Gibco, Invitrogen). Next, the HBSS solution was removed and aliquots of nanoparticle formulation were added to each well. The formulations were removed after 5 h of incubation and replaced by growth media supplemented with PEST.

4.6 Luminometry
For analysis of luciferase gene expression post-transfection, cells were washed with PBS (Gibco, Invitrogen) and lysed using luciferase lysis buffer (Promega). The luciferase activity was measured using a LMax II luminometer (Molecular Devices). Total cell protein content was measured using a bicinchoninic acid assay (Pierce) for normalizing the luciferase activity to the amount of cells.

4.7 Flow cytometry
Measurements of cellular delivery or expression of fluorescent molecules were performed using a Gallios flow cytometer (Beckman Coulter). At the time of analysis the cells were washed in PBS, trypsinized and resuspended in ice-cold PBS supplemented with 5% FBS. For each sample, 10,000 gated events were counted and a dot plot of forward scatter versus side scatter established a collection gate for cells to exclude cellular debris, dead and aggregated cells. The analyzed fluorescent molecules were exited using appropriate lasers and emitted light was collected using filters avoiding spectral overlap.

4.8 GAPDH protein activity assay
The effect of transfection with GAPDH (Glyceraldehyde-3-phosphate dehydrogenase) targeting siRNA on the GAPDH protein activity was measured using the commercial available KDalert GAPDH assay kit (Ambion) according to the manufacturer's protocol.

4.9 Quantitative real-time RT-PCR

Knockdown was measured at mRNA levels using the ABI 7500 real-time PCR system (Applied Biosystems). The mRNA was harvested, and cDNA was synthesized and amplified using the Cells-to-C_T kit (Applied Biosystems) as described in the manufacturer's protocol. Primer efficiencies were determined using standard curves. The percentage of mRNA expression relative to untreated cells was calculated using the comparative C_t method, where the target sample was normalized to the endogenous β-actin expression.

4.10 Confocal laser scanning microscopy

Cells were seeded onto 8-chamber microscopic slides (Ibidi) and transfected. At the time of analysis, cells were imaged using appropriate lasers and filters for the fluorescent molecules that were investigated. The live cells were examined using a LSM 510 (Carl Zeiss) confocal laser scanning microscope (CLSM) equipped with a c-Apochromat 40x/1.2 NA W corr objective. The acquired images had resolutions of 512x512 pixels.

4.11 Toxicity

4.11.1 Metabolic activity

The effect of transfection on metabolic activity was measured using an Alamar Blue assay (Invitrogen). The sample absorbances were measured 4 h after adding the assay reagent using a spectrophotometer (Molecular Devices, USA) at 570- and 600-nm. The metabolic activity of the cells was evaluated as the reduction in Alamar Blue reagent.

4.11.2 Cellular membrane integrity

The effects on the cellular membrane integrity from transfection were evaluated using the LDH (lactate dehydrogenase) cytotoxicity assay (Cayman), which measures levels of cellular cytoplasmic LDH leakage. Measurements of absorbance at 490 nm were performed in serum-free medium using a spectrophotometer.

4.12 Rhodamine 123 efflux assay

A 10 μM solution with the P-gp substrate rhodamine 123 (R123, Sigma) diluted in Opti-MEM was added to the cells. After 45 min of incubation, R123 was removed and replaced with growth medium. Two hours after removing the R123, cells were prepared for analysis by flow cytometry or CLSM.

4.13 Doxorubicin delivery and efficacy

One day after transfection the RBE4 cells were added growth medium with concentrations of the P-gp substrate, and DNA intercalating agent, doxorubicin (Pharmacia) ranging from 0 to 5 μM. The cells were incubated with doxorubicin for two days before the effect on metabolic activity was measured using the Alamar Blue assay. Intracellular doxorubicin delivery was measured two days after transfection by flow cytometry or CLSM by incubating the cells in growth medium with 50 μM doxorubicin for 3 h.

4.14 Statistical analysis

The measured values were collected and given as mean values ± standard deviation (s.d.). Statistical differences between the raw data were investigated using the SigmaPlot 11.0 software package with one-way ANOVA in conjunction with a multiple comparison test (Holm-Sidak).

4.15 Summary of analytical techniques

A summary of the different plasmids and siRNAs used in the study with corresponding measured parameters and analytical techniques are given in Table 4-1.

Table 4-1: A summary of the plasmids and siRNA duplexes, measured parameters and analytical methods used in the transfection experiments in Paper I-III.

pDNA	Measured parameter post-transfection	Analytical method	Paper
Cy3 labeled	pDNA uptake	CLSM	I
GFP encoding	GFP expression, number of GFP positive cells	FC	I
Luciferase encoding	Luciferase expression	Luminometry	I
YOYO-1 labeled	pDNA uptake, number of YOYO-1 positive cells	FC	I

siRNA	Measured parameter post-transfection	Analytical method	Paper
Alexa-647 labeled	siRNA uptake, number of Alexa-647 positive cells	FC, CLSM	II, III
EGFP targeting	EGFP silencing, number of EGFP positive cells	FC, CLSM	II
GAPDH targeting	Reduction in mRNA levels and protein activity	qRT-PCR, KDalert	II, III
NT	Non-specific effects, nanoparticle toxicity	FC, CLSM, qRT-PCR, KDalert	II, III
P-gp targeting	Reduction in mRNA levels and protein function	qRT-PCR, FC, CLSM	III

Alexa-647: Alexa Fluor 647, CLSM: Confocal laser scanning microscopy, FC: Flow cytometry,
KDalert: KDalert GAPDH knockdown assay kit, NT: Non-targeting, qRT-PCR: Quantitative real-time RT-PCR.

5. Results and discussion

The initial investigations to be presented in this thesis aimed to characterize chitosan molecular and formulation properties, e.g. chain length, chain architecture, F_A or N/P favoring efficient gene delivery (Paper I) or silencing (Paper II). Nanoparticles selected on the basis of the results in Paper II were utilized to silence the drug efflux pump P-gp in rat brain endothelial cells, to improve drug delivery across the BBB (Paper III). This section highlights the main findings addressing the aims of this study. For further details, the reader is referred to the attached papers.

5.1 Self-branching of chitosans for improved pDNA delivery (Paper I)

Previous studies have illustrated that chitosan mediated pDNA delivery can be optimized by balancing parameters affecting the nanoparticle stability and kinetics of intracellular dissociation[95,97,106]. The interest in branched chitosan architectures was initiated by a recent study wherein self-branching was used as a tool to increase the colloidal stability of nanoparticles formed with AAM-substituted chitosans[77]. The resulting SBTCO was shown to possess higher solubility at pH>7, less aggregation in PBS and it mediated higher transgene expression than linear chitosans in HEK293 cells[77]. Consequently, a systematic investigation of the pDNA delivery efficiency of branched chitosans was initiated to identify structures with high gene transfer potential and to explain the mechanism behind their improved performance.

5.1.1 Transgene expression

The transfection efficiencies of the self-branched chitosans were found to depend on the molecular size (Figure 2 in Paper I). Furthermore, the highest transgene expression in the HeLa cells was obtained using formulations with a certain combination of MW and N/P. As the MW and N/P determine the physical stability of chitosan based nanoparticles[95,97,105], the structure-activity relationship observed can be explained in terms of a balance between nanoparticle stability and dissociation. The efficient gene transfer mediated by nanoparticles with SB or SBTCO with M_w 20-30 kDa indicates that these possess optimal stability with protection of the nucleic acids, but also allow intracellular dissociation and expression of pDNA. Increasing the MW of the chitosan generally lead to more stable particles[97,102] that may dissociate too slowly and reside in lysosomes[106]. Also, reducing the N/P have been shown to reduce the stability of pDNA-chitosan nanoparticles[77,97,102,115]. Thus, to maintain transgene expression the nanoparticles assembled with higher MW chitosans must be destabilized by using a lower N/P and vice versa. Nanoparticles falling outside the optimal stability window are likely to possess interaction strengths that are too high or too low between the chitosan and pDNA. For the AAM-substituted SBTCO chitosans in this study, the range of optimal stability was shifted towards higher N/P and higher MW. This was likely a consequence of the trimer substitution, which previously has shown to reduce the physical stability of pDNA-chitosan nanoparticles[77,97,116]. The rationale behind the impaired stability is probably a combination of reduced charge density and steric hindrance of pDNA interactions from the AAM-substitutions[97].

Previously, it has been indicated that HeLa cells are difficult to transfect with conventional linear chitosans[102,115]. The discovery that self-branched, but not linear, chitosans efficiently transfected HeLa cells (Figure 1 in Paper I) was surprising and

demonstrated that the molecular architecture of chitosan can be crucial for the pDNA delivery efficiency. Thus, direct comparison of nanoparticles based on chitosans derived from a linear chitosan with a M_w of 10 kDa was performed to characterize possible mechanisms explaining their differing pDNA delivery efficiencies.

The combination of self-branching and substitution of the linear chitosan (SBTCO) resulted in high transfection efficiency, exceeding that of the tested commercial transfection reagents Exgen and Lipofectamine 2000, as shown from the luciferase analysis in Figure 5-1.

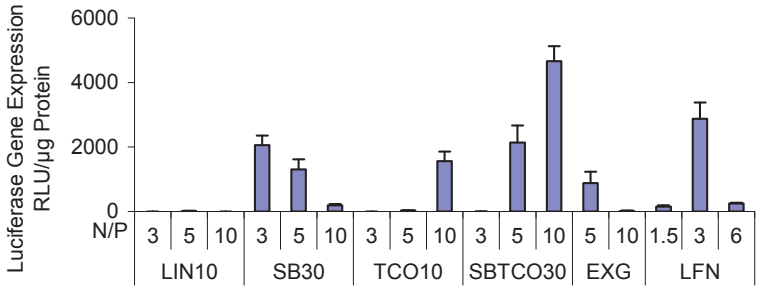

Figure 5-1: Effect of self-branching and glycosylation on the gene delivery efficiency of chitosan in HeLa cells. Self-branched (SB), trisaccharide substituted (TCO), or self-branched trisaccharide substituted (SBTCO) chitosans were derived from linear chitosan (LIN) with a M_w of 10 kDa. Luciferase gene expression was measured 24 h after transfection using pDNA-chitosan nanoparticles prepared at N/P 3-10. The commercial transfection reagents Exgen (EXG) and Lipofectamine 2000 (LFN) were also included. SBTCO30 at N/P 10 yielded significantly higher ($p<0.05$) luciferase gene expression compared with all other formulations. The number used in the chitosan notation is the measured M_w. Data represent mean values ± s.d., n=4.

5.1.2 Nanoparticle uptake and aggregation kinetics

The results from flow cytometry analysis of fluorescent labeled pDNA uptake mediated by the linear chitosan derived nanoparticles are shown in Figure 5-2. To distinguish between internalized and cell surface bound nanoparticles, cells were analyzed before and after incubation with trypan blue (TB) used as a quencher of extracellular fluorescence.

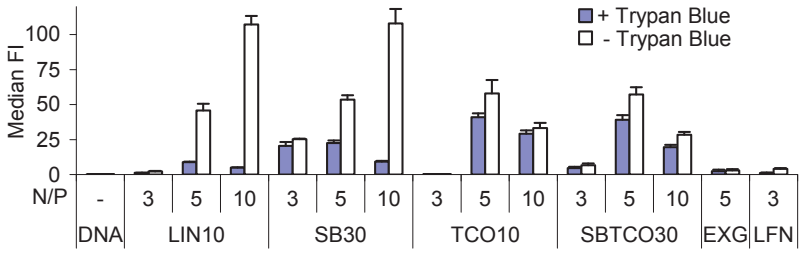

Figure 5-2: Cellular uptake of pDNA-chitosan nanoparticles in HeLa cells. The measurements are presented as the relative amount of internalized pDNA expressed as median fluorescence intensity (FI) of the YOYO-1-positive cells. To distinguish between cell surface-bound and internalized nanoparticles, the cells were quenched with trypan blue (TB). Blue bars show measurements after TB treatment (corresponding to internalized pDNA), whereas white bars show the measurements in the absence of TB (surface-bound and internalized pDNA). The cells were analyzed 3 h after transfection. The number used in the chitosan notation is the measured M_w. Data represent mean values ± s.d., n=4.

Although almost all cells internalized some amount of nanoparticles (Figure 4A in Paper I), the flow cytometry analysis revealed large differences in the relative amount of cell surface bound (without quenching) and internalized pDNA (quenching with TB) among the different formulations. The amount of pDNA delivered intracellularly by LIN formulations was considerably lower compared to the other chitosans, and may thus be a reason for its poor transfection efficiency. Indeed, most chitosan formulations showing poor cellular uptake also mediated poor transfection. Formulations with TCO or SBTCO at higher N/P seem to have reduced amounts of internalized pDNA, but higher levels of transgene expression. This indicates better intracellular protective capabilities and/or dissociation kinetics. Furthermore, cells treated with the commercial transfection reagents exhibited very low uptake of pDNA, with levels comparable to the LIN formulations, but they showed quite high levels of transgene expression. Therefore, the relationship between the amount of internalized pDNA and the amount of transgene produced seems to be strongly dependent on the delivery system. This indicates that the tested commercial reagents based on PEI and cationic lipids mediate more efficient intracellular processing of the internalized pDNA, which has also been suggested elsewhere[237-239].

The differences in transfection efficiency of the chitosans cannot solely be explained by relative differences in the cellular uptake levels of the nanoparticles, as some of the formulations mediated similar uptake but different transgene expression. The lack of transgene expression using the linear chitosans may be related to poor uptake or poor intracellular trafficking. As reported previously, the nanoparticles of LIN, TCO and SBTCO possessed similar sizes and properties[77,89]. However, the nanoparticles of TCO and SBTCO have been shown to be less prone to aggregation at physiological pH values in PBS[77]. Despite aggregating, the linear chitosans have previously shown to mediate high pDNA uptake levels and to transfect HEK293 cells[95,97]. This illustrates cell line-specific differences related to the uptake and cellular processing of the different particles, as previously reported for pDNA-PEI nanoparticles[240]. HeLa cells may be unable to take up larger aggregates or alternatively, different endocytic mechanisms may be involved in the uptake and intracellular trafficking of different types of nanoparticles. These differences may also be due to a different occurrence of nucleases or chitosan-degrading enzymes in the endosomes, making molecular properties affecting the intracellular processing more important in certain cell lines.

An extensive binding of LIN and SB nanoparticles to the cell surface was observed in the nanoparticle uptake experiments as shown in Figure 5-2. This binding seemed to increase with the N/P and was accompanied by a decreasing amount of internalized pDNA. This may be a consequence of the increasing amounts of free chitosan in the formulations, which competes for cell surface binding via electrostatic interactions. It has previously been shown that at N/P 10, 50–70% of the chitosan is unbound to pDNA[89]. Despite possibly reducing the uptake of pDNA-chitosan nanoparticles, the occurrence of free chitosan appears to be important for efficient transfection[84,96,114]. This has been linked to facilitation of particle release from the lysosomes[114]. Regarding *in vivo* applications of the pDNA-chitosan nanoparticles, the need for unbound chitosan to obtain efficient transfection can be difficult to fulfill as the free fraction may not follow the particles e.g. in the blood stream.

The dynamic light scattering analysis of the formulations performed at transfection conditions, quantitatively confirmed the severe aggregation of nanoparticles based on LIN and SB chitosans, as shown in Figure 5-3A.

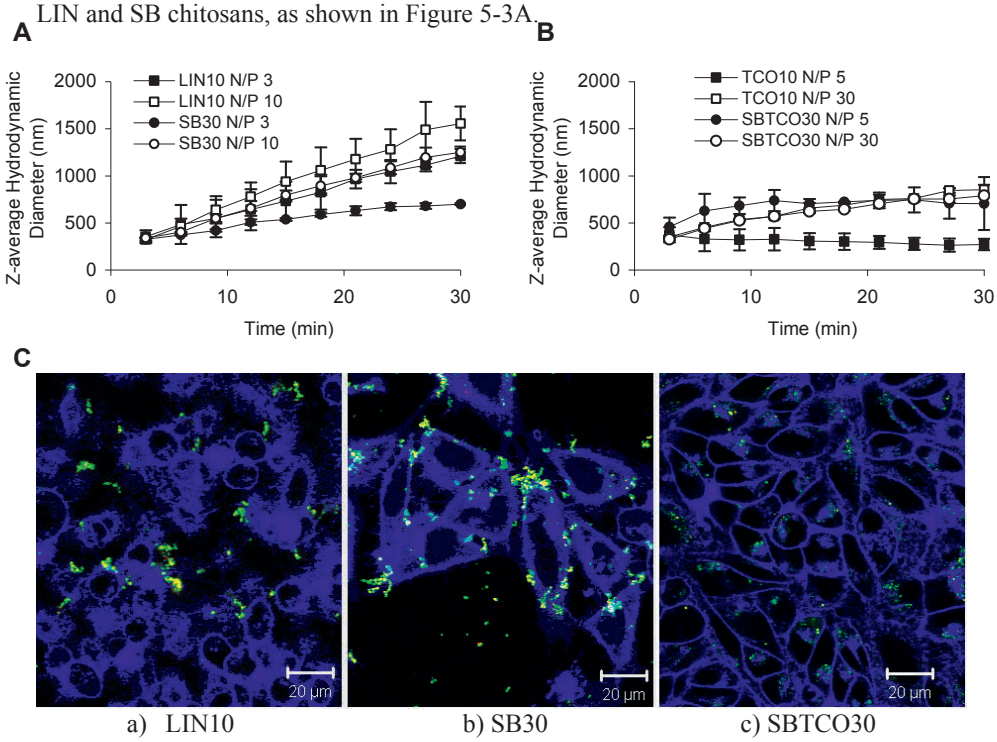

Figure 5-3: Aggregation of pDNA-chitosan nanoparticles. A) Aggregation of nanoparticles formed with unsubstituted chitosans LIN10 and SB30 at N/P 3-10. B) Aggregation of nanoparticles formed with the substituted chitosans TCO10 and SBTCO30 at N/P 5-30. The z-average hydrodynamic diameter of the particles was measured after diluting the samples with an equal volume of CO_2-saturated hypertonic Opti-MEM to obtain isotonic formulations with a pH of 7.2 and an osmolarity of 300 mOsm/kg. Data represent mean values ± s.d., n=3. C) Representative CLSM images of HeLa cells incubated for 2 h with nanoparticles of a) LIN10, b) SB30, or c) SBTCO30 at N/P 5. The chitosans were labeled with Alexa Fluor 488 (green), pDNA was labeled with YOYO-1 (red), and the cellular plasma membrane was stained with CellMask (blue). The number used in the chitosan notation is the measured M_w. The bar size is 20 µm.

Apparently, the aggregating formulations made from unsubstituted chitosans (LIN and SB) sediment on and bind to cell surfaces, as also confirmed by the CLSM imaging as shown in Figure 5-3C. In contrast, as shown in Figure 5-3B and C, the nanoparticles based on SBTCO with increased colloidal stability were intracellularly located.

The internalization of large aggregates is clearly limited and leads to accumulation of aggregated nanoparticles and free chitosan. Interestingly, there was no straightforward correlation between the extent of nanoparticle aggregation and the pDNA delivery efficiency. The most colloidal stable formulations, SBTCO with M_w 70 kDa at N/P 30 (Figure 5B in Paper I), and TCO with M_w 10 at N/P 5 (Figure 5-3B), mediated poor transfection. On the other hand, the aggregating formulations of SBTCO with M_w 30 kDa

were far more efficient (Figure 2 in Paper I). This indicates that colloidal stability of the nanoparticles itself does not guarantee successful gene transfer. Possibly, the pDNA transported by the colloidal stable particles from TCO with M_w 10 at N/P 5 that showed efficient uptake but no transgene expression, was easily degraded by intracellular nucleases. In contrast, the stable nanoparticles obtained from SBTCO with M_w 70 at N/P 30 did possibly not dissociate after internalization. However, a high degree of aggregation does seem to correlate with poor transgene expression. For instance, the formulations with the most severe aggregation, i.e. LIN with M_w 10 kDa at N/P 3 or 10 and SB with M_w 30 kDa at N/P 10, failed to transfect the HeLa cells. In contrast, the nanoparticles assembled from SB with M_w 30 kDa at N/P 3 and SBTCO with M_w 30 at N/P 30 that had lower degrees of aggregation were able to mediate the most efficient transfections.

These results illustrate a need for strategies to increase the colloidal stability of pDNA-chitosan nanoparticles without negatively influencing the physical stability and cellular uptake. Such strategies could include grafting of chitosan with PEG, which has been previously shown to increase the nanoparticle solubility and prevent aggregation in physiological fluids[140,141,241]. Alternatively, the net positive charge of chitosan based nanoparticles could be neutralized with hyaluronic acid[142] to reduce the interactions with negatively charged components.

5.1.3 Cytotoxicity

The chitosan-based nanoparticles were based solely on chitosan and no other synthetic components, thereby maintaining the high safety profile of chitosan. Analysis of post-transfection cellular metabolic activity and morphological observation of the nanoparticle treated cells confirmed the low toxicity of chitosan (Figure 6 in Paper I), despite the changes in molecular architecture from linear to self-branched chains. The result correlates well with many previous studies, implying that chitosan is a safe nonviral delivery vehicle for potential use in gene therapy *in vivo*[77,105,111,119,139-141].

5.2 Molecular optimization of chitosan for siRNA delivery (Paper II)

Most siRNA delivery studies have been performed with conventional partially *N*-acetylated linear chitosans[108-110,242]. These studies have typically depended on high siRNA doses and N/P values to obtain efficient knockdown of the target gene. To rationalize the use of chitosans as siRNA delivery vehicles, this study was initiated to identify fundamental molecular properties favoring efficient silencing of genes in mammalian cells.

*5.2.1 Effect of the degree of de-*N*-acetylation and chain architecture*

The maximum charge density obtained by fully de-*N*-acetylation of chitosan appears crucial to obtain high knockdown efficiencies. This is illustrated by the flow cytometry analysis of EGFP fluorescence shown in Figure 5-4A and B. The partially *N*-acetylated chitosan with F_A 0.15 and the AAM-substituted SBTCO that contains uncharged GlcNAc units, show lower siRNA mediated EGFP knockdown in H1299 cells compared to their fully de-*N*-acetylated counterparts LIN and SB, respectively.

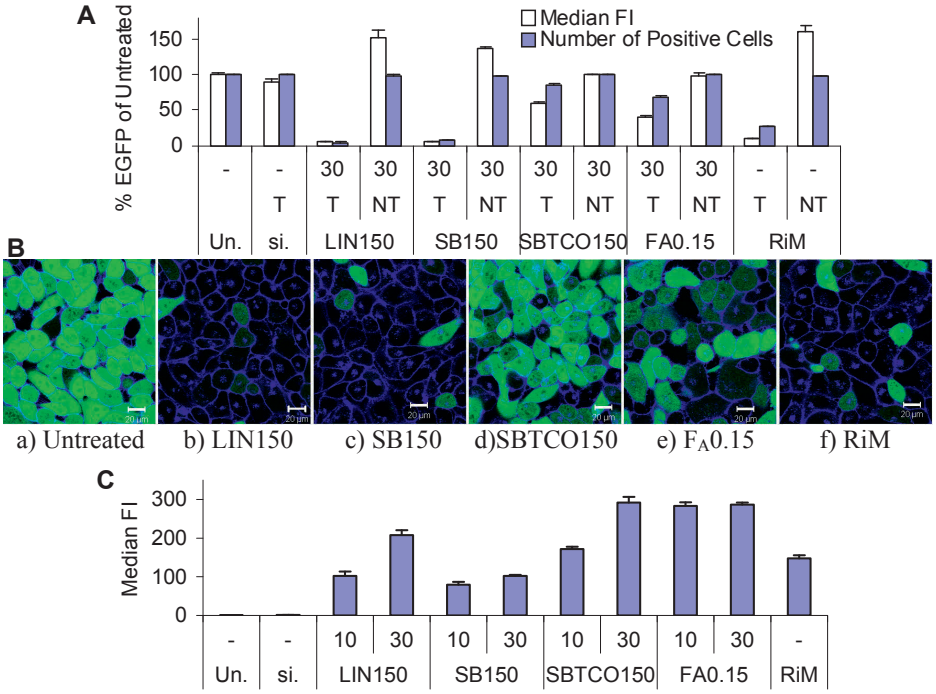

Figure 5-4: Effect of chitosan chain architecture and *N*-acetylation on siRNA delivery and knockdown of EGFP in H1299 cells. A) Knockdown of EGFP measured as the median FI or the number of EGFP positive cells relative to untreated cells (Un.) 48 h after transfection with anti-EGFP (targeting, T) or non-targeting (NT) siRNA. B) Representative CLSM images of a) untreated H1299 cells, 48 h after transfection with b) LIN150, c) SB150, d) SBTCO150, e) F_A0.15 at N/P 30, or f) RNAiMAX (RiM). The cellular plasma membrane was stained with CellMask (blue) and EGFP is indicated with the green colour. The bar size is 20 µm. C) Relative amount of internalized Alexa-647 conjugated siRNA expressed as the median fluorescence intensity (FI) of the Alexa-647 positive cells. The cells were analyzed 4 h after transfection. The number used in the chitosan notation is the measured DP_n. The siRNA was delivered at a concentration of 90 nM. Data represent mean values ± s.d., n=3.

Results from the flow cytometry analysis of internalized fluorescent siRNA are shown in Figure 5-4C. Interestingly, despite lower knockdown efficiencies, the SBTCO and partially *N*-acetylated chitosan showed better cellular uptake of siRNA. This observation indicates that the chitosans are able to form stable nanoparticles with siRNA that are internalized, but their intracellular protection and/or cellular processing seem less efficient than that for the LIN and SB chitosans. This can be compared to the results from the substituted chitosan (TCO10 at N/P 5) shown in Figure 5-2 that showed high pDNA uptake, however, the transfection efficiency was minimal (Figure 5-1). Possibly, the acetylated chitosans release siRNA in the endo/lysosomal compartments, as earlier reported for chitosan mediated pDNA delivery[106], which results in rapid degradation. Indeed, a previous study have shown that siRNA-chitosan nanoparticles are destabilized when increasing the F_A[84], suggesting that the nucleic acids could more easily be degraded after uptake. The lower density of protonable amino groups may also render the chitosans less efficient in escaping the endosomes, due to reduced buffering capacity and ability to mediate endosomal rupture[105].

5.2.2 Effect of the chain length of linear chitosans

Based on the initial experiments showing that fully de-*N*-acetylated linear chitosans mediate efficient siRNA delivery and gene silencing, the effect of the chain length, i.e. the size (MW/DP), was investigated as shown in Figure 5-5.

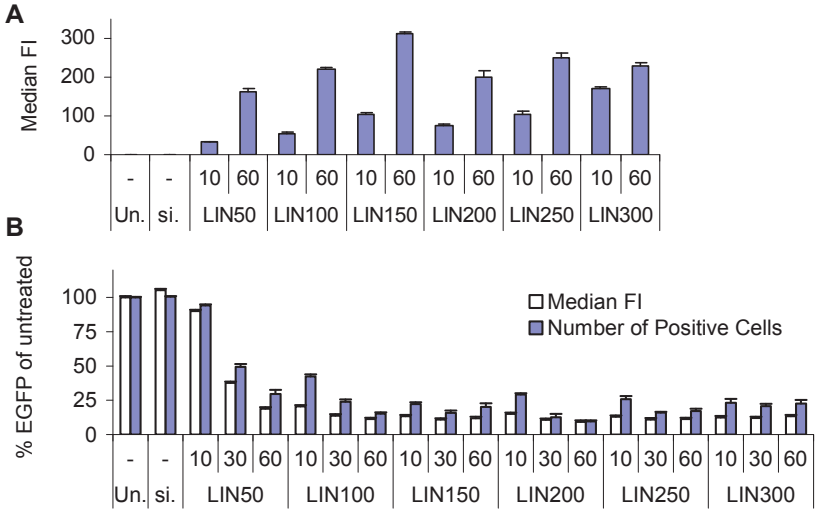

Figure 5-5: Effect of chain length and N/P on siRNA uptake and EGFP knockdown efficiency in H1299 cells, using fully de-*N*-acetylated linear chitosans. A) Relative amount of internalized Alexa-647 conjugated siRNA expressed as median FI of the Alexa-647 positive cells. The cells were analyzed 4 h after transfection. B) Knockdown of EGFP measured as the median FI or the number of EGFP positive cells relative to untreated cells (Un.) 48 h after transfection with anti-EGFP siRNA. The number used in the chitosan notation is the measured DP_n. The siRNA was delivered at a concentration of 45 nM. Data represent mean values ± s.d., n=3.

As shown by flow cytometry analysis of the siRNA uptake and EGFP knockdown, the siRNA delivery appears relatively unaffected by the chitosan chain length, particularly

for chitosans equal to and above DP_n 100 (M_w 35 kDa). When compared to other studies using N/P in the range of 50-150[84,108-110], the fully de-*N*-acetylated chitosan nanoparticles reach maximum knockdown efficiency at relatively low N/P values such as N/P 10. Only the knockdown efficiency of LIN with DP_n 50, and partially with DP_n 100, increased with the N/P, suggesting that some of the chains in the polydisperse sample with average DP_n 50 (PDI 1.52) are able to form stable complexes with siRNA. This is in agreement with the results for pDNA delivery where an increase in N/P could compensate for low MW (Paper I). The possibility of compensating for the lower DP_n of chitosans by increasing their N/P is generally not considered an optimal strategy, as higher N/P imply a large excess of free chitosans that can bind to the cell surface (as shown for pDNA delivery in Figure 5-2), increase the potential for unspecific interactions and complicate the use of the nanoparticles *in vivo*. Therefore, chitosan nanoparticles with low N/P are highly beneficial. A plausible explanation for the low N/P needed is that the fully de-*N*-acetylated chitosans are able to bind siRNA more tightly, thereby reducing the need for excess chitosan.

A significant knockdown of EGFP was achieved at a siRNA concentration as low as 15 nM (Figure 3 in Paper II), and the maximum gene knockdown was reached at 45 nM where the knockdown was found to have duration of at least five days (Figure 4 in Paper II). Compared to other studies on polycation mediated siRNA delivery, concentrations in the range of 50–200 nM have typically been used to obtain efficient gene silencing, with the majority of studies in the upper concentration range of 100-200 nM[108-110,159,242,243]. Similar knockdown efficiencies were also obtained for HEK293 (unpublished data), HeLa (unpublished data) and primary HUVEC cells, in addition to MCF-7 cells (Figure 5 in Paper II) that have previously proved difficult to transfect. This demonstrates that the chitosans used in this study could be used as efficient delivery vehicles for siRNA in a broad range of cell lines.

5.2.3 Side effects from transfection

Off-target effects of siRNA, toxicity of the carrier and other non-specific effects have repeatedly been lifted as serious concerns in the field of siRNA delivery[244-246]. Some examples of siRNA mediated side effects are induction of the interferon response, unspecific intracellular interactions between the material of the delivery vehicle and endogenous proteins or nucleic acids, but also possible effects on the global gene expression as a consequence of silencing the target gene[244,246-248]. There is also the possibility of unspecific binding of siRNA to mRNA and thereby translational repression of genes not intended to be affected by the delivered siRNA. Furthermore, it has been suggested that transfection with siRNA can saturate components in the RNAi machinery such as RISC, and thereby lead to non-specific effects by perturbing the endogenous function of RNAi[247]. Therefore, in all experiments, appropriate non-targeting (NT) siRNA have been used as negative control to distinguish non-sequence specific effects. Furthermore, mock transfections with chitosan only were also performed. The analysis of EGFP expression presented in Figure 5-6A shows that the delivery of NT siRNA in some cases increased the cellular protein levels whereas the naked chitosan in mock transfections (M) mediated a decrease in EGFP of approximately 10%.

In contrast to EGFP, the levels of GAPDH mRNA or protein activity did not seem to be affected by delivery of NT siRNA or the mock transfection (Figure 4A in Paper II). This indicates that the off-target effects influence random genes and not the global gene expression in treated cells. Chitosan released from nanoparticles after their dissociation may also possibly bind to EGFP and reduce its turnover rate. The extent of increased EGFP seems to be more pronounced for chitosans of mid-range DP_n around 100–250. Interestingly, as shown by the flow cytometry analysis in Figure 5-6B, mock transfections performed at increased chitosan concentrations of 3.5, 35 and 70 μg/mL (corresponding to N/P 10, 100, and 200) in a time course of 1–3 days show 75–100% EGFP compared to the untreated cells. However, the decrease seems to be random with respect to the chitosan concentration and is most prominent two days after transfection.

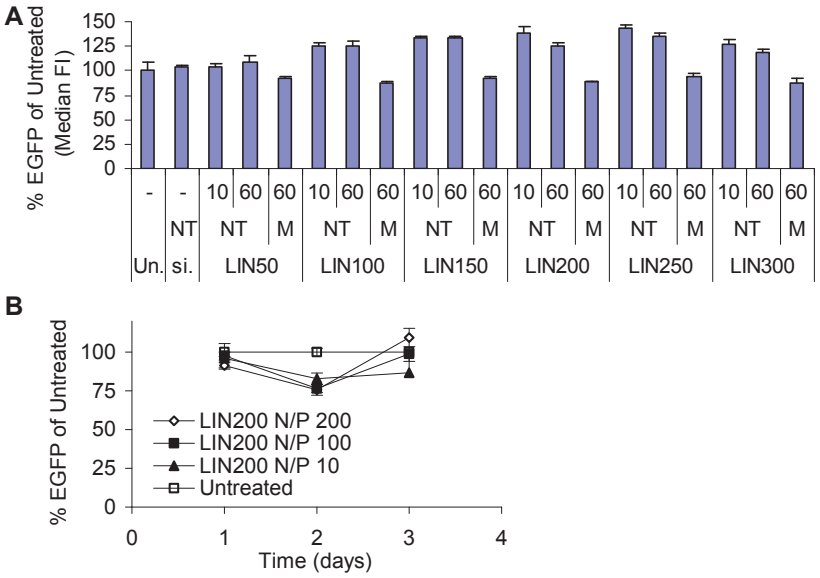

Figure 5-6: The effect of chitosan and siRNA-chitosan nanoparticles on EGFP expression. A) The effect on EGFP expression from mock transfection (M) or transfection with non-targeting (NT) siRNA. siRNA was delivered at a concentration of 45 nM. B) The effect of chitosan concentration (N/P) on EGFP expression in H1299 cells measured over three days, using a fully de-*N*-acetylated linear chitosan with DP_n 200. The effect is measured as the median FI from EGFP relative to untreated cells after mock transfection with chitosan only. The number used in the chitosan notation is the measured DP_n. Data represent mean values ± s.d., n=3.

The siRNA-chitosan nanoparticles showed minimal cytotoxicity as assessed by the analysis of metabolic activity and membrane integrity (Figure 6 in Paper II). Similar as mentioned earlier for pDNA delivery, the low toxicity of chitosan is in agreement with previous studies that recognize different types of siRNA-chitosan nanoparticles as safe delivery reagents[110,118,242]. The optimization of the nucleic acid carrier allows reduction of the siRNA dose and N/P, thereby reducing the probability of deleterious side effects.

5.3 Chitosan mediated pDNA vs. siRNA delivery (Paper I and II)

The gene silencing was efficient when using nanoparticles assembled from linear fully-de-*N*-acetylated chitosans with DP_n>50 and N/P>10. This observation is in contrast to the pDNA delivery, where the efficiency of gene transfer had a critical dependency on the chitosan molecular size and N/P. A balance have previously been implicated between the nanoparticle stability and its ability to undergo intracellular dissociation; the kinetics of the intracellular dissociation can be optimized by combining the proper size and N/P values[97]. Since the length of pDNA (typically several kbp) largely exceeds that of siRNA, pDNA molecules are able to form multiple inter-chain bridges with chitosan molecules, and the electrostatic interactions between pDNA and chitosan are thus much stronger. Therefore, by using short chitosan chains (low MW/DP), the interaction strength between pDNA and chitosan may be reduced, promoting intracellular dissociation. Short siRNA duplexes on the other hand have substantially weaker interaction with chitosan and this limits the stability of the nanoparticles. Therefore, above a certain DP_n the stability of the nanoparticles will not depend on the chitosan chain length. This is in agreement with the results presented in this thesis, showing that chitosans below DP_n 100 mediate weak siRNA uptake and knockdown, probably due to insufficient stability of the nanoparticles. This is also in agreement with results reported by Liu et al.[84], where a chitosan of approximately DP_n 50 and F_A 0.05 has been shown to form unstable nanoparticles at N/P 50 mediating poor gene silencing[84]. This stability hypothesis is supported by observations showing that pDNA compared to siRNA seem to form more stable nanoparticles at lower N/P values[84,97]. Increasing the N/P can further increase the stability of the nanoparticles, and this can prevent intracellular release. Hence, the pDNA nanoparticles have a lower critical N/P compared to siRNA, where no upper limit was detected in the range of N/P values tested herein.

Both gene delivery and silencing could be performed with the SB chitosans. The SBTCO on the other hand was only able to mediate efficient gene delivery. This is probably caused by the reduced charge density and steric hindrance from the AAM-substitution, preventing proper association of the chitosan and siRNA, but not the long pDNA molecules. However, the SBTCO was able to efficiently silence genes with siRNA in HeLa cells (unpublished results). For any conclusion to be drawn from the direct comparison of the siRNA and pDNA investigations, the delivery should have been performed in the same cell line.

The effects of chitosan chain length, chain architecture, F_A and N/P of formulation on nucleic acid delivery is summarized in Table 5-1.

Table 5-1: Overview of the effects of chitosan molecular and formulation parameters on the nucleic acid delivery.

Chitosan parameter	Optimal for pDNA delivery in HeLa cells	Optimal for siRNA delivery in H1299 cells
Size (MW/DP)	Optimal window depending on the chain architecture. Typically M_w 10-40 kDa.	DP_n>50 (M_w>16 kDa)
Chain architecture	TCO, SB and SBTCO perform well	LIN and SB perform well
F_A	Low F_A increases the efficiency	Low F_A increases the efficiency
N/P	Optimal window depending on the size. Typically N/P 3-30.	N/P>10

5.4 siRNA-chitosan mediated P-gp silencing in a blood-brain barrier model (Paper III)

The xenobiotic efflux pump P-gp is expressed in cells at anatomical and physiological barriers in mammalian tissues and in malignant cells[208-213]. Several of the identified P-gp substrates are drugs, and thus a considerable research effort has focused on finding ways to overcome drug efflux from P-gp expressing cells. Temporarily silencing of the P-gp gene by RNAi is a possible way to inhibit the efflux. Previously, this approach has been applied to overcome drug resistance in cancer cells by improving the delivery and efficacy of chemotherapeutic agents[214-216,249]. Recently, a preliminary study showed reduction in P-gp expression in brain endothelial cells *in vivo* by repeated hydrodynamic injections of naked siRNA intravenously in mice[236], but extremely high doses of siRNA were used in this study. The delivery of siRNA with nanoparticles may represent a more rational approach as the nanoparticles will protect the siRNA from degradation and facilitate the uptake, thereby allowing the use of lower doses.

5.4.1 P-gp silencing in rat brain endothelial cells

A fully de-*N*-acetylated linear chitosan with a DP_n of approximately 400 was selected as siRNA delivery vehicle on the basis of the results presented in Paper II. This chitosan mediated efficient uptake of siRNA into the RBE4 cells (Figure 1 in Paper III). As shown in Figure 5-7, the delivery of anti-P-gp siRNA resulted in efficient silencing of the P-gp expression with a reduction in mRNA levels of approximately 80% compared to the untreated cells.

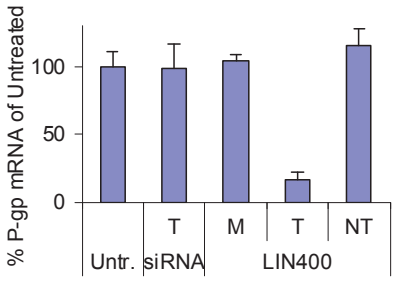

Figure 5-7: Knockdown of P-gp in RBE4 cells measured at mRNA level by qRT-PCR. The cells were transfected with only chitosan (mock, M) or nanoparticles having N/P 30 and P-gp targeting (T) or non-targeting (NT) siRNA at 100 nM. Cells were also treated with naked siRNA (siRNA). The number used in the chitosan notation is the measured DP_n. Data represents mean values ± s.d., n=3.

Despite measuring similar concentration of nanoparticles in the formulations (Figure 2 in Paper III), the degree of nanoparticle uptake decreased at increasing N/P (Figure 1 in Paper III). This indicates that the higher the N/P, the higher is the excess of chitosan in the formulation. The excess of unbound chitosan at higher N/P values may inhibit the uptake of siRNA by binding to cellular surfaces and preventing the attachment of siRNA-chitosan nanoparticles. This is similar as earlier mentioned for the pDNA delivery (Figure 5-2).

5.4.2 The effect of P-gp silencing on substrate efflux, drug delivery and efficacy

Functional activity of the P-gp efflux pump was evaluated using a rhodamine 123 (R123) efflux assay (Figure 5 in Paper III). The concentration-response analysis showed a considerably lower R123 efflux as the concentration of anti-P-gp siRNA increased from 10 to 100 nM. A concentration of 45 nM siRNA was shown sufficient for gene silencing in a number of cell lines when using fully de-*N*-acetylated chitosans as delivery vehicles (Paper II). However, this may depend on the cell line and the expression of the target gene. The P-gp gene is known to be relatively weakly expressed in the RBE4 cell line[230] and this was confirmed by qRT-PCR in this study (unpublished data). Silencing a weakly expressed gene could require a higher delivered dose of siRNA before the effect is observed due to strong regulation and low availability of target mRNA[250,251]. This was supported by experiments with transfection of C6 cells with even weaker expression of P-gp compared to the RBE4 cells (unpublished results). In this case, efficient silencing of P-gp was not achieved despite promising preliminary GAPDH silencing experiments at low siRNA concentrations. Furthermore, the knockdown kinetics (Figure 5 in Paper III) show that the reduced P-gp mediated efflux lasted only from one to four days post-transfection. Such short duration of P-gp knockdown has also been observed in other studies with different cancer cell lines, where the protein expression was shown to reach its lowest levels one to two days after transfection, and recovered after two to three days[215,216]. A short duration of P-gp knockdown is beneficial since it allows rapid reestablishment of the protective function of the BBB after drug therapy. However, it was shown that if necessary, it is possible to further reduce the substrate efflux and increase the duration of knockdown by repeated transfections (unpublished results).

The reduction in P-gp mediated efflux following successful siRNA transfection improved the delivery and considerably increased the efficacy of doxorubicin (Figure 5-8). Doxorubicin is a DNA intercalating cytostatic used as a model drug in this study. As shown from the metabolic activity assay in Figure 5-8A, cells with silenced P-gp were considerably more sensitive to doxorubicin, even at doxorubicin concentrations as low as 0.5 μM. The efficacy of doxorubicin treatment was even higher at 1 μM, where up to 60% reduction in metabolic activity was observed compared to untreated cells with normal P-gp expression.

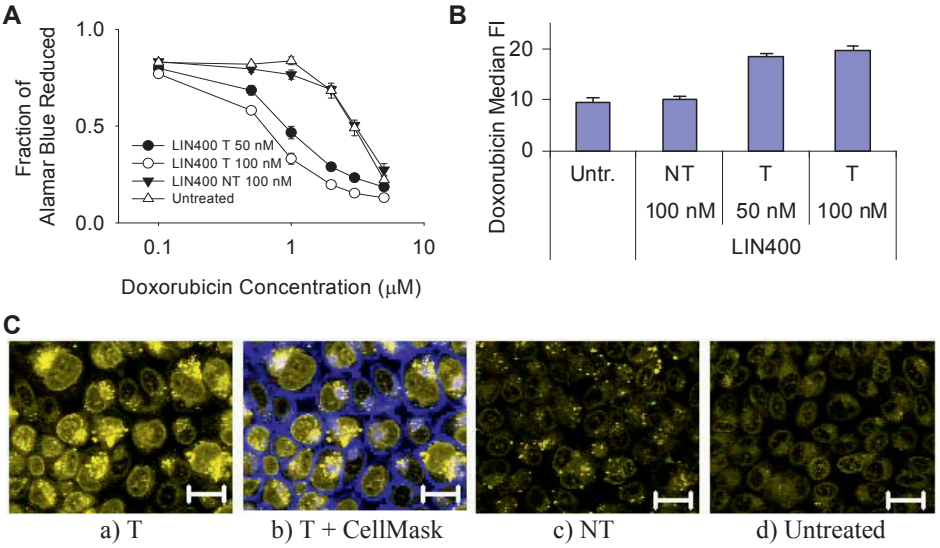

Figure 5-8: The effect of P-gp knockdown on doxorubicin efficacy and delivery. A) Drug efficacy measured as the reduced metabolic activity after 48 h incubation with doxorubicin in untreated or transfected cells. The cells were transfected with LIN400 nanoparticles at N/P 30 with P-gp targeting (T) or non-targeting (NT) siRNA concentrations of 50 or 100 nM. Data represents mean values ± s.d., n=4. B) Levels of intracellular doxorubicin expressed as the median FI of the cells. Data represents mean values ± s.d., n=3. D) Representative CLSM images after transfection with a, b) T or c) NT siRNA or d) untreated cells. The cellular plasma membranes in b) were stained with CellMask (blue) and doxorubicin fluorescence is indicated with the green color. siRNA was delivered at a concentration of 100 nM. The number used in the chitosan notation is the measured DP_n. The bar size is 20 μm.

As shown by the flow cytometry (Figure 5-8B) and CLSM (Figure 5-8C) analysis, doxorubicin was located intracellularly both in transfected and non-transfected cells. However, the measured doxorubicin fluorescence intensities were doubled in cells transfected with anti-P-gp siRNA as compared to the untreated or NT transfected cells. Furthermore, the drug was only able to intercalate with DNA in the nucleus after P-gp knockdown. This suggests that P-gp is located both at the cellular membrane (as indicated by the R123 experiments) and at the nuclear envelope. Indeed, the expression and localization of P-gp in RBE4 cells have previously been confirmed at both sites[252]. Furthermore, doxorubicin has been shown to depend on P-gp silencing for delivery to the nucleus of the multi-drug resistant cell line KB-V1[214]. This illustrates that an improved delivery of drugs does not necessarily enhance their efficacy as efflux pumps still can prevent them from reaching their final destination, such as the nucleus in the case of doxorubicin. Similarly, the dose of drugs needed to obtain a therapeutic window could be considerably reduced if a larger fraction reaches its target. This in turn will reduce potential deleterious side effects from the drug.

One obvious limitation of using a two-dimensional *in vitro* model to represent the BBB is the lack of a brain interstitium, basal membrane, astrocytes and pericytes. The drugs targeting the brain need to cross the layer of endothelial cells and not accumulate inside

the capillaries. However, if a drug reaches higher levels in the cytoplasm of the brain endothelial cells more of it is expected to enter the brain. Even if a drug is able to cross the endothelial cells it can still be prevented from further transport, or even be effluxed back to the blood because of efflux pumps in the astrocyte end-feet ensheating the capillaries. Thus, the nanoparticles should also penetrate the BBB and transfect cells in the brain to even further increase the drug delivery and efficacy. This probably requires labeling of the nanoparticles with ligands targeting receptors expressed by brain endothelial cells or receptor antibodies facilitating transcytosis. This has previously been performed with drug-loaded liposomes labeled with insulin[253] and transferrin[254] receptor antibodies. Receptor-binding nanoparticles also have the benefit of promoting a targeted delivery with reduced uptake by irrelevant cells.

Another crucial property of nanoparticles applied *in vivo* is that they must be stable in the blood when administered intravenously. There are several strategies to accomplish this, and as mentioned earlier conjugating particles with PEG or shielding the positive charge with hyaluronic acid are possible approaches to prevent nanoparticle aggregation. Both these approaches were investigated for improved siRNA delivery in this study. However, the resulting nanoparticles showing high levels of uptake appeared to have an unbalanced stability, either resulting in inefficient intracellular release or alternatively the siRNA became degraded due to weak protection from nucleases, resulting in poor gene silencing (data not shown). This is similar to the results in Paper I, where the colloidal stable pDNA-chitosan nanoparticles failed to mediate efficient transgene expression, even when internalized at high levels. Furthermore, the *N*-acetylated and substituted chitosans in Paper II were inefficient in mediating gene silencing despite high levels of siRNA uptake.

Any P-gp substrate can also be a substrate for other drug efflux pumps, e.g. R123 has been reported to be transported by Mrp1[255] which is also expressed in RBE4 cells[230]. Therefore, even though the P-gp is successfully downregulated, efflux by other pumps may still occur. In addition, P-gp is encoded by two different genes in rodents, *mdr1a* and *mdr1b*, with partly overlapping substrate specificity and efflux efficiency[228]. In this study the focus was on delivering siRNA targeting *mdr1a* as no effect was measured on R123 efflux when silencing *mdr1b* (unpublished data). Despite the possibility of having to deal with several different drug efflux pumps to improve the drug delivery, it would be simple to assemble nanoparticles with a pooled library of siRNAs targeting several different mRNA sequences.

6. Concluding remarks

The work presented in this thesis demonstrates the application of tailored chitosans in nucleic acid delivery *in vitro*. The optimized chitosans showed efficient gene delivery and silencing with minimal toxic effects, proving their potential for *in vivo* applications. The major findings in this study as presented in Paper I, II and III were:

- Self-branched chitosans can be optimized for pDNA delivery by adjusting parameters determining the physical stability of nanoparticles. The self-branched chitosans mediate better pDNA delivery efficiency compared to their linear counterparts due to their improved colloidal stability and increased uptake in HeLa cells (Paper I).

- Fully de-*N*-acetylated chitosans of DP_n>50 mediate efficient long-term gene silencing at low N/P values and siRNA doses (Paper II).

- Silencing the P-gp gene with nanoparticles selected on basis of the results in Paper II improved the delivery of P-gp substrates and the efficacy of doxorubicin in an *in vitro* BBB model (Paper III).

7. Future studies

The *in vitro* promising siRNA-chitosan nanoparticles developed herein should be further investigated *in vivo* to realize their potential in gene therapy. In this study, initial *in vivo* experiments aiming for P-gp silencing in rat brain endothelial cells were performed. However, these experiments highlighted several challenges that need to be addressed. First, the nanoparticles should have a proper targeting molecule, e.g. ligand or antibody, directing the particles to endothelial cells in the brain to reduce the dose needed for an effect. Furthermore, the particles should be stable in serum but as emphasized they need to be able to dissociate and release siRNA intracellularly. Ideally, the nanoparticles should mediate an effect after intravenous injection in the tail vein. After successful silencing of P-gp, the penetration of P-gp substrate drugs into the brain tissue following systemic administration could be evaluated. Also, the effect on drug efficacy after P-gp knockdown *in vivo* should be characterized.

In order to develop stable ligand conjugated nanoparticles for systemic administration, further studies need to be performed *in vitro* to investigate the relationship between stability and intracellular trafficking. This can be addressed by using confocal and electron microscopy techniques, combined with evaluation of gene silencing efficiency. Stabilization of the nanoparticles can possibly be obtained by substitution with a neutral oligomer, e.g. PEG, or by shielding the net positive charge using a suitable anionic molecule. Furthermore, these approaches can be combined with a layer-by-layer design tailoring the nanoparticles with multiple functional layers for optimal performance. After the development, promising nanoparticles could be investigated for their accumulation in various tissues *in vivo* after intravenous administration to evaluate the targeting specificity.

Since siRNA and pDNA delivery seem to share some common requirements of the nucleic acid carrier molecule, strategies mediating efficient siRNA delivery *in vivo* might also very well result in efficient gene delivery with pDNA. By using different ligands, these nanoparticles could target different cells in tissues, aiming for the treatment of many diseases.

8. References

1. Pons B, Mouhoubi L, Adib A, Godzina P, Behr J-P, Zuber G. ω-Hydrazino Linear Polyethylenimine: A Monoconjugation Building Block for Nucleic Acid Delivery. *ChemBioChem* 2006;**7**:303-309.
2. Pack DW, Hoffman AS, Pun S, Stayton PS. Design and development of polymers for gene delivery. *Nature Reviews Drug Discovery* 2005;**4**:581-593.
3. Mintzer MA, Simanek EE. Nonviral Vectors for Gene Delivery. *Chemical Reviews* 2008;**109**:259-302.
4. Howard KA. Delivery of RNA interference therapeutics using polycation-based nanoparticles. *Advanced Drug Delivery Reviews* 2009;**61**:710-720.
5. Anderson W, Human gene therapy: The initial concepts, in: Bingham K (Ed.), *Gene therapy for the diseases of the lung*, Marcel Dekker Inc, New York, 1997, pp. 3-16.
6. Blaese RM, Culver KW, Miller AD, Carter CS, Fleisher T, Clerici M, et al. T Lymphocyte-Directed Gene Therapy for ADA$^-$ SCID: Initial Trial Results After 4 Years. *Science* 1995;**270**:475-480.
7. Anderson W. Human gene therapy. *Nature* 1998;**392**:25-30.
8. Venter JC, Adams MD, Myers EW, Li PW, Mural RJ, Sutton GG, et al. The Sequence of the Human Genome. *Science* 2001;**291**:1304-1351.
9. Wilhelm J A. Next-generation DNA sequencing techniques. *New Biotechnology* 2009;**25**:195-203.
10. http://www.wiley.com//legacy/wileychi/genmed/clinical/. Accessed 29.02.2012.
11. Ma G, Shimada H, Hiroshima K, Tada Y, Suzuki N, Tagawa M. Gene medicine for cancer treatment: Commercially available medicine and accumulated clinical data in China. *Drug Design , Development and Therapy* 2008;**6**:115-122.
12. Jia H. Controversial Chinese gene-therapy drug entering unfamiliar territory. *Nature Reviews Drug Discovery* 2006;**5**:269-270.
13. Pearson S, Jia H, Kandachi K. China approves first gene therapy. *Nature Biotechnology* 2004;**22**:3-4.
14. Garber K. China Approves World's First Oncolytic Virus Therapy For Cancer Treatment. *Journal of the National Cancer Institute* 2006;**98**:298-300.
15. Colosimo A, Goncz KK, Holmes AR, Kunzelmann KHP, Novelli G, Malone RW, et al. Transfer and expression of foreign genes in mammalian cells. *Biotechniques* 2000;**29**:314-331.
16. Abdallah B, Sachs L, Demeneix BA. Non-viral gene transfer: Applications in developmental biology and gene therapy. *Biology of the Cell* 1995;**85**:1-7.
17. Vigna E, Naldini L. Lentiviral vectors: excellent tools for experimental gene transfer and promising candidates for gene therapy. *The Journal of Gene Medicine* 2000;**2**:308-316.
18. Wurm FM. Production of recombinant protein therapeutics in cultivated mammalian cells. *Nature Biotechnology* 2004;**22**:1393-1398.
19. Liu MA. DNA vaccines: a review. *Journal of Internal Medicine* 2003;**253**:402-410.
20. Cheng L, Sapieha P, Kittlerova P, Hauswirth WW, Di Polo A. TrkB Gene Transfer Protects Retinal Ganglion Cells from Axotomy-Induced Death In Vivo. *The Journal of Neuroscience* 2002;**22**:3977-3986.

21. Kells AP, Fong DM, Dragunow M, During MJ, Young D, Connor B. AAV-Mediated Gene Delivery of BDNF or GDNF is Neuroprotective in a Model of Huntington Disease. *Molecular Therapy* 2004;**9**:682-688.
22. Bowman K, Sarkar R, Raut S, Leong KW. Gene transfer to hemophilia A mice via oral delivery of FVIII-chitosan nanoparticles. *Journal of Controlled Release* 2008;**132**:252-259.
23. Guoping L, Zhigang L, Bin L, Nanshan Z. Induction of Th1-Type Immune Response by Chitosan Nanoparticles Containing Plasmid DNA Encoding House Dust Mite Allergen Der p 2 for Oral Vaccination in Mice. *Cellular and Molecular Immunology* 2009;**6**:45-50.
24. Lee J, Hargest R, Wasan H, Phillips RKS. Liposome-Mediated Adenomatous Polyposis Coli Gene Therapy: A Novel Anti-Adenoma Strategy in Multiple Intestinal Neoplasia Mouse Model. *Diseases of the Colon & Rectum* 2004;**47**:2105-2113.
25. LeWitt PA, Rezai AR, Leehey MA, Ojemann SG, Flaherty AW, Eskandar EN, et al. AAV2-GAD gene therapy for advanced Parkinson's disease: a double-blind, sham-surgery controlled, randomised trial. *The Lancet Neurology* 2010;**10**:309-319.
26. Noone PG, Hohneker KW, Zhou Z, Johnson LG, Foy C, Gipson C, et al. Safety and Biological Efficacy of a Lipid-CFTR Complex for Gene Transfer in the Nasal Epithelium of Adult Patients with Cystic Fibrosis. *Molecular Therapy* 2000;**1**:105-114.
27. Sidi AA, Ohana P, Benjamin S, Shalev M, Ransom JH, Lamm D, et al. Phase I/II Marker Lesion Study of Intravesical BC-819 DNA Plasmid in H19 Over Expressing Superficial Bladder Cancer Refractory to Bacillus Calmette-Guerin. *The Journal of Urology* 2008;**180**:2379-2383.
28. Konstan MW, Davis PB, Wagene JS, Hilliard KA, Stern RC, Milgram LJH, et al. Compacted DNA Nanoparticles Administered to the Nasal Mucosa of Cystic Fibrosis Subjects Are Safe and Demonstrate Partial to Complete Cystic Fibrosis Transmembrane Regulator Reconstitution. *Human gene therapy* 2004;**15**:1255-1269.
29. Becker W, Kleinsmith L, Hardin J. *The world of the cell*: Pearson/Benjamin Cummings; 2006.
30. Hannon GJ. RNA interference. *Nature* 2002;**418**:244-251.
31. Tijsterman M, Ketting RF, Okihara KL, Sijen T, Plasterk RHA. RNA Helicase MUT-14-Dependent Gene Silencing Triggered in C. elegans by Short Antisense RNAs. *Science* 2002;**295**:694-697.
32. Fire A, Xu S, Montgomery MK, Kostas SA, Driver SE, Mello CC. Potent and specific genetic interference by double-stranded RNA in Caenorhabditis elegans. *Nature* 1998;**391**:806-811.
33. Elbashir SM, Harborth J, Lendeckel W, Yalcin A, Weber K, Tuschl T. Duplexes of 21-nucleotide RNAs mediate RNA interference in cultured mammalian cells. *Nature* 2001;**411**:494-498.
34. Song E, Lee S-K, Wang J, Ince N, Ouyang N, Min J, et al. RNA interference targeting Fas protects mice from fulminant hepatitis. *Nature Medicine* 2003;**9**:347-351.
35. Jo W. First clinical data on RNAi. *Drug discovery today* 2005;**10**:1014-1015.
36. Paddison PJ, Caudy AA, Hannon GJ. Stable suppression of gene expression by RNAi in mammalian cells. *Proceedings of the National Academy of Sciences of the United States of America* 2002;**99**:1443-1448.

37. Howard KA, Paludan SR, Behlke MA, Besenbacher F, Deleuran B, Kjems J. Chitosan/siRNA Nanoparticle-mediated TNF-α Knockdown in Peritoneal Macrophages for Anti-inflammatory Treatment in a Murine Arthritis Model. *Molecular Therapy* 2008;**17**:162-168.
38. Baigude H, McCarroll J, Yang C-s, Swain PM, Rana TM. Design and Creation of New Nanomaterials for Therapeutic RNAi. *ACS Chemical Biology* 2007;**2**:237-241.
39. Davis ME, Zuckerman JE, Choi CHJ, Seligson D, Tolcher A, Alabi CA, et al. Evidence of RNAi in humans from systemically administered siRNA via targeted nanoparticles. *Nature* 2010;**464**:1067-1070.
40. DeVincenzo J, Cehelsky JE, Alvarez R, Elbashir S, Harborth J, Toudjarska I, et al. Evaluation of the safety, tolerability and pharmacokinetics of ALN-RSV01, a novel RNAi antiviral therapeutic directed against respiratory syncytial virus (RSV). *Antiviral Research* 2008;**77**:225-231.
41. Gish RG, Satishchandran C, Young M, Pachuk C. RNA interference and its potential applications to chronic HBV treatment: results of a Phase I safety and tolerability study. *Antiviral Therapy* 2011;**16**:547-554.
42. Kaiser PK, Symons RCA, Shah SM, Quinlan EJ, Tabandeh H, Do DV, et al. RNAi-Based Treatment for Neovascular Age-Related Macular Degeneration by Sirna-027. *American Journal of Ophthalmology* 2010;**150**:33-39.e32.
43. Leachman SA, Hickerson RP, Schwartz ME, Bullough EE, Hutcherson SL, Boucher KM, et al. First-in-human Mutation-targeted siRNA Phase Ib Trial of an Inherited Skin Disorder. *Molecular Therapy* 2009;**18**:442-446.
44. Peer D, Park EJ, Morishita Y, Carman CV, Shimaoka M. Systemic Leukocyte-Directed siRNA Delivery Revealing Cyclin D1 as an Anti-Inflammatory Target. *Science* 2008;**319**:627-630.
45. Schiffelers RM, Ansari A, Xu J, Zhou Q, Tang Q, Storm G, et al. Cancer siRNA therapy by tumor selective delivery with ligand-targeted sterically stabilized nanoparticle. *Nucleic Acids Research* 2004;**32**:e149.
46. Thomas M, Lu JJ, Ge Q, Zhang C, Chen J, Klibanov AM. Full deacylation of polyethylenimine dramatically boosts its gene delivery efficiency and specificity to mouse lung. *Proceedings of the National Academy of Sciences of the United States of America* 2005;**102**:5679-5684.
47. Castanotto D, Rossi JJ. The promises and pitfalls of RNA-interference-based therapeutics. *Nature* 2009;**457**:426-433.
48. de Fougerolles A, Vornlocher H-P, Maraganore J, Lieberman J. Interfering with disease: a progress report on siRNA-based therapeutics. *Nature Reviews Drug Discovery* 2007;**6**:443-453.
49. Yi R, Qin Y, Macara IG, Cullen BR. Exportin-5 mediates the nuclear export of pre-microRNAs and short hairpin RNAs. *Genes & Development* 2003;**17**:3011-3016.
50. Hutvágner G, McLachlan J, Pasquinelli AE, Bálint É, Tuschl T, Zamore PD. A Cellular Function for the RNA-Interference Enzyme Dicer in the Maturation of the let-7 Small Temporal RNA. *Science* 2001;**293**:834-838.
51. Manche L, Green SR, Schmedt C, Mathews MB. Interactions between double-stranded RNA regulators and the protein kinase DAI. *Molecular and Cellular Biology* 1992;**12**:5238-5248.

52. Matranga C, Tomari Y, Shin C, Bartel DP, Zamore PD. Passenger-Strand Cleavage Facilitates Assembly of siRNA into Ago2-Containing RNAi Enzyme Complexes. *Cell* 2005;**123**:607-620.
53. Valencia-Sanchez MA, Liu J, Hannon GJ, Parker R. Control of translation and mRNA degradation by miRNAs and siRNAs. *Genes & Development* 2006;**20**:515-524.
54. Matzke MA, Birchler JA. RNAi-mediated pathways in the nucleus. *Nature Reviews Genetics* 2005;**6**:24-35.
55. Verdel A, Jia S, Gerber S, Sugiyama T, Gygi S, Grewal SIS, et al. RNAi-Mediated Targeting of Heterochromatin by the RITS Complex. *Science* 2004;**303**:672-676.
56. He L, Hannon GJ. MicroRNAs: small RNAs with a big role in gene regulation. *Nature Reviews Genetics* 2004;**5**:522-531.
57. Kurita K, Sannan T, Iwakura Y. Studies on chitin, 4. Evidence for formation of block and random copolymers of N-acetyl-D-glucosamine and D-glucosamine by hetero- and homogeneous hydrolyses. *Die Makromolekulare Chemie* 1977;**178**:3197-3202.
58. Vårum KM, Antohonsen MW, Grasdalen H, Smidsrød O. Determination of the degree of N-acetylation and the distribution of N-acetyl groups in partially N-deacetylated chitins (chitosans) by high-field n.m.r. spectroscopy. *Carbohydrate Research* 1991;**211**:17-23.
59. Vårum K, Smidsrød O, Structure-Property Relationship in Chitosans, in: Dumitriu S (Ed.), *Polysaccharides: Structural diversity and functional versatility*, 2nd ed, CRC Press, New York, 2004, pp. 625 - 643.
60. Dahiya N, Chitin Metabolism In Fungi, in: Rai M, Kövics G editors, *Progress in Mycology*, Springer Netherlands, 2010, pp. 409-423.
61. Bartnicki-Garcia S, Nickerson WJ. Isolation, composition, and structure of cell walls of filamentous and yeast-like forms of Mucor rouxii. *Biochimica et Biophysica Acta* 1962;**58**:102-119.
62. Synowiecki Jz, Al-Khateeb NAAQ. Mycelia of Mucor rouxii as a source of chitin and chitosan. *Food Chemistry* 1997;**60**:605-610.
63. Vårum KM, Ottøy MH, Smidsrød O. Acid hydrolysis of chitosans. *Carbohydrate Polymers* 2001;**46**:89-98.
64. Anthonsen MW, Vårum KM, Smidsrød O. Solution properties of chitosans: conformation and chain stiffness of chitosans with different degrees of N-acetylation. *Carbohydrate Polymers* 1993;**22**:193-201.
65. Vårum KM, Ottøy MH, Smidsrød O. Water-solubility of partially N-acetylated chitosans as a function of pH: effect of chemical composition and depolymerisation. *Carbohydrate Polymers* 1994;**25**:65-70.
66. Strand SP, Tømmeraas K, Vårum KM, Østgaard K. Electrophoretic Light Scattering Studies of Chitosans with Different Degrees of N-acetylation. *Biomacromolecules* 2001;**2**:1310-1314.
67. Schipper NGM, Vårum KM, Artursson P. Chitosans as Absorption Enhancers for Poorly Absorbable Drugs. 1: Influence of Molecular Weight and Degree of Acetylation on Drug Transport Across Human Intestinal Epithelial (Caco-2) Cells. *Pharmaceutical Research* 1996;**13**:1686-1692.
68. Agnihotri SA, Mallikarjuna NN, Aminabhavi TM. Recent advances on chitosan-based micro- and nanoparticles in drug delivery. *Journal of Controlled Release* 2004;**100**:5-28.

69. Schipper NGM, Olsson S, Hoogstraate JA, deBoer AG, Vårum KM, Artursson P. Chitosans as Absorption Enhancers for Poorly Absorbable Drugs 2: Mechanism of Absorption Enhancement. *Pharmaceutical Research* 1997;**14**:923-929.
70. Schipper NGM, Vårum KM, Stenberg P, Ocklind G, Lennernäs H, Artursson P. Chitosans as absorption enhancers of poorly absorbable drugs 3: Influence of mucus on absorption enhancement. *European Journal of Pharmaceutical Sciences* 1999;**8**:335-343.
71. Thanou M, Verhoef JC, Junginger HE. Chitosan and its derivatives as intestinal absorption enhancers. *Advanced Drug Delivery Reviews* 2001;**50, Supplement 1**:S91-S101.
72. Seferian PG, Martinez ML. Immune stimulating activity of two new chitosan containing adjuvant formulations. *Vaccine* 2000;**19**:661-668.
73. Ong S-Y, Wu J, Moochhala SM, Tan M-H, Lu J. Development of a chitosan-based wound dressing with improved hemostatic and antimicrobial properties. *Biomaterials* 2008;**29**:4323-4332.
74. Tømmeraas K, Strand SP, Christensen BE, Smidsrød O, Vårum KM. Preparation and characterization of branched chitosans. *Carbohydrate Polymers* 2011;**83**:1558-1564.
75. Tømmeraas K, Vårum KM, Christensen BE, Smidsrød O. Preparation and characterisation of oligosaccharides produced by nitrous acid depolymerisation of chitosans. *Carbohydrate Research* 2001;**333**:137-144.
76. Tømmeraas K, Köping-Höggård M, Vårum KM, Christensen BE, Artursson P, Smidsrød O. Preparation and characterisation of chitosans with oligosaccharide branches. *Carbohydrate Research* 2002;**337**:2455-2462.
77. Strand SP, Issa MM, Christensen BE, Vårum KM, Artursson P. Tailoring of Chitosans for Gene Delivery: Novel Self-Branched Glycosylated Chitosan Oligomers with Improved Functional Properties. *Biomacromolecules* 2008;**9**:3268-3276.
78. Miyata K, Christie RJ, Kataoka K. Polymeric micelles for nano-scale drug delivery. *Reactive and Functional Polymers* 2011;**71**:227-234.
79. Kay MA, Glorioso JC, Naldini L. Viral vectors for gene therapy: the art of turning infectious agents into vehicles of therapeutics. *Nature Medicine* 2001;**7**:33-40.
80. Kim W, Kim S. Efficient siRNA Delivery with Non-viral Polymeric Vehicles. *Pharmaceutical Research* 2009;**26**:657-666.
81. Thomas CE, Ehrhardt A, Kay MA. Progress and problems with the use of viral vectors for gene therapy. *Nature Reviews Genetics* 2003;**4**:346-358.
82. Al-Dosari M, Gao X. Nonviral Gene Delivery: Principle, Limitations, and Recent Progress. *The AAPS Journal* 2009;**11**:671-681.
83. MacLaughlin FC, Mumper RJ, Wang J, Tagliaferri JM, Gill I, Hinchcliffe M, et al. Chitosan and depolymerized chitosan oligomers as condensing carriers for in vivo plasmid delivery. *Journal of Controlled Release* 1998;**56**:259-272.
84. Liu X, Howard KA, Dong M, Andersen MØ, Rahbek UL, Johnsen MG, et al. The influence of polymeric properties on chitosan/siRNA nanoparticle formulation and gene silencing. *Biomaterials* 2007;**28**:1280-1288.
85. Wolfert MA, Schacht E, Toncheva V, Ulbrich K, Nazarova O, Seymour LW. Characterization of vectors for gene therapy formed by self-assembly of DNA with synthetic block co-polymers. *Human gene therapy* 1996;**7**:2123-2133.

86. Matulis D, Rouzina I, Bloomfield VA. Thermodynamics of DNA binding and condensation: isothermal titration calorimetry and electrostatic mechanism. *Journal of Molecular Biology* 2000;**296**:1053-1063.
87. Danielsen S, Vårum KM, Stokke BT. Structural Analysis of Chitosan Mediated DNA Condensation by AFM: Influence of Chitosan Molecular Parameters. *Biomacromolecules* 2004;**5**:928-936.
88. Layman JM, Ramirez SM, Green MD, Long TE. Influence of Polycation Molecular Weight on Poly(2-dimethylaminoethyl methacrylate)-Mediated DNA Delivery In Vitro. *Biomacromolecules* 2009;**10**:1244-1252.
89. Reitan NK, Maurstad G, de Lange Davies C, Strand SP. Characterizing DNA Condensation by Structurally Different Chitosans of Variable Gene Transfer Efficacy. *Biomacromolecules* 2009;**10**:1508-1515.
90. Scholz C, Wagner E. Therapeutic plasmid DNA versus siRNA delivery: Common and different tasks for synthetic carriers. *Journal of Controlled Release* 2012;**161**:554-565.
91. Zhang S, Zhao B, Jiang H, Wang B, Ma B. Cationic lipids and polymers mediated vectors for delivery of siRNA. *Journal of Controlled Release* 2007;**123**:1-10.
92. Mumper RJ, Wang JJ, Claspell JM, Rolland AP. Novel polymeric condensing carriers for gene delivery. *Proceedings of the International Symposium on Controlled Release Bioactive Materials* 1995;**22**:178-179.
93. Lai W-F, Lin MC-M. Nucleic acid delivery with chitosan and its derivatives. *Journal of Controlled Release* 2009;**134**:158-168.
94. Mao S, Shuai X, Unger F, Simon M, Bi D, Kissel T. The depolymerization of chitosan: effects on physicochemical and biological properties. *International Journal of Pharmaceutics* 2004;**281**:45-54.
95. Lavertu M, Méthot S, Tran-Khanh N, Buschmann MD. High efficiency gene transfer using chitosan/DNA nanoparticles with specific combinations of molecular weight and degree of deacetylation. *Biomaterials* 2006;**27**:4815-4824.
96. Köping-Höggard M, Vårum KM, Issa M, Danielsen S, Christensen BE, Stokke BT, et al. Improved chitosan-mediated gene delivery based on easily dissociated chitosan polyplexes of highly defined chitosan oligomers. *Gene Therapy* 2004;**11**:1441-1452.
97. Strand SP, Lelu S, Reitan NK, de Lange Davies C, Artursson P, Vårum KM. Molecular design of chitosan gene delivery systems with an optimized balance between polyplex stability and polyplex unpacking. *Biomaterials* 2009;**31**:975-987.
98. Mao S, Sun W, Kissel T. Chitosan-based formulations for delivery of DNA and siRNA. *Advanced Drug Delivery Reviews* 2010;**62**:12-27.
99. Eide KB, Norberg AL, Heggset EB, Lindbom AR, Vårum KM, Eijsink VGH, et al. Human Chitotriosidase-Catalyzed Hydrolysis of Chitosan. *Biochemistry* 2012;**51**:487-495.
100. Nordtveit RJ, Vårum KM, Smidsrød O. Degradation of partially N-acetylated chitosans with hen egg white and human lysozyme. *Carbohydrate Polymers* 1996;**29**:163-167.
101. Vårum KM, Myhr MM, Hjerde RJN, Smidsrød O. In vitro degradation rates of partially N-acetylated chitosans in human serum. *Carbohydrate Research* 1997;**299**:99-101.

102. Kiang T, Wen J, Lim HW, Leong KWKW. The effect of the degree of chitosan deacetylation on the efficiency of gene transfection. *Biomaterials* 2004;**25**:5293-5301.
103. Köping-Höggård M, Tubulekas I, Guan H, Edwards K, Nilsson M, Vårum KM, et al. Chitosan as a nonviral gene delivery system. Structure-property relationships and characteristics compared with polyethylenimine in vitro and after lung administration in vivo. *Gene Therapy* 2001;**8**:1108-1121.
104. Huang M, Fong C-W, Khor E, Lim L-Y. Transfection efficiency of chitosan vectors: Effect of polymer molecular weight and degree of deacetylation. *Journal of Controlled Release* 2005;**106**:391-406.
105. Köping-Höggard M, Tubulekas I, Guan H, Edwards K, Nilsson M, Vårum K, et al. Chitosan as a nonviral gene delivery system. Structure-property relationships and characteristics compared with polyethyleneimine in vitro and after lung admnistration in vivo. *Gene Therapy* 2001;**8**:1108-1121.
106. Thibault M, Nimesh S, Lavertu M, Buschmann MD. Intracellular Trafficking and Decondensation Kinetics of Chitosan-pDNA Polyplexes. *Molecular Therapy* 2010;**18**:1787-1795.
107. Richardson SW, Kolbe HJ, Duncan R. Potential of low molecular mass chitosan as a DNA delivery system: biocompatibility, body distribution and ability to complex and protect DNA. *International Journal of Pharmaceutics* 1999;**178**:231-243.
108. Rojanarata T, Opanasopit P, Techaarpornkul S, Ngawhirunpat T, Ruktanonchai U. Chitosan-Thiamine Pyrophosphate as a Novel Carrier for siRNA Delivery. *Pharmaceutical Research* 2008;**25**:2807-2814.
109. Techaarpornkul S, Wongkupasert S, Opanasopit P, Apirakaramwong A, Nunthanid J, Ruktanonchai U. Chitosan-Mediated siRNA Delivery In Vitro: Effect of Polymer Molecular Weight, Concentration and Salt Forms. *AAPS PharmSciTech* 2010;**11**:64-72.
110. Howard KA, Rahbek UL, Liu X, Damgaard CK, Glud SZ, Andersen MO, et al. RNA Interference in Vitro and in Vivo Using a Chitosan/siRNA Nanoparticle System. *Molecular Therapy* 2006;**14**:476-484.
111. Lee M, Nah J-W, Kwon Y, Koh JJ, Ko KS, Kim SW. Water-Soluble and Low Molecular Weight Chitosan-Based Plasmid DNA Delivery. *Pharmaceutical Research* 2001;**18**:427-431.
112. De Smedt SC, Demeester J, Hennink WE. Cationic Polymer Based Gene Delivery Systems. *Pharmaceutical Research* 2000;**17**:113-126.
113. Suh J, Wirtz D, Hanes J. Efficient active transport of gene nanocarriers to the cell nucleus. *Proceedings of the National Academy of Sciences* 2003;**100**:3878-3882.
114. Thibault M, Astolfi M, Tran-Khanh N, Lavertu M, Darras V, Merzouki A, et al. Excess polycation mediates efficient chitosan-based gene transfer by promoting lysosomal release of the polyplexes. *Biomaterials* 2011;**32**:4639-4646.
115. Gao S, Chen J, Xu X, Ding Z, Yang Y-H, Hua Z, et al. Galactosylated low molecular weight chitosan as DNA carrier for hepatocyte-targeting. *International Journal of Pharmaceutics* 2003;**255**:57-68.
116. Issa MM, Köping-Höggård M, Tømmeraas K, Vårum KM, Christensen BE, Strand SP, et al. Targeted gene delivery with trisaccharide-substituted chitosan oligomers in vitro and after lung administration in vivo. *Journal of Controlled Release* 2006;**115**:103-112.

117. Katas H, Oya AH. Develpment and characterisation of chitosan nanoparticles for siRNA delivery. *Journal of Controlled Release* 2006;**115**:216-225.
118. Lee DW, Yun K-S, Ban H-S, Choe W, Lee SK, Lee KY. Preparation and characterization of chitosan/polyguluronate nanoparticles for siRNA delivery. *Journal of Controlled Release* 2009;**139**:146-152.
119. Nimesh S, Thibault M, Lavertu M, Buschmann M. Enhanced Gene Delivery Mediated by Low Molecular Weight Chitosan/DNA Complexes: Effect of pH and Serum. *Molecular Biotechnology* 2010;**46**:182-196.
120. Gao S, Dagnaes-Hansen F, Nielsen EJB, Wengel J, Besenbacher F, Howard KA, et al. The Effect of Chemical Modification and Nanoparticle Formulation on Stability and Biodistribution of siRNA in Mice. *Molecular Therapy* 2009;**17**:1225-1233.
121. Sato T, Ishii T, Okahata Y. In vitro gene delivery mediated by chitosan. Effect of pH, serum, and molecular mass of chitosan on the transfection efficiency. *Biomaterials* 2001;**22**:2075-2080.
122. Xu S, Dong M, Liu X, Howard KA, Kjems J, Besenbacher F. Direct Force Measurements between siRNA and Chitosan Molecules Using Force Spectroscopy. *Biophysical Journal* 2007;**93**:952-959.
123. Hashimoto M, Morimoto M, Saimoto H, Shigemasa Y, Sato T. Lactosylated Chitosan for DNA Delivery into Hepatocytes: The Effect of Lactosylation on the Physicochemical Properties and Intracellular Trafficking of pDNA/Chitosan Complexes. *Bioconjugate Chemistry* 2006;**17**:309-316.
124. Gao S, Chen J, Dong L, Ding Z, Yang Y-h, Zhang J. Targeting delivery of oligonucleotide and plasmid DNA to hepatocyte via galactosylated chitosan vector. *European Journal of Pharmaceutics and Biopharmaceutics* 2005;**60**:327-334.
125. Eisenberg C, Seta N, Appel M, Feldmann G, Durand G, Feger J. Asialoglycoprotein receptor in human isolated hepatocytes from normal liver and its apparent increase in liver with histological alterations. *Journal of Hepatology* 1991;**13**:305-309.
126. Nakase I, Lai H, Singh NP, Sasaki T. Anticancer properties of artemisinin derivatives and their targeted delivery by transferrin conjugation. *International Journal of Pharmaceutics* 2008;**354**:28-33.
127. Mao H-Q, Roy K, Troung-Le VL, Janes KA, Lin KY, Wang Y, et al. Chitosan-DNA nanoparticles as gene carriers: synthesis, characterization and transfection efficiency. *Journal of Controlled Release* 2001;**70**:399-421.
128. Jiang W, Swiggard WJ, Heufler C, Peng M, Mirza A, Steinman RM, et al. The receptor DEC-205 expressed by dendritic cells and thymic epithelial cells is involved in antigen processing. *Nature* 1995;**375**:151-155.
129. Kim TH, Nah JW, Cho M-H, Park TG, Cho CS. Receptor-Mediated Gene Delivery into Antigen Presenting Cells Using Mannosylated Chitosan/DNA Nanoparticles. *Journal of Nanoscience and Nanotechnology* 2006;**6**:2796-2803.
130. Lee D, Lockey R, Mohapatra S. Folate Receptor-Mediated Cancer Cell Specific Gene Delivery Using Folic Acid-Conjugated Oligochitosans. *Journal of Nanoscience and Nanotechnology* 2006;**6**:2860-2866.
131. Fernandes JC, Wang H, Jreyssaty C, Benderdour M, Lavigne P, Qiu X, et al. Bone-protective Effects of Nonviral Gene Therapy With Folate-Chitosan DNA Nanoparticle Containing Interleukin-1 Receptor Antagonist Gene in Rats With Adjuvant-induced Arthritis. *Molecular Therapy* 2008;**16**:1243-1251.

132. Zhao XB, Lee RJ. Tumor-selective targeted delivery of genes and antisense oligodeoxyribonucleotides via the folate receptor. *Advanced Drug Delivery Reviews* 2004;**56**:1193-1204.
133. Han HD, Mangala LS, Lee JW, Shahzad MMK, Kim HS, Shen D, et al. Targeted Gene Silencing Using RGD-Labeled Chitosan Nanoparticles. *Clinical Cancer Research* 2010;**16**:3910-3922.
134. Thanou M, Florea BI, Geldof M, Junginger HE, Borchard G. Quaternized chitosan oligomers as novel gene delivery vectors in epithelial cell lines. *Biomaterials* 2002;**23**:153-159.
135. Kean T, Roth S, Thanou M. Trimethylated chitosans as non-viral gene delivery vectors: Cytotoxicity and transfection efficiency. *Journal of Controlled Release* 2005;**103**:643-653.
136. Jintapattanakit A, Mao S, Kissel T, Junyaprasert VB. Physicochemical properties and biocompatibility of N-trimethyl chitosan: Effect of quaternization and dimethylation. *European Journal of Pharmaceutics and Biopharmaceutics* 2008;**70**:563-571.
137. Dehousse V, Garbacki N, Jaspart S, Castagne D, Piel G, Colige A, et al. Comparison of chitosan/siRNA and trimethylchitosan/siRNA complexes behaviour in vitro. *International Journal of Biological Macromolecules* 2010;**46**:342-349.
138. Noh SM, Park MO, Shim G, Han SE, Lee HY, Huh JH, et al. Pegylated poly-l-arginine derivatives of chitosan for effective delivery of siRNA. *Journal of Controlled Release* 2010;**145**:159-164.
139. Jiang H-L, Kwon J-T, Kim E-M, Kim Y-K, Arote R, Jere D, et al. Galactosylated poly(ethylene glycol)-chitosan-graft-polyethylenimine as a gene carrier for hepatocyte-targeting. *Journal of Controlled Release* 2008;**131**:150-157.
140. Germershaus O, Mao S, Sitterberg J, Bakowsky U, Kissel T. Gene delivery using chitosan, trimethyl chitosan or polyethylenglycol-graft-trimethyl chitosan block copolymers: Establishment of structure-activity relationships in vitro. *Journal of Controlled Release* 2008;**125**:145-154.
141. Jiang X, Dai H, Leong KW, Goh SH, Mao HQ, Yang YY. Chitosan-g-PEG/DNA complexes deliver gene to the rat liver via intrabiliary and intraportal infusions. *The Journal of Gene Medicine* 2006;**8**:477-487.
142. Raviña M, Cubillo E, Olmeda D, Novoa-Carballal R, Fernandez-Megia E, Riguera R, et al. Hyaluronic Acid/Chitosan-g-Poly(ethylene glycol) Nanoparticles for Gene Therapy: An Application for pDNA and siRNA Delivery. *Pharmaceutical Research* 2010;**27**:2544-2555.
143. Kurisawa M, Yokoyama M, Okano T. Transfection efficiency increases by incorporating hydrophobic monomer units into polymeric gene carriers. *Journal of Controlled Release* 2000;**68**:1-8.
144. Sang Yoo H, Eun Lee J, Chung H, Chan Kwon I, Young Jeong S. Self-assembled nanoparticles containing hydrophobically modified glycol chitosan for gene delivery. *Journal of Controlled Release* 2005;**103**:235-243.
145. Chae SY, Son S, Lee M, Jang M-K, Nah J-W. Deoxycholic acid-conjugated chitosan oligosaccharide nanoparticles for efficient gene carrier. *Journal of Controlled Release* 2005;**109**:330-344.

146. Hu F-Q, Zhao M-D, Yuan H, You J, Du Y-Z, Zeng S. A novel chitosan oligosaccharide-stearic acid micelles for gene delivery: Properties and in vitro transfection studies. *International Journal of Pharmaceutics* 2006;**315**:158-166.
147. Wong K, Sun G, Zhang, Dai H, Liu Y, He, et al. PEI-g-chitosan, a Novel Gene Delivery System with Transfection Efficiency Comparable to Polyethylenimine in Vitro and after Liver Administration in Vivo. *Bioconjugate Chemistry* 2005;**17**:152-158.
148. Jiang H-L, Kim Y-K, Arote R, Nah J-W, Cho M-H, Choi Y-J, et al. Chitosan-graft-polyethylenimine as a gene carrier. *Journal of Controlled Release* 2007;**117**:273-280.
149. Lu B, Xu X-D, Zhang X-Z, Cheng S-X, Zhuo R-X. Low Molecular Weight Polyethylenimine Grafted N-Maleated Chitosan for Gene Delivery: Properties and In Vitro Transfection Studies. *Biomacromolecules* 2008;**9**:2594-2600.
150. Kim TH, Ihm JE, Choi YJ, Nah JW, Cho CS. Efficient gene delivery by urocanic acid-modified chitosan. *Journal of Controlled Release* 2003;**93**:389-402.
151. Behr J-P. The Proton Sponge: a Trick to Enter Cells the Viruses Did Not Exploit. *CHIMIA International Journal for Chemistry* 1997;**51**:34-36.
152. Schmitz T, Bravo-Osuna I, Vauthier C, Ponchel G, Loretz B, Bernkop-Schnürch A. Development and in vitro evaluation of a thiomer-based nanoparticulate gene delivery system. *Biomaterials* 2007;**28**:524-531.
153. Liao Z-X, Ho Y-C, Chen H-L, Peng S-F, Hsiao C-W, Sung H-W. Enhancement of efficiencies of the cellular uptake and gene silencing of chitosan/siRNA complexes via the inclusion of a negatively charged poly(γ-glutamic acid). *Biomaterials* 2010;**31**:8780-8788.
154. Godbey WT, Wu KK, Mikos AG. Size matters: Molecular weight affects the efficiency of poly(ethylenimine) as a gene delivery vehicle. *Journal of Biomedical Materials Research* 1999;**45**:268-275.
155. Fischer D, Bieber T, Li Y, Elsässer H-P, Kissel T. A Novel Non-Viral Vector for DNA Delivery Based on Low Molecular Weight, Branched Polyethylenimine: Effect of Molecular Weight on Transfection Efficiency and Cytotoxicity. *Pharmaceutical Research* 1999;**16**:1273-1279.
156. Kunath K, von Harpe A, Fischer D, Petersen H, Bickel U, Voigt K, et al. Low-molecular-weight polyethylenimine as a non-viral vector for DNA delivery: comparison of physicochemical properties, transfection efficiency and in vivo distribution with high-molecular-weight polyethylenimine. *Journal of Controlled Release* 2003;**89**:113-125.
157. Dunlap DD, Maggi A, Soria MR, Monaco L. Nanoscopic structure of DNA condensed for gene delivery. *Nucleic Acids Research* 1997;**25**:3095-3101.
158. Wightman L, Kircheis R, Rössler V, Carotta S, Ruzicka R, Kursa M, et al. Different behavior of branched and linear polyethylenimine for gene delivery in vitro and in vivo. *The Journal of Gene Medicine* 2001;**3**:362-372.
159. Grayson AR, Doody A, Putnam D. Biophysical and Structural Characterization of Polyethylenimine-Mediated siRNA Delivery in Vitro. *Pharmaceutical Research* 2006;**23**:1868-1876.
160. Werth S, Urban-Klein B, Dai L, Höbel S, Grzelinski M, Bakowsky U, et al. A low molecular weight fraction of polyethylenimine (PEI) displays increased transfection efficiency of DNA and siRNA in fresh or lyophilized complexes. *Journal of Controlled Release* 2006;**112**:257-270.

161. Gary DJ, Puri N, Won Y-Y. Polymer-based siRNA delivery: Perspectives on the fundamental and phenomenological distinctions from polymer-based DNA delivery. *Journal of Controlled Release* 2007;**121**:64-73.
162. Harada A, Cammas S, Kataoka K. Stabilized α-Helix Structure of Poly(l-lysine)-block-poly(ethylene glycol) in Aqueous Medium through Supramolecular Assembly. *Macromolecules* 1996;**29**:6183-6188.
163. Midoux P, Monsigny M. Efficient Gene Transfer by Histidylated Polylysine/pDNA Complexes. *Bioconjugate Chemistry* 1999;**10**:406-411.
164. Read ML, Singh S, Ahmed Z, Stevenson M, Briggs SS, Oupicky D, et al. A versatile reducible polycation-based system for efficient delivery of a broad range of nucleic acids. *Nucleic Acids Research* 2005;**33**:e86.
165. Kwoh DY, Coffin CC, Lollo CP, Jovenal J, Banaszczyk MG, Mullen P, et al. Stabilization of poly-l-lysine/DNA polyplexes for in vivo gene delivery to the liver. *Biochimica et Biophysica Acta (BBA) - Gene Structure and Expression* 1999;**1444**:171-190.
166. Wolfert MA, Seymour LW. Atomic force microscopic analysis of the influence of the molecular weight of poly(L)lysine on the size of polyelectrolyte complexes formed with DNA. *Gene therapy* 1996;**3**:269-273.
167. Liu G, Molas M, Grossmann GA, Pasumarthy M, Perales JC, Cooper MJ, et al. Biological Properties of Poly-l-lysine-DNA Complexes Generated by Cooperative Binding of the Polycation. *Journal of Biological Chemistry* 2001;**276**:34379-34387.
168. van de Wetering P, Moret EE, Schuurmans-Nieuwenbroek NME, van Steenbergen MJ, Hennink WE. Structure-Activity Relationships of Water-Soluble Cationic Methacrylate/Methacrylamide Polymers for Nonviral Gene Delivery. *Bioconjugate Chemistry* 1999;**10**:589-597.
169. van de Wetering P, Cherng J-Y, Talsma H, Hennink WE. Relation between transfection efficiency and cytotoxicity of poly(2-(dimethylamino)ethyl methacrylate)/plasmid complexes. *Journal of Controlled Release* 1997;**49**:59-69.
170. Verbaan FJ, Oussoren C, van Dam IM, Takakura Y, Hashida M, Crommelin DJA, et al. The fate of poly(2-dimethyl amino ethyl)methacrylate-based polyplexes after intravenous administration. *International Journal of Pharmaceutics* 2001;**214**:99-101.
171. Funhoff AM, van Nostrum CF, Koning GA, Schuurmans-Nieuwenbroek NME, Crommelin DJA, Hennink WE. Endosomal Escape of Polymeric Gene Delivery Complexes Is Not Always Enhanced by Polymers Buffering at Low pH. *Biomacromolecules* 2003;**5**:32-39.
172. Gonzalez H, Hwang SJ, Davis ME. New Class of Polymers for the Delivery of Macromolecular Therapeutics. *Bioconjugate Chemistry* 1999;**10**:1068-1074.
173. Hu-Lieskovan S, Heidel JD, Bartlett DW, Davis ME, Triche TJ. Sequence-Specific Knockdown of EWS-FLI1 by Targeted, Nonviral Delivery of Small Interfering RNA Inhibits Tumor Growth in a Murine Model of Metastatic Ewing's Sarcoma. *Cancer Research* 2005;**65**:8984-8992.
174. Li W, Szoka F. Lipid-based Nanoparticles for Nucleic Acid Delivery. *Pharmaceutical Research* 2007;**24**:438-449.
175. Filion MC, Phillips NC. Toxicity and immunomodulatory activity of liposomal vectors formulated with cationic lipids toward immune effector cells. *Biochimica et Biophysica Acta (BBA) - Biomembranes* 1997;**1329**:345-356.

176. Tang D-c, DeVit M, Johnston SA. Genetic immunization is a simple method for eliciting an immune response. *Nature* 1992;**356**:152-154.
177. Neumann E, Schaefer-Ridder M, Wang Y, Hofschneider PH. Gene transfer into mouse lyoma cells by electroporation in high electric fields. *The EMBO journal* 1982;**1**:841-845.
178. Dufès C, Uchegbu IF, Schätzlein AG. Dendrimers in gene delivery. *Advanced Drug Delivery Reviews* 2005;**57**:2177-2202.
179. Naldini L. Ex vivo gene transfer and correction for cell-based therapies. *Nature Reviews Genetics* 2011;**12**:301-315.
180. Whitehead KA, Langer R, Anderson DG. Knocking down barriers: advances in siRNA delivery. *Nature Reviews Drug Discovery* 2009;**8**:129-138.
181. Rettig GR, Behlke MA. Progress Toward In Vivo Use of siRNAs-II. *Molecular Therapy* 2012;**20**:483-512.
182. Yildirimer L, Thanh NTK, Loizidou M, Seifalian AM. Toxicology and clinical potential of nanoparticles. *Nano Today* 2011;**6**:585-607.
183. Plank C, Mechtler K, Szoka FC, Wagner E. Activation of the complement system by synthetic DNA complexes: a potential barrier for intravenous gene delivery. *Human gene therapy* 1996;**7**:1437-1446.
184. Alexis F, Pridgen E, Molnar LK, Farokhzad OC. Factors Affecting the Clearance and Biodistribution of Polymeric Nanoparticles. *Molecular Pharmaceutics* 2008;**5**:505-515.
185. Kawabata K, Takakura Y, Hashida M. The Fate of Plasmid DNA After Intravenous Injection in Mice: Involvement of Scavenger Receptors in Its Hepatic Uptake. *Pharmaceutical Research* 1995;**12**:825-830.
186. Lélu S, Strand SP, Steine J, Davies CdL. Effect of PEGylation on the Diffusion and Stability of Chitosan–DNA Polyplexes in Collagen Gels. *Biomacromolecules* 2011;**12**:3656-3665.
187. Medina-Kauwe LK, Xie J, Hamm-Alvarez S. Intracellular trafficking of nonviral vectors. *Gene Therapy* 2005;**12**:1734-1751.
188. Pathak A, Patnaik S, Gupta KC. Recent trends in non-viral vector-mediated gene delivery. *Biotechnology Journal* 2009;**4**:1559-1572.
189. Lukacs GL, Haggie P, Seksek O, Lechardeur D, Freedman N, Verkman AS. Size-dependent DNA Mobility in Cytoplasm and Nucleus. *Journal of Biological Chemistry* 2000;**275**:1625-1629.
190. Dauty E, Verkman AS. Actin Cytoskeleton as the Principal Determinant of Size-dependent DNA Mobility in Cytoplasm. *Journal of Biological Chemistry* 2005;**280**:7823-7828.
191. Dean DA, Strong DD, Zimmer WE. Nuclear entry of nonviral vectors. *Gene Therapy* 2005;**12**:881-890.
192. Abbott NJ, Patabendige AAK, Dolman DEM, Yusof SR, Begley DJ. Structure and function of the blood-brain barrier. *Neurobiology of Disease* 2009;**37**:13-25.
193. Yadav A, Collman R. CNS Inflammation and Macrophage/Microglial Biology Associated with HIV-1 Infection. *Journal of Neuroimmune Pharmacology* 2009;**4**:430-447.
194. Ming GL, Song HJ, Adult neurogenesis in the mammalian central nervous system, *Annual Review of Neuroscience*, Annual Reviews, Palo Alto, 2005, pp. 223-250.

195. Weiss N, Miller F, Cazaubon S, Couraud P-O. The blood-brain barrier in brain homeostasis and neurological diseases. *Biochimica et Biophysica Acta (BBA) - Biomembranes* 2009;**1788**:842-857.
196. Löscher W, Potschka H. Role of drug efflux transporters in the brain for drug disposition and treatment of brain diseases. *Progress in Neurobiology* 2005;**76**:22-76.
197. Nazer B, Hong S, Selkoe DJ. LRP promotes endocytosis and degradation, but not transcytosis, of the amyloid-β peptide in a blood–brain barrier in vitro model. *Neurobiology of Disease* 2008;**30**:94-102.
198. Carvey PM, Hendey B, Monahan AJ. The blood–brain barrier in neurodegenerative disease: a rhetorical perspective. *Journal of Neurochemistry* 2009;**111**:291-314.
199. Pardridge WM. Blood-Brain Barrier Genomics. *Stroke* 2007;**38**:686-690.
200. Pardridge WM. Blood-brain barrier drug targeting: the future of brain drug development. *Molecular interventions* 2003;**3**:90-105, 151.
201. Cecchelli R, Berezowski V, Lundquist S, Culot M, Renftel M, Dehouck M-P, et al. Modelling of the blood-brain barrier in drug discovery and development. *Nature Reviews Drug Discovery* 2007;**6**:650-661.
202. Leslie EM, Deeley RG, Cole SPC. Multidrug resistance proteins: role of P-glycoprotein, MRP1, MRP2, and BCRP (ABCG2) in tissue defense. *Toxicology and Applied Pharmacology* 2005;**204**:216-237.
203. de Klerk OL, Willemsen ATM, Bosker FJ, Bartels AL, Hendrikse NH, den Boer JA, et al. Regional increase in P-glycoprotein function in the blood-brain barrier of patients with chronic schizophrenia: A PET study with [11C]verapamil as a probe for P-glycoprotein function. *Psychiatry Research: Neuroimaging* 2010;**183**:151-156.
204. Weiss J, Dormann S-MG, Martin-Facklam M, Kerpen CJ, Ketabi-Kiyanvash N, Haefeli WE. Inhibition of P-Glycoprotein by Newer Antidepressants. *Journal of Pharmacology and Experimental Therapeutics* 2003;**305**:197-204.
205. Kemper EM, van Zandbergen AE, Cleypool C, Mos HA, Boogerd W, Beijnen JH, et al. Increased Penetration of Paclitaxel into the Brain by Inhibition of P-Glycoprotein. *Clinical Cancer Research* 2003;**9**:2849-2855.
206. Lee CGL, Gottesman MM, Cardarelli CO, Ramachandra M, Jeang K-T, Ambudkar SV, et al. HIV-1 Protease Inhibitors Are Substrates for the MDR1 Multidrug Transporter. *Biochemistry* 1998;**37**:3594-3601.
207. Tishler DM, Weinberg KI, Hinton DR, Barbaro N, Annett GM, Raffel C. MDR1 Gene Expression in Brain of Patients with Medically Intractable Epilepsy. *Epilepsia* 1995;**36**:1-6.
208. Scheffer GL, Pijnenborg ACLM, Smit EF, Müller M, Postma DS, Timens W, et al. Multidrug resistance related molecules in human and murine lung. *Journal of Clinical Pathology* 2002;**55**:332-339.
209. Thiebaut F, Tsuruo T, Hamada H, Gottesman MM, Pastan I, Willingham MC. Cellular localization of the multidrug-resistance gene product P-glycoprotein in normal human tissues. *Proceedings of the National Academy of Sciences* 1987;**84**:7735-7738.
210. Schinkel AH, Smit JJM, van Tellingen O, Beijnen JH, Wagenaar E, van Deemter L, et al. Disruption of the mouse mdr1a P-glycoprotein gene leads to a deficiency in the blood-brain barrier and to increased sensitivity to drugs. *Cell* 1994;**77**:491-502.
211. Cordon-Cardo C, O'Brien JP, Casals D, Rittman-Grauer L, Biedler JL, Melamed MR, et al. Multidrug-resistance gene (P-glycoprotein) is expressed by endothelial cells at

blood-brain barrier sites. *Proceedings of the National Academy of Sciences* 1989;**86**:695-698.
212. Demeule M, Labelle M, Régina A, Berthelet F, Béliveau R. Isolation of Endothelial Cells from Brain, Lung, and Kidney: Expression of the Multidrug Resistance P-Glycoprotein Isoforms. *Biochemical and Biophysical Research Communications* 2001;**281**:827-834.
213. Chen C-j, Chin JE, Ueda K, Clark DP, Pastan I, Gottesman MM, et al. Internal duplication and homology with bacterial transport proteins in the mdr1 (P-glycoprotein) gene from multidrug-resistant human cells. *Cell* 1986;**47**:381-389.
214. Meng H, Liong M, Xia T, Li Z, Ji Z, Zink JI, et al. Engineered Design of Mesoporous Silica Nanoparticles to Deliver Doxorubicin and P-Glycoprotein siRNA to Overcome Drug Resistance in a Cancer Cell Line. *ACS Nano* 2010;**4**:4539-4550.
215. Susa M, Iyer AK, Ryu K, Choy E, Hornicek FJ, Mankin H, et al. Inhibition of ABCB1 (MDR1) Expression by an siRNA Nanoparticulate Delivery System to Overcome Drug Resistance in Osteosarcoma. *PLoS ONE* 2010;**5**:e10764.
216. Wu H, Hait WN, Yang J-M. Small Interfering RNA-induced Suppression of MDR1 (P-Glycoprotein) Restores Sensitivity to Multidrug-resistant Cancer Cells. *Cancer Research* 2003;**63**:1515-1519.
217. Wu C, Ivars F, Anderson P, Hallmann R, Vestweber D, Nilsson P, et al. Endothelial basement membrane laminin α5 selectively inhibits T lymphocyte extravasation into the brain. *Nature Medicine* 2009;**15**:519-527.
218. upload.wikimedia.org/wikipedia/commons/d/d8/Blood-brain_barrier_02.png. Accessed on 05.03.2012.
219. Nag S. Morphology and Properties of Brain Endothelial Cells *Methods in Molecular Biology* 2011;**686**:3-47.
220. Nag S. Morphology and properties of astrocytes. *Methods in Molecular Biology* 2011;**686**:69-100.
221. Abbott NJ, Ronnback L, Hansson E. Astrocyte-endothelial interactions at the blood-brain barrier. *Nature Reviews Neuroscience* 2006;**7**:41-53.
222. Nag S. Morphology and properties of pericytes. *Methods in Molecular Biology* 2011;**686**:49-68.
223. Armulik A, Genove G, Mae M, Nisancioglu MH, Wallgard E, Niaudet C, et al. Pericytes regulate the blood-brain barrier. *Nature* 2010;**468**:557-561.
224. Daneman R, Zhou L, Kebede AA, Barres BA. Pericytes are required for blood-brain barrier integrity during embryogenesis. *Nature* 2010;**468**:562-566.
225. Dean M, Hamon Y, Chimini G. The human ATP-binding cassette (ABC) transporter superfamily. *Journal of Lipid Research* 2001;**42**:1007-1017.
226. Paolinelli R, Corada M, Orsenigo F, Dejana E. The molecular basis of the blood brain barrier differentiation and maintenance. Is it still a mystery? *Pharmacological Research* 2011;**63**:165-171.
227. Loo TW, Clarke DM. Do drug substrates enter the common drug-binding pocket of P-glycoprotein through "gates"? *Biochemical and Biophysical Research Communications* 2005;**329**:419-422.
228. Gros P, Dhir R, Croop J, Talbot F. A single amino acid substitution strongly modulates the activity and substrate specificity of the mouse mdr1 and mdr3 drug efflux pumps. *Proceedings of the National Academy of Sciences* 1991;**88**:7289-7293.

229. Cui YJ, Cheng X, Weaver YM, Klaassen CD. Tissue Distribution, Gender-Divergent Expression, Ontogeny, and Chemical Induction of Multidrug Resistance Transporter Genes (Mdr1a, Mdr1b, Mdr2) in Mice. *Drug Metabolism and Disposition* 2009;**37**:203-210.
230. Regina A, Koman A, Piciotti M, El Hafny B, Center MS, Bergmann R, et al. Mrp1 Multidrug Resistance-Associated Protein and P-Glycoprotein Expression in Rat Brain Microvessel Endothelial Cells. *Journal of Neurochemistry* 1998;**71**:705-715.
231. Ramakrishnan P. The role of P-glycoprotein in the blood-brain barrier. *Einstein Quarterly Journal of Biology and Medicine* 2003;**19**:160-165.
232. Fellner S, Bauer B, Miller DS, Schaffrik M, Fankhänel M, Spruß T, et al. Transport of paclitaxel (Taxol) across the blood-brain barrier in vitro and in vivo. *The Journal of Clinical Investigation* 2002;**110**:1309-1318.
233. List AF, Kopecky KJ, Willman CL, Head DR, Persons DL, Slovak ML, et al. Benefit of cyclosporine modulation of drug resistance in patients with poor-risk acute myeloid leukemia: a Southwest Oncology Group study. *Blood* 2001;**98**:3212-3220.
234. Lee G, Piquette-Miller M. Cytokines alter the expression and activity of the multidrug resistance transporters in human hepatoma cell lines; analysis using RT-PCR and cDNA microarrays. *Journal of Pharmaceutical Sciences* 2003;**92**:2152-2163.
235. Gupta Y, Jain A, Jain SK. Transferrin-conjugated solid lipid nanoparticles for enhanced delivery of quinine dihydrochloride to the brain. *Journal of Pharmacy and Pharmacology* 2007;**59**:935-940.
236. Fuest C, Bankstahl M, Winter P, Helm M, Pekcec A, Potschka H. In vivo down-regulation of mouse brain capillary P-glycoprotein: A preliminary investigation. *Neuroscience Letters* 2009;**464**:47-51.
237. Cohen RN, van der Aa MAEM, Macaraeg N, Lee AP, Szoka Jr FC. Quantification of plasmid DNA copies in the nucleus after lipoplex and polyplex transfection. *Journal of Controlled Release* 2009;**135**:166-174.
238. Hama S, Akita H, Ito R, Mizuguchi H, Hayakawa T, Harashima H. Quantitative Comparison of Intracellular Trafficking and Nuclear Transcription between Adenoviral and Lipoplex Systems. *Molecular Therapy* 2006;**13**:786-794.
239. Chen HH, Ho Y-P, Jiang X, Mao H-Q, Wang T-H, Leong KW. Quantitative Comparison of Intracellular Unpacking Kinetics of Polyplexes by a Model Constructed From Quantum Dot-FRET. *Molecular Therapy* 2008;**16**:324-332.
240. von Gersdorff K, Sanders NN, Vandenbroucke R, De Smedt SC, Wagner E, Ogris M. The Internalization Route Resulting in Successful Gene Expression Depends on both Cell Line and Polyethylenimine Polyplex Type. *Molecular Therapy* 2006;**14**:745-753.
241. Ogris M, Brunner S, Schüller S, Kircheis R, Wagner E. PEGylated DNA/transferrin-PEI complexes: reduced interaction with blood components, extended circulation in blood and potential for systemic gene delivery. *Gene Therapy* 1999;**6**:595-605.
242. Mittnacht U, Hartmann H, Hein S, Oliveira H, Dong M, P. Pego A, et al. Chitosan/siRNA Nanoparticles Biofunctionalize Nerve Implants and Enable Neurite Outgrowth. *Nano Letters* 2010;**10**:3933-3939.
243. Veiseh O, Kievit FM, Fang C, Mu N, Jana S, Leung MC, et al. Chlorotoxin bound magnetic nanovector tailored for cancer cell targeting, imaging, and siRNA delivery. *Biomaterials* 2009;**31**:8032-8042.

244. Akhtar S, Benter I. Toxicogenomics of non-viral drug delivery systems for RNAi: Potential impact on siRNA-mediated gene silencing activity and specificity. *Advanced Drug Delivery Reviews* 2007;**59**:164-182.
245. Tschuch C, Schulz A, Pscherer A, Werft W, Benner A, Hotz-Wagenblatt A, et al. Off-target effects of siRNA specific for GFP. *BMC Molecular Biology* 2008;**9**:60.
246. Jackson AL, Linsley PS. Recognizing and avoiding siRNA off-target effects for target identification and therapeutic application. *Nature Reviews Drug Discovery* 2010;**9**:57-67.
247. Khan AA, Betel D, Miller ML, Sander C, Leslie CS, Marks DS. Transfection of small RNAs globally perturbs gene regulation by endogenous microRNAs. *Nature Biotechnology* 2009;**27**:549-555.
248. Tang G. siRNA and miRNA: an insight into RISCs. *Trends in Biochemical Sciences* 2005;**30**:106-114.
249. Matsui Y, Kobayashi N, Nishikawa M, Takakura Y. Sequence-Specific Suppression of mdr1a/1b Expression in Mice via RNA Interference. *Pharmaceutical Research* 2005;**22**:2091-2098.
250. Saito T, Saetrom P. Target gene expression levels and competition between transfected and endogenous microRNAs are strong confounding factors in microRNA high-throughput experiments. *Silence* 2012;**3**:3.
251. Larsson E, Sander C, Marks D. mRNA turnover rate limits siRNA and microRNA efficacy. *Molecular Systems Biology* 2010;**6**:
252. Babakhanian K, Bendayan M, Bendayan R. Localization of P-glycoprotein at the nuclear envelope of rat brain cells. *Biochemical and Biophysical Research Communications* 2007;**361**:301-306.
253. Pardridge WM, Kang Y-S, Buciak JL, Yang J. Human Insulin Receptor Monoclonal Antibody Undergoes High Affinity Binding to Human Brain Capillaries in Vitro and Rapid Transcytosis Through the Blood–Brain Barrier in Vivo in the Primate. *Pharmaceutical Research* 1995;**12**:807-816.
254. Pardridge WM, Buciak JL, Friden PM. Selective transport of an anti-transferrin receptor antibody through the blood-brain barrier in vivo. *Journal of Pharmacology and Experimental Therapeutics* 1991;**259**:66-70.
255. Daoud R, Kast C, Gros P, Georges E. Rhodamine 123 Binds to Multiple Sites in the Multidrug Resistance Protein (MRP1). *Biochemistry* 2000;**39**:15344-15352.

Paper I

Biomacromolecules

ARTICLE

pubs.acs.org/Biomac

Effect of Chitosan Chain Architecture on Gene Delivery: Comparison of Self-Branched and Linear Chitosans

Jostein Malmo, Kjell M. Vårum, and Sabina P. Strand*

Department of Biotechnology, Norwegian Biopolymer Laboratory (NOBIPOL), Norwegian University of Science and Technology (NTNU), N-7491 Trondheim, Norway

Supporting Information

ABSTRACT: Chitosan possesses many characteristics of an ideal gene delivery system. However, the transfection efficiency of conventional chitosans is generally found to be low. In this study, we investigated the self-branching of chitosans as a strategy to improve its gene transfer properties without compromising its safety profile. Self-branched (SB) and self-branched trisaccharide-substituted (SBTCO) chitosans with molecular weights of 11−71 kDa were synthesized, characterized, and compared with their linear counterparts with respect to transfection efficiency, cellular uptake, formulation stability, and cytotoxicity. Our studies show that in contrast with unmodified linear chitosans that were unable to transfect HeLa cells, self-branched chitosans mediated high transfection efficiencies. The most efficient chitosan, SBTCO30, yielded gene expression levels two and five times higher than those of Lipofectamine and Exgen, respectively, and was nontoxic to cells. Nanoparticles formed with SBTCO chitosans exhibited a higher colloidal stability of formulation, efficient internalization without excessive cell surface binding, and low cytotoxicity.

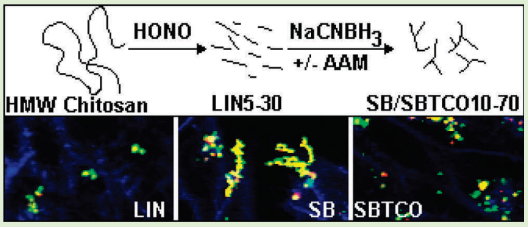

INTRODUCTION

The cellular delivery of nucleic acids is the foundation of gene therapy and has the potential to treat many currently incurable diseases. The large size and negative charge of the DNA molecule as well as its susceptibility toward degradation are considerable obstacles to efficient delivery, and numerous viral and nonviral delivery systems have been investigated. Genetically modified viruses have been the carrier of choice in many clinical studies. However, complications associated with vector safety[1−3] as well as manufacturing and restrictions in therapeutic cargo size[4] have triggered a search for nonviral alternatives. One of the promising candidates for nonviral gene delivery is the cationic polysaccharide chitosan, a linear copolymer consisting of β-1,4 linked *N*-acetyl-D-glucosamine (GlcNAc) and D-glucosamine (GlcN) derived from chitin. The interest in chitosans has been increasing over the past decade, owing to their availability, excellent safety profile, biodegradability, ease of modification, and interesting biological properties. The major disadvantage of chitosan is its poor solubility at physiological pH values that results from the deprotonation of the primary amine groups of GlcNs, which have a pK_a around 6.5 (25 °C, 100 mM NaCl).[5,6]

Off-the-shelf chitosans usually mediate poor gene transfer efficiencies. It is often assumed that this is a consequence of the low charge density of chitosan near physiological pH values, which is manifested in the poor physical and colloidal stabilities of DNA−chitosan nanoparticles. One strategy to improve chitosan properties in gene delivery applications is the tailoring of its structure. The fraction of acetylated units (F_A) and molecular weight (MW) have been found to be important for the condensation of DNA[7] and gene transfer efficiency.[8−10] It has been recently reported that the efficiency of gene delivery using chitosans is related to the polyplex stability and kinetics of intracellular unpacking.[11] Our studies also indicate the importance of an optimal balance between DNA protection and polyplex unpacking.[10]

However, the optimization of F_A and MW is not always sufficient to achieve efficient transfection with chitosan. Some cell lines appear to be difficult to transfect with linear chitosan, and modifications are necessary to improve the gene transfer.[10,12,13] Glycosylation with oligosaccharides such as lactose[14] or a GlcNAc-containing trisaccharide (AAM),[15,16] originally applied to target lectin receptors on hepatocytes, has also been shown to improve the solubility and reduce the aggregation rate of chitosan nanoparticles.[16] Substitution with short oligosaccharide chains may also be used as a tool to control the unpacking of polyplexes.[10] Self-branching has been recently employed as another tailoring tool, and we showed that the self-branching of glycosylated chitosan oligomers enhanced the transfection.[16] However, only one self-branched chitosan was used in this study, and the effects of self-branching and glycosylation were not studied

Received: November 12, 2010
Revised: January 11, 2011
Published: February 04, 2011

Table 1. Characterization of Chitosans Used in the Study[a]

linear/starting material				SB				SBTCO				
notation	M_n kDa	M_w kDa	PDI	Notation	M_n kDa	M_w kDa	PDI	Notation	M_n kDa	M_w kDa	PDI	d.s. % AAM
LIN5	4.2	4.7	1.12	SB10	8.3	11.3	1.36	SBTCO10	8.3	11.6	1.40	8.8
LIN8	6.3	8.0	1.28	SB20	12.1	19.8	1.64	SBTCO20	13.0	20.6	1.59	8.4
LIN10	8.5	11.6	1.37	SB30	15.3	27.3	1.78	SBTCO30	15.8	27.1	1.71	8.4
LIN15	10.8	16.4	1.52	SB40	21.3	40.1	1.88	SBTCO40	20.3	38.1	1.88	8.7
LIN25	14.5	24.8	1.71	SB60	28.4	56.6	1.99	SBTCO60	29.8	56.7	1.90	8.5
LIN30	17.6	32.9	1.87	SB70	33.4	67.4	2.02	SBTCO70	33.9	71.0	2.09	8.3

[a] Unsubstituted chitosans denoted as linear (LIN) have been used as the starting material for self-branched (SB) and self-branched trisaccharide (AAM)-substituted chitosan oligomers (SBTCO). The weight- and number-averages of molecular weight (M_w, M_n) and molecular weight distribution (PDI) were analyzed by SEC-MALLS. The degree of AAM-substitution (d.s.) was determined by ^{1}H NMR.

separately. Self-branched chitosans may be considered to be a novel and interesting class of chitosans that possess other properties beyond the conventional linear chains. In a similar manner as that for linear and branched polyethylenimine,[17] linear and branched chitosans may differ in both transfection efficiency and cytotoxicity.

The aim of this study was to investigate the gene delivery performance of self-branched chitosans compared with their linear counterparts and to evaluate the impact of self-branching on the various steps of the gene transfer process. For this purpose, we synthesized a series of self-branched chitosans with and without oligosaccharide substituents at MWs 11.3−71.0 kDa. Their transfection efficiencies, cellular uptake rates, formulation stabilities, and cytotoxicities were investigated. This study shows that in contrast with unmodified linear chitosans, which are unable to transfect HeLa cells, self-branched chitosans mediate efficient nanoparticle uptake and transfection with negligible cytotoxicity.

MATERIALS AND METHODS

Plasmid DNA. Reporter plasmids containing a cytomegalovirus promoter, firefly luciferase or a GFP (green fluorescence protein) encoding gene were purchased from Aldevron. When appropriate, plasmid DNA (pDNA) was labeled with the fluorescent dye YOYO-1 (Molecular Probes) using a molar ratio of 1 dye per 100 base pairs. For confocal microscopy, a noncoding control Cy3-labeled pDNA (Mirus) was used.

Chitosans. All chitosans used in this study are listed and characterized in Table 1.

Chitosans with MWs (weight average, M_w) ranging from 11.3 to 71.0 kDa were prepared by nitrous acid depolymerization of fully de-*N*-acetylated chitosan (F_A < 0.002, M_w 146 kDa), as previously described.[18] To produce the linear oligomers, depolymerized chitosan was conventionally reduced by $NaBH_4$, dialyzed, and lyophilized. Self-branched chitosans were prepared directly after depolymerization by omitting the reduction step and incubating the chitosan solution under selective reduction conditions ($NaCNBH_3$) for 48 h. The details of the synthesis may be found elsewhere.[19] The glycosylation of chitosans using the trimer 2-acetamido-2-deoxy-D-glucopyranosyl-β-(1−4)-2-acetamido-2-deoxy-D-glucopyranosyl-β-(1−4)-2,5-anhydro-D-mannofuranose (AAM) was carried out as previously described.[20]

To determine the degree of substitution, the chitosan samples were characterized by ^{1}H NMR (Avance DPX 400, Bruker). The weight and number averages of MW and MW distribution were determined by size-exclusion chromatography (SEC) with a refractive index detector (RI, Dawn Optilab 903, Wyatt Technology) and a multi-angle laser light scattering detector (MALLS, Dawn DSP, Wyatt Technology). All samples were dissolved in Milli-Q (MQ) deionized water (5−7 mg/mL) and filtered through a 0.22 μm syringe filter (Millipore). A TSK 3000 PWXL column (Tosoh Bioscience) was used, and the sample was eluted with 0.2 M ammonium acetate (pH 4.5) at a low flow rate of 0.5 mL/min.

The four different structure types of chitosan oligomers are denoted as linear (LIN), self-branched (SB), trisaccharide-substituted (TCO), and self-branched trisaccharide-substituted (SBTCO). The number used in the notation is the measured M_w.

For confocal microscopy, the chitosans were labeled with an Alexa Fluor 488 succinimidyl ester (Molecular Probes) using a molar ratio of 1 dye per 200 glucosamine residues.

Commercial Transfection Reagents. The lipid-based transfection reagent Lipofectamine 2000 (LFN) was purchased from Invitrogen. Exgen 500 (EXG), a linear polyethyleneimine (M_w 22 kDa)-based transfection reagent, was purchased from Fermentas. Both reagents were used as described in the manufacturers' protocol.

Preparation of pDNA−Chitosan Polyplexes. Formulations with different amino/phosphate (N/P) ratios were prepared by a self-assembly method while keeping the amount of pDNA constant (13.3 μg/mL). A stock solution of pDNA (0.5 mg/mL) was diluted with the necessary amount of sterile MQ water. Subsequently, the required amount of chitosan was added from a sterile filtered stock solution (2 mg/mL) during vortex mixing (1200 rpm). The assembled complexes were incubated for 30 min at room temperature before transfection.

Size Analysis. Nanoparticle size determination was performed using dynamic light scattering (DLS) on a Zetasizer Nano ZS (Malvern Instruments). Measurements were performed at a 173° angle and a temperature of 25 °C when analyzing samples in MQ water. Aggregation kinetics was measured by diluting the samples with an equal volume of hypertonic Opti-MEM (as described in the In Vitro Transfection section), and the analysis was performed at 37 °C. Each sample was analyzed in triplicate over a time span of 30 min. The polyplex size is expressed as the *z*-average hydrodynamic diameter obtained by a cumulative analysis of the correlation function using the viscosity and refractive index of water in the calculations.

Cell Culture. The HeLa cells used in these experiments were a gift from Prof. Marit Otterlei (Dept. of Cancer Research and Molecular Medicine, NTNU). The cells were grown in DMEM (Gibco, Invitrogen) supplemented with 1 mM nonessential amino acids (Gibco, Invitrogen), 10% FBS (Gibco, Invitrogen), and 1 mM L-glutamine (Sigma). When seeding cells for experiments, DMEM supplemented with 1% penicillin and streptomycin (PEST, Sigma) was used. The cells were cultivated at 37 °C in a humidified atmosphere with 5% CO_2.

In Vitro Transfection. HeLa cells were seeded in tissue culture wells 24 h prior to transfection experiments in densities giving 90% confluency on the day of transfection. The nanoparticles assembled in MQ water were diluted with an equal volume of Opti-MEM (Gibco, Invitrogen), supplemented with 270 mM mannitol (Sigma) and 20 mM HEPES (Sigma) for adjustment of the osmolarity to 300 mOsm/kg and pH to 7.2. Prior to the addition of the nanoparticles, the cells were incubated 20 min in HBSS (Gibco, Invitrogen) at 37 °C and 5% CO_2. A volume of 50 μL of polyplexes containing 0.33 μg pDNA was added to each well when using 96-well plates. The formulations were removed after 5 h of incubation and replaced by 200 μL of DMEM supplemented with PEST. For measurements of luciferase gene expression, the cells were washed with PBS and lysed using luciferase lysis buffer (Promega). Luciferase activity (expressed in relative light units, RLU) was measured using a luminometer (Molecular Devices). Total cell protein content was measured using the bicinchoninic acid assay (Pierce, IL) for normalizing the luciferase activity to the amount of cells. GFP expression was determined using flow cytometry, as described below.

Flow Cytometry. GFP expression and cellular uptake of YOYO-1-labeled pDNA were measured using a Gallios flow cytometer (Beckman Coulter). Cells expressing GFP were analyzed 24 h after transfection. The cells were washed in PBS, trypsinized, resuspended in ice-cold PBS supplemented with 4% FBS, filtered through 40 μm nylon mesh (BD), and kept on ice until the time of analysis. The cellular uptake of pDNA was determined by transfection with YOYO-1-labeled pDNA. After incubating with polyplexes for 3 h, the cells were washed with PBS and further incubated with DMEM for 30 min. Afterward, the cells were washed twice with warm PBS, trypsinized, resuspended in ice-cold PBS supplemented with 4% FBS, and centrifuged. The supernatant was removed, and the pellet was resuspended in ice-cold HBSS. These samples were subsequently analyzed. To estimate the contribution from extracellularly bound, labeled pDNA, the same samples were also analyzed after incubation with trypan blue (TB, 400 μg/mL) for 5 min.[21] Following TB treatment, the cells were centrifuged, resuspended in ice-cold HBSS, and analyzed. For each sample, 10 000 gated events were counted, and a dot plot of forward scatter versus side scatter was used to establish a collection gate for cells, excluding cellular debris, dead, and aggregated cells. The GFP- or YOYO-1-positive cells were excited using a 488 nm laser, and emitted light was collected at FL1 using a 525/40 band-pass filter. Nontransfected cells were analyzed as negative controls to set a threshold for fluorescence intensity (FI) above the level of autofluorescence. The percentage of GFP- or YOYO-1-positive cells was calculated, and the relative amount of internalized YOYO-1 was estimated from the median FI of the YOYO-1-positive population.

CLSM and Light Microscopy. HeLa cells were seeded onto eight-chamber microscopic slides (Ibidi GmbH, Germany) and transfected as described previously. After 2 h of incubation with nanoparticles, the cells to be investigated by CLSM were treated with 5 μg/mL of a CellMask plasma membrane stain (Invitrogen). Live cells were examined using a LSM 510 (Carl Zeiss Jena GmbH, Germany) equipped with a c-Apochromat 40x/1.2 NA W corr objective. Alexa 488-labeled chitosan, Cy3-labeled pDNA and CellMask were excited using the 488-nm argon, 543-nm HeNe and 633-nm HeNe laser lines, respectively. The emitted light was collected using 500−530 nm band-pass, 565−615 nm band-pass and 650 nm long pass filters. All of the images had resolutions of 512 × 512 pixels.

Images for evaluating the effects on cell morphology were captured with a 10×/0.25 objective using a CCD camera (Nikon DS Fi-1) equipped with a digital image recorder (Nikon Digital Sight DS-U2) that was mounted on a Nikon Eclipse TS100 microscope.

Alamar Blue Assay. The effect of transfection on metabolic activity was measured using an Alamar blue assay (Invitrogen). A total of 10 000 cells were seeded in wells and transfected as previously described. A volume of 10 μL of the Alamar blue assay reagent that was diluted in 100 μL of growth medium was added to the transfected cells 4 and 24 h post-transfection. The sample absorbances were measured 4 h after adding the assay reagent using a spectrophotometer (Molecular Devices) at 570 and 600 nm. The metabolic activity of the cells was evaluated as a percentage of reduction of the Alamar blue reagent relative to the nontransfected cells that were treated only with growth medium and assay reagent.

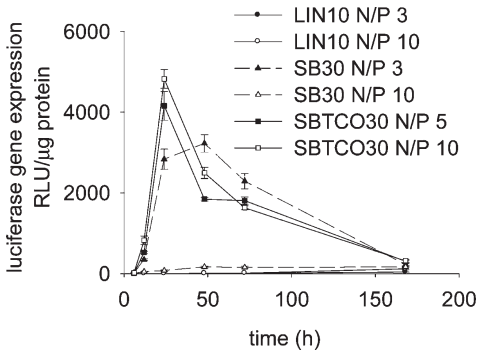

Figure 1. Time course of luciferase gene expression in HeLa cells transfected using nanoparticles formed with linear (LIN), self-branched (SB), and self-branched trisaccharide-substituted (SBTCO) chitosans at amino-phosphate (N/P) ratios of 3−10. Data represent mean values ± s.d., $n = 4$.

Statistical Analysis. The measured values were collected and expressed as mean values ± standard deviation (s.d.). Statistical differences between raw data were investigated using the SigmaPlot 11.0 software package with one-way ANOVA, in conjunction with a multiple comparison test (Holm-Sidak).

RESULTS

Gene Transfer Efficiency. In our preliminary experiments using HeLa cells, conventional chitosans with different chain lengths and degrees of acetylation exhibited extremely poor transfection efficiencies or no transfection at all (data not shown). In contrast, the self-branched and glycosylated chitosan previously developed in our laboratory[16] showed a transfection efficiency comparable to that of commercial transfection reagents, such as Exgen or Lipofectamine. Therefore, using HeLa cells as a model cell line, we decided to focus on self-branched chitosans and investigate the structure−activity relationships related to gene transfer. As illustrated in Figure 1, self-branched chitosans both with and without trisaccharide substitutions mediated transgene expression in HeLa cells. The transgene expression peaked at 24−48 h and then rapidly declined, even when the cells were split and kept under growing conditions.

However, the corresponding linear chitosan used as a starting material for the synthesis of self-branched chitosans did not transfect the cells. The same results were obtained with other linear chitosans having MWs from 6 to 150 kDa and degrees of acetylation from F_A 0 to 0.2 (data not shown).

Next, we synthesized a series of completely de-*N*-acetylated self-branched chitosans (F_A < 0.002) with and without the trisaccharide substitution. The synthesis and characterization of these compounds has been recently reported elsewhere.[19] As shown in Table 1, the branched chitosans had two- to three-fold higher MWs (M_w) compared with their linear precursors, reaching approximate M_w in the range of 10−70 kDa. Several

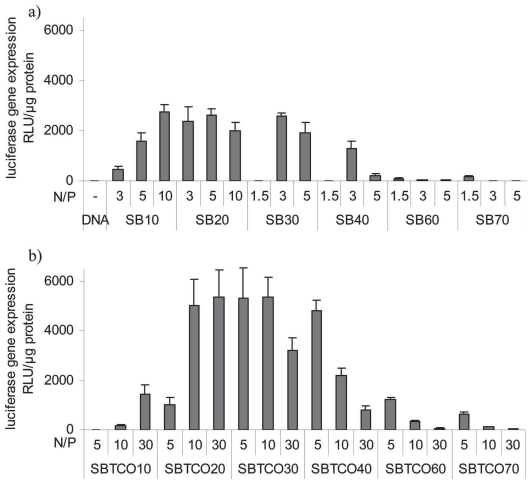

Figure 2. Effect of MW on transfection efficiency of self-branched chitosans. Luciferase gene expression 24 h after transfection using (a) self-branched (SB) or (b) self-branched trisaccharide-substituted (SBTCO) nanoparticles at different N/P ratios. Data represents mean values ± s.d., $n = 4$.

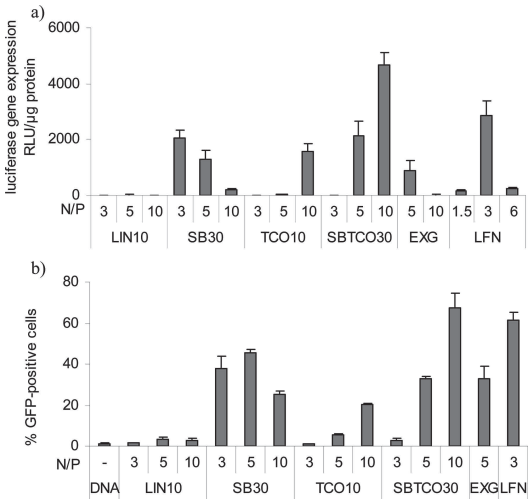

Figure 3. Effect of self-branching and glycosylation on transfection efficiency of chitosan in HeLa cells. Self-branched (SB), trisaccharide-substituted (TCO), or self-branched trisaccharide-substituted (SBTCO) chitosan were derived from linear chitosan (LIN) with a M_w of 10 kDa. The commercially available transfection reagents Exgen (EXG) and Lipofectamine 2000 (LFN) were also included. (a) Luciferase gene expression 24 h after transfection using pDNA−chitosan nanoparticles prepared at N/P ratios of 3−10. SBTCO30 at a N/P ratio of 10 yielded significantly higher ($p < 0.05$) luciferase gene expression compared with all other formulations. (b) Percentage of GFP-positive cells 24 h after transfection. SBTCO30 at a N/P ratio of 10 yielded significantly higher ($p < 0.05$) percentage of GFP-positive cells compared with all other formulations. Data represent mean values ± s.d., $n = 4$.

nanoparticles varying in the relative amount of chitosan, defined as ratio between protonable amines and phosphate (N/P), were prepared from each chitosan. The N/P ratios were chosen to cover the interval of optimal performance for each chitosan and varied due to large variation in the chitosan structures. For comparison purposes, nanoparticles with a N/P ratio of 5 were prepared from all chitosans. In total, 36 formulations were prepared and used to transfect HeLa cells. Figure 2 shows the dependence of gene transfer on the MW and amount of chitosan in the formulation for SB and SBTCO chitosans.

In the case of the SB chitosans (Figure 2a), the highest luciferase gene expression was mediated by formulations based on SB10, SB20 and SB30. The substitution of self-branched chitosans by the AAM trimer resulted in a significant increase in transfection efficiency and the highest luciferase expression was obtained with SBTCO20 and SBTCO30 (Figure 2b). Figure 2 also shows that luciferase gene expression decreased as the M_w of the chitosans increased above 40 kDa. For all chitosans, the transfection efficiency varied with the N/P ratio of the polyplexes. The optimal N/P ratio, where the maximum level of gene expression was observed, decreased with increasing MW. The formulations formed with SBTCO chitosan generally required higher N/P ratios than those with SB chitosans of comparable MW.

On the basis of the results presented in Figure 2, the self-branched chitosans SB30 and SBTCO30 were chosen for further experiments, in which the transfection efficiency was directly compared to their linear counterparts and two commercial transfection reagents, Exgen (EXG) and Lipofectamine 2000 (LFN). Figure 3a shows that LIN10, which was the starting material for production of SB30, TCO10, and SBTCO30 was not able to transfect the HeLa cells at all.

Substitution of LIN10 by AAM improved the ability to transfect the HeLa cells, and TCO10 required a N/P ratio of 10 to mediate transgene expression. Self-branching of LIN10 had a similar positive effect on transfection, and SB30 showed optimal transfection at N/P ratios of 3 and 5. The combination of self-branching and substitution was the most successful strategy and SBTCO30 at N/P 10 mediated an approximately three-fold higher luciferase expression level than SB30 and TCO10. SBTCO30 was the most effective gene carrier overall, showing approximately two- and five-fold higher luciferase expression levels than LFN and EXG, respectively (Figure 3a).

To compare the transfection efficiency of the chitosans at the single-cell level, HeLa cells were transfected with the same plasmid construct expressing GFP as a reporter and analyzed by flow cytometry. The results presented in Figure 3b show the percentage of GFP-positive cells after transfection using pDNA−chitosan nanoparticles based on LIN10, SB30, TCO10, SBTCO30, LFN, and EXG. In a similar manner to Figure 3a, LIN10-mediated poor transfection, giving a percentage of positive cells similar to that of naked pDNA. Transfection using SB30 resulted in up to 40% GFP-positive cells at N/P ratios of 3 and 5, whereas the TCO10 transfected up to 20% of the cells. SBTCO30 mediated the most successful transfection, reaching almost 70% transfection of cells at a N/P ratio of 10, which is similar to the results for LFN.

Nanoparticle Uptake. The most obvious reason for different transfection efficiencies may be differences in the cellular uptake of nanoparticles. Therefore, internalization of nanoparticles containing YOYO-1-labeled pDNA by HeLa cells was investigated. To distinguish between internalized and cell surface bound nanoparticles resistant to extensive washing, we analyzed the cells before and after incubation with TB, which is used as a

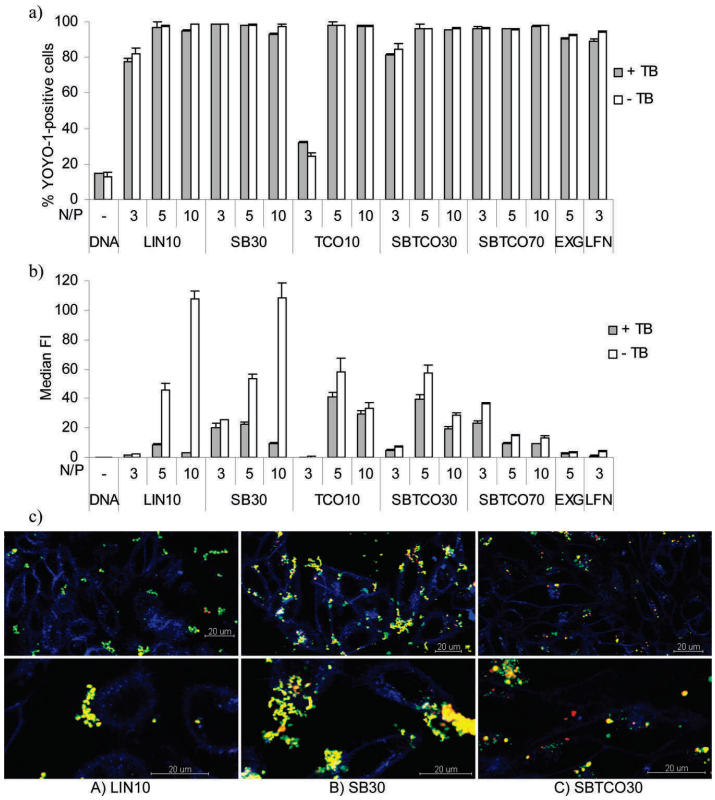

Figure 4. Cellular uptake of pDNA−chitosan polyplexes in HeLa cells. To distinguish between cell-surface-bound and internalized nanoparticles, the cells were quenched with trypan blue (TB). Gray bars show measurements after TB treatment (corresponding to internalized pDNA), whereas white bars show the measurements in the absence of TB (corresponding to both surface-bound and internalized DNA). (a) Percentage of YOYO-1-positive cells after the uptake of pDNA−chitosan polyplexes. (b) Relative amount of internalized pDNA expressed as median fluorescence intensity (FI) of the YOYO-1-positive cells. Data represent mean values ± s.d., $n = 4$. (c) Representative CLSM images of HeLa cells incubated for 2 h with polyplexes of (A) LIN10, (B) SB30, or (C) SBTCO30 at a N/P ratio of 5. The chitosans were labeled with Alexa Fluor 488 (green), pDNA was labeled with YOYO-1 (red), and the cellular plasma membrane was stained with CellMask (blue). The bar size is 20 μm.

quencher of extracellular fluorescence. Figure 4a shows that with a few exceptions, typically >95% of cells in the population internalized the nanoparticles.

The poor uptake of TCO10 at a N/P ratio of 3 likely resulted from premature dissociation due to the poor physical stability of TCO polyplexes at low N/P ratios. The percentage of YOYO-1-positive cells remained very similar both in the presence and absence of TB. However, Figure 4b shows that the relative amount of internalized pDNA was strongly dependent on the type of chitosan and the N/P ratio of the formulation. Furthermore, formulations based on LIN and SB chitosan showed a high amount of extracellularly bound pDNA, as evidenced by the substantial reduction in FI after incubation of the cells with TB.

The median values of FI following the TB treatment presented in Figure 4b show that TCO10 and SBTCO30 chitosans mediated the highest uptake of pDNA. The cells transfected with these chitosans showed relatively low amounts of surface-bound nanoparticles. Compared with SBTCO30, a lower amount of pDNA was delivered by SBTCO70. The fluorescence displayed by the cells transfected with the LIN and SB chitosans was significantly quenched by TB and was therefore mediated by extracellular nanoparticles. In the formulations with increasing amounts of chitosan, such as LIN10 and SB30 at a N/P ratio of 10, the median FI decreased 22- and 12-fold, respectively, after incubation with TB. Therefore, Figure 4b demonstrates that the HeLa cells transfected with TCO and SBTCO chitosans internalized most pDNA, whereas cells transfected with LIN and SB chitosans exhibited a high amount of cell surface-associated pDNA. Compared with chitosans in general, transfections performed with EXG or LFN led to a weak internalization of pDNA. Figure 4b confirms that naked pDNA was not taken up by the cells.

The cellular uptake of polyplex formulations of LIN10, SB30, and SBTCO30 at a N/P ratio of 5 was also investigated by CLSM, as presented in Figure 4c. These images show large aggregates of LIN10 and SB30 nanoparticles bound to the cell surface, and only a few particles appear to have been internalized. In contrast, cells transfected with SBTCO30 showed fewer extracellular nanoparticles, and the internalized nanoparticles were smaller and more abundant compared with cells transfected with LIN10 or SB30.

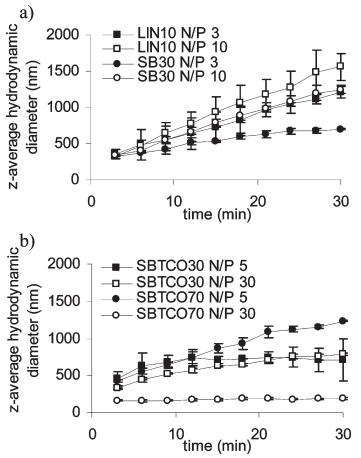

Figure 5. Time-dependent aggregation of pDNA−chitosan polyplexes during transfection. (a) Aggregation of polyplexes formed with unsubstituted chitosans LIN10 and SB30 at N/P ratios of 3−10. (b) Aggregation of polyplexes formed with substituted chitosans SBTCO30 and SBTCO70 at N/P ratios of 5−30. The *z*-average hydrodynamic diameter of the particles was measured after diluting the samples with an equal volume of CO_2-saturated hypertonic Opti-MEM to obtain isotonic formulations with a pH of 7.2 and an osmolarity of 300 mOsm/kg. Data represent mean values ± s.d., $n = 3$.

Formulation Stability. Because of differences in the apparent size of the nanoparticles, as revealed in the CLSM images (Figure 4c), we investigated the colloidal stability of different chitosan formulations after dilution in a CO_2-saturated hypertonic Opti-MEM at 37 °C. Previously, it has been shown that AAM-substitution of chitosan renders the nanoparticles more stable toward aggregation.[16] However, the analysis was performed in PBS or in Hanks balanced salt solution and not in a cell culture medium under conditions identical to the transfection experiment. Initially, all pDNA−chitosan nanoparticles prepared in MQ water had comparable *z*-average hydrodynamic diameters of approximately 80−100 nm (Table 2, Supporting Information). However, following dilution in cell culture media at 37 °C, the nanoparticles rapidly increased in size and aggregated (Figure 5).

The rate of aggregation was strongly dependent on the type of chitosan and the N/P ratio of the formulation. Figure 5a shows that in the case of nanoparticles formed with the unsubstituted chitosans, SB30 nanoparticles aggregated to a lower extent than LIN10. For both chitosans, the aggregation rate increased as the N/P ratio was increased from 3 to 10. The AAM substitution of chitosan clearly reduced the rate of aggregation (Figure 5b). However, formulations of SBTCO30 still formed aggregates with a *z*-average diameter of ∼600 nm over 30 min. Surprisingly, no effect of the N/P ratio on the aggregation rate was observed for SBTCO30. In contrast, the formulation prepared from SBTCO70 at a N/P ratio of 30 showed no aggregation at all, and the nanoparticles remained well below 200 nm in diameter.

Nanoparticle Cytotoxicity. Changes in chain architecture of chitosan may have an influence on the cytotoxicity of this compound. Therefore, cytotoxicity mediated by pDNA−chitosan formulations was investigated using the Alamar blue assay, and the metabolic activity of HeLa cells was measured 4 and 24 h after transfection. Figure 6a shows that cells treated with SBTCO chitosans of different MW retained high metabolic activity after transfection. No obvious relationship between MW and cytotoxicity was found.

However, a few formulations of SBTCO40 and SBTCO60 mediated a minor but significant decrease in metabolic activity compared with untreated cells. Furthermore, Figure 6b shows that the self-branching of chitosan did not result in higher toxicity compared with their linear counterparts. When comparing the cytotoxicity of chitosans with that of the commercial transfection reagents (Figure 6b,c), it is apparent that both EXG and LFN exerted significantly higher toxicity. The metabolic activity in cells treated with EXG and LFN was further reduced 24 h after transfection, whereas cells transfected using chitosan remained unaffected. As shown in Figure 6c, cells treated with EXG or LFN also displayed severe changes in morphology 24 h after transfection, whereas the chitosan-treated cells appeared comparable to untreated cells.

DISCUSSION

This study demonstrates that self-branching of chitosan yields efficient and safe gene delivery in cells not transfected by linear chitosans. The interest in branched chitosan architectures was initiated by a recent study in which self-branching was used as a tool to increase the physical stability of polyplexes formed with glycosylated chitosan oligomers.[16] The resulting self-branched and glycosylated chitosan has been shown to possess higher solubility at pH > 7 and mediated significantly higher transgene expression than the optimized linear oligomers in HEK293 and HepG2 cells.[16] Therefore, we decided to investigate systematically transfection efficiency of branched chitosans and identify structures with high gene transfer efficiency.

As shown in this study, the transfection efficiency of self-branched chitosans was found to depend on MW, and the highest gene transfer was obtained using formulations with a certain combination of MW and N/P. Because MW and N/P determine physical stability of nanoparticles,[8,10,22] the structure−activity relationship observed in Figure 2 may be explained in terms of a balance between polyplex stability and unpacking. The efficient gene transfer mediated by nanoparticles formed with SB/SBTCO20−30 indicates that these possess optimal stability, allowing the intracellular unpacking and expression of pDNA. Increasing the MW of the chitosan lead to more stable polyplexes[10] that may dissociate too slowly, as recently shown by Thibault et al.[11] To maintain transgene expression, the resulting higher MW must be compensated by a lower N/P ratio and vice versa (Figure 2). Nanoparticles falling outside the optimal stability window are likely to possess interaction strengths that are too high or too low between the chitosan and pDNA. One example of the former is the nanoparticles formed with high MW chitosans, such as SB/SBTCO60−70, especially at a high N/P ratio. For the AAM-substituted SBTCO chitosans, the range of optimal stability was shifted toward higher N/P ratios and higher MW (Figure 2b). This was likely a consequence of the glycosylation, which has been previously shown to weaken the physical stability of pDNA−chitosan nanoparticles.[10,16]

It has been previously reported that HeLa cells are difficult to transfect with chitosans.[12,13] The discovery that only self-branched but not linear chitosans efficiently transfected HeLa cells was rather surprising. Direct comparison of chitosans derived from the linear chitosan LIN10 (Figure 3), which was previously

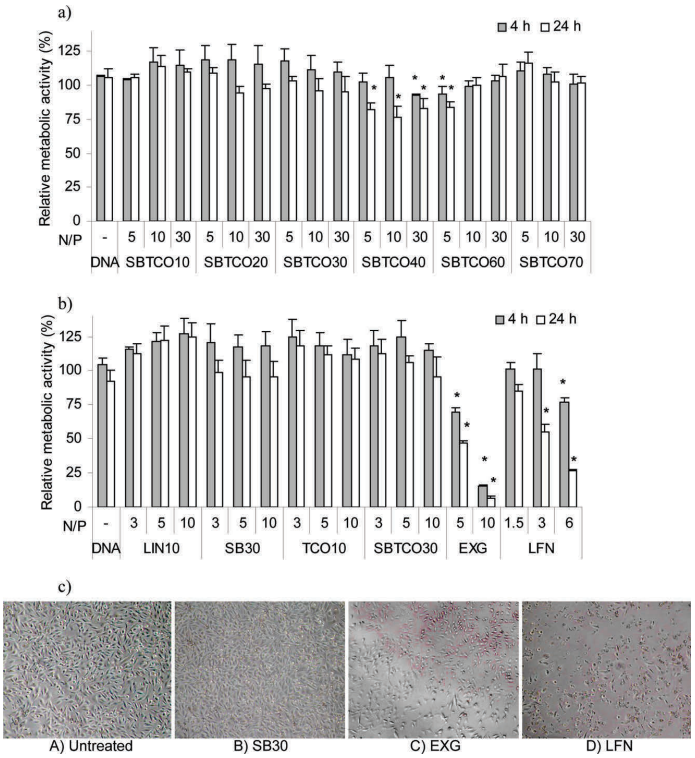

Figure 6. Metabolic activity of transfected HeLa cells relative to untreated cells measured by the Alamar blue assay. Activity was measured 4 h (gray bars) and 24 h (white bars) after transfection using pDNA formulated with (a) self-branched chitosans of different MW and (b) chitosans varying in molecular architecture (LIN10, SB30, TCO10, SBTCO30), Exgen (EXG), and Lipofectamine (LFN). Data represent mean values ± s.d., $n = 4$. Formulations that yielded significantly reduced ($p < 0.05$) metabolic activity compared with untreated cells are indicated with asterisks ("*"). (c) Representative microscopy images at 10× magnification of (A) untreated HeLa cells and (B) cells 24 h after treatment with SB30 at N/P 5 or complexes of (C) EXG at N/P 5 or (D) LFN at a weight ratio of 3.

tailored for the transfection of HEK293 cells, demonstrates that the molecular architecture of chitosan is crucial for gene transfer performance. The combination of self-branching and substitution of the linear chitosan resulted in a high transfection efficiency, exceeding that of EXG and LFN (Figure 3). The lack of transgene expression using the linear chitosans may be related to poor uptake or poor intracellular trafficking. As previously reported, the polyplexes of LIN, TCO, and SBTCO possessed similar sizes and properties.[16,23] However, the nanoparticles of TCO and SBTCO have been shown to be less prone to aggregation at physiological pH values.[16] Despite aggregation, the linear chitosans showed high uptake levels and were able to transfect HEK293 cells.[8,10] This illustrates cell-line-specific differences related to the uptake and cellular processing of the different nanoparticles, as previously reported by von Gersdorff.[24] HeLa cells may be unable to take up larger aggregates, or, alternatively, different endocytic mechanisms may be involved in the uptake and intracellular trafficking of different types of nanoparticles. These differences may also be due to a different occurrence of chitosan-degrading enzymes in the endosomes, making protection of the pDNA more important in certain cell lines.

For most chitosan formulations, the efficiency of transfection on the single-cell level correlates with the amount of transgene produced, indicating a similar level of GFP-production per cell. EXG gives a relatively high percentage of positive cells but still yields very low levels of luciferase transgene expression. This may also indicate high cytotoxicity because dying cells will be excluded from flow cytometry analysis but not from the luciferase analysis.

The differences in transfection efficiency of the chitosans cannot only be explained by relative differences in cellular uptake levels of the nanoparticles. All chitosan nanoparticles showed efficient cellular uptake compared with naked pDNA, but there was no correlation between the percentage of YOYO-1-positive cells in Figure 4a and the transfection efficiency.

Although almost all cells internalized the nanoparticles, there were large differences in the relative amount of cell surface bound and internalized pDNA among the different formulations (Figure 4b). The amount of DNA delivered by LIN formulations was considerably lower compared with the other chitosans and may thus be a reason for the poor transfection efficiency. Furthermore, most chitosan formulations showing poor cellular uptake also mediated poor transfection (Figure 3a). In general, formulations with higher N/P ratio seem to have reduced amounts of internalized pDNA but higher levels of transgene expression. However, cells transfected with LFN and EXG also exhibited

very low uptake of pDNA, with levels comparable to the LIN formulations, but they showed reasonably high levels of luciferase expression. Therefore, the relationship between the amount of internalized pDNA and the amount of transgene produced seems to be strongly carrier-dependent. This indicates that LFN and EXG transfection leads to more efficient intracellular processing of internalized pDNA, which has also been suggested in several previous studies.[25−27]

The extensive binding of LIN and SB nanoparticles to the cell surface seemed to increase with N/P ratio and was accompanied by decreasing amount of internalized pDNA. This may be a consequence of increasing amounts of free chitosan in the formulations, which competes for cell-surface binding. It has been previously shown that at a N/P ratio of 10, 50−70% of the chitosan in polyplex formulations is unbound to pDNA.[23] The higher uptake of SB nanoparticles compared with LIN, despite a similar extent of cell surface binding, may be related to a lower aggregation rate of SB nanoparticles.

The CLSM images (Figure 4c) qualitatively confirm the flow cytometry data, showing large amounts of extracellular LIN and SB nanoparticles that appear to be aggregated. On the contrary, cells transfected with SBTCO exhibited mostly intracellular nanoparticles. The DLS analysis of the formulations performed under transfection conditions confirmed the aggregation (Figure 5). Apparently, the aggregating formulations made from linear chitosans sediment on and bind to cell surfaces. The internalization of large aggregates is clearly limited and leads to accumulation of aggregated nanoparticles and free chitosan. SB chitosans also showed aggregation and extensive binding to the cell surface (Figure 4c), and CLSM did not show any apparent differences compared to LIN. However, because SB nanoparticles were taken up (Figure 4b) and able to transfect the cells (Figures 2 and 3), CLSM failed to visualize these intracellular complexes in the presence of the large and highly fluorescent aggregates.

Interestingly, there was no straightforward correlation between the extent of polyplex aggregation (Figure 5) and gene transfer efficiency (Figures 2 and 3). The most stable formulation, SBTCO70 at a N/P ratio of 30, mediated poor gene transfer (Figure 2b). The aggregating formulations of SBTCO30 were far more efficient. Similarly, the two SBTCO30 formulations showed a similar degree of aggregation but exhibited different transfection efficiencies. This indicates that colloidal stability of formulation itself does not guarantee successful gene transfer. However, a high degree of aggregation seems to correlate with poor transfection. For instance, the formulations with the highest degree of aggregation, LIN10 with a N/P ration of 3 or 10 and SB30 with an N/P ratio of 10, failed to transfect the HeLa cells. However, the polyplexes of SB30 (N/P ratio of 3), TCO10, and SBTCO30 (N/P ratio of 30) that had lower degrees of aggregation were able to mediate the most efficient transfections. Therefore, strategies to increase the colloidal stability of chitosan nanoparticles without negatively influencing the physical stability and cellular uptake are needed. Such strategies could include the grafting of chitosan with polyethylene glycol (PEG), which has been previously shown to prevent aggregation in the presence of serum and bile.[28] Another possible approach is to coat the nanoparticles with multivalent polymers, such as copolymers of *N*-(2-hydroxy-propyl)methacrylamide (PHPMA), as described by Oupicky et al.[29]

The chitosan-based nanoparticles presented in this study were based solely on chitosan and no other synthetic components, thereby maintaining the high safety profile that is a hallmark of chitosan. The analysis of post-transfection cellular metabolic activity and the morphological observation of the transfected cells (Figure 6) once again confirm the low toxicity of chitosan. Although some formulations showed a subtle but significant reduction in metabolic activity, these effects were minor compared with EXG or LFN, which also exerted a visible effect on cellular morphology (Figure 6c). This result correlates well with many previous studies, implying that chitosan is a safe nonviral vector for potential use as a vector in gene therapy in vivo.[22,28,30−32]

■ CONCLUSIONS

This study shows that small modifications in the chitosan architecture, such as the self-branching of linear chitosan, that do not involve substantial changes in chemical composition can profoundly enhance gene transfer performance. The poor transfection efficiency of linear chitosans in HeLa cells seems to be related to low cellular uptake because of poor formulation stability and extensive binding of the aggregated nanoparticles to the cell surface. Compared with linear chitosans, nanoparticles formed with self-branched chitosans show higher colloidal stabilities and enhanced cellular uptake levels and were able to mediate high transgene expression in HeLa cells. The glycosylation of self-branched chitosans reduced extensive binding to the cell surface and improved the uptake of nanoparticles. However, high uptake of nanoparticles did not always correlate with high transgene expression. Only the nanoparticles within a certain range of MW and N/P ratio yielded efficient gene transfer, indicating the importance of the balance between DNA protection and DNA dissociation. Structure−activity relationships revealed that self-branched chitosans in the M_w range of 20−30 kDa are the most potent gene transfer vehicles, showing high transfection efficiencies and low cytotoxicity.

■ ASSOCIATED CONTENT

Supporting Information. Size determination of pDNA−chitosan nanoparticles prepared in MQ-water. This material is available free of charge via the Internet at http://pubs.acs.org.

■ AUTHOR INFORMATION

Corresponding Author
*E-mail: sabina.strand@biotech.ntnu.no.

■ ACKNOWLEDGMENT

This work was supported by a Ph.D. grant from NTNU (J.M.) and by the Norwegian Research Council (grant 182695/40). We are grateful to Ann-Sissel Ulset (Dept. of Biotechnology, NTNU) for performing the SEC-MALLS analysis and Kristin G. Sæterbø (Dept. of Physics, NTNU) for assistance with cell culture and flow cytometry. We are also grateful to Prof. Catharina de L. Davies for giving us the opportunity to use the equipment and facilities at the Dept. of Physics (Biophysics and Medical Technology, NTNU). We would also like to thank Elen K. Møller for performing the preliminary nanoparticle uptake experiments.

■ REFERENCES

(1) Sun, J. Y.; Anand-Jawa, V.; Chatterjee, S.; Wong, K. K. Immune responses to adeno-associated virus and its recombinant vectors. *Gene Ther.* **2003**, *10*, 964–976.

(2) Check, E. Gene therapy put on hold as third child develops cancer. *Nature* **2005**, *433*, 561.
(3) Graham, A.; Walker, R.; Baird, P.; Hahn, C. N.; Fazakerley, J. K. CNS gene therapy applications of the semliki forest virus 1 vector are limited by neurotoxicity. *Mol Ther.* **2006**, *13*, 631–635.
(4) Thomas, C. E.; Ehrhardt, A.; Kay, M. A. Progress and problems with the use of viral vectors for gene therapy. *Nat. Rev. Genet.* **2003**, *4*, 346–358.
(5) Filion, D.; Lavertu, M.; Buschmann, M. D. Ionization and solubility of chitosan solutions related to thermosensitive chitosan/glycerol-phosphate systems. *Biomacromolecules.* **2007**, *8*, 3224–3234.
(6) Strand, S. P.; Tømmeraas, K.; Vårum, K. M.; Østgaard, K. Electrophoretic light scattering studies of chitosans with different degrees of N-acetylation. *Biomacromolecules.* **2001**, *2*, 1310–1314.
(7) Danielsen, S.; Vårum, K. M.; Stokke, B. T. Structural analysis of chitosan mediated DNA condensation by AFM: influence of chitosan molecular parameters. *Biomacromolecules.* **2004**, *5*, 928–936.
(8) Lavertu, M.; Méthot, S.; Tran-Khanh, N.; Buschmann, M. D. High efficiency gene transfer using chitosan/DNA nanoparticles with specific combinations of molecular weight and degree of deacetylation. *Biomaterials* **2006**, *27*, 4815–4824.
(9) Köping-Höggard, M.; Vårum, K. M.; Issa, M.; Danielsen, S.; Christensen, B. E.; Stokke, B. T.; Artursson, P. Improved chitosan-mediated gene delivery based on easily dissociated chitosan polyplexes of highly defined chitosan oligomers. *Gene Ther.* **2004**, *11*, 1441–1452.
(10) Strand, S. P.; Lelu, S.; Reitan, N. K.; de Lange Davies, C.; Artursson, P.; Vårum, K. M. Molecular design of chitosan gene delivery systems with an optimized balance between polyplex stability and polyplex unpacking. *Biomaterials* **2009**, *31*, 975–987.
(11) Thibault, M.; Nimesh, S.; Lavertu, M.; Buschmann, M. D. Intracellular trafficking and decondensation kinetics of chitosan-pDNA polyplexes. *Mol Ther.* **2010**, *18*, 1787–1795.
(12) Gao, S.; Chen, J.; Xu, X.; Ding, Z.; Yang, Y.-H.; Hua, Z.; Zhang, J. Galactosylated low molecular weight chitosan as DNA carrier for hepatocyte-targeting. *Int. J. Pharm.* **2003**, *255*, 57–68.
(13) Kiang, T.; Wen, J.; Lim, H. W.; Leong, K. W. K. W. The effect of the degree of chitosan deacetylation on the efficiency of gene transfection. *Biomaterials* **2004**, *25*, 5293–5301.
(14) Hashimoto, M.; Morimoto, M.; Saimoto, H.; Shigemasa, Y.; Sato, T. Lactosylated chitosan for DNA delivery into hepatocytes: the effect of lactosylation on the physicochemical properties and intracellular trafficking of pDNA/chitosan complexes. *Bioconjugate Chem.* **2006**, *17*, 309–316.
(15) Issa, M. M.; Köping-Höggård, M.; Tømmeraas, K.; Vårum, K. M.; Christensen, B. E.; Strand, S. P.; Artursson, P. Targeted gene delivery with trisaccharide-substituted chitosan oligomers in vitro and after lung administration in vivo. *J. Controlled Release* **2006**, *115*, 103–112.
(16) Strand, S. P.; Issa, M. M.; Christensen, B. E.; Vårum, K. M.; Artursson, P. Tailoring of chitosans for gene delivery: novel self-branched glycosylated chitosan oligomers with improved functional properties. *Biomacromolecules* **2008**, *9*, 3268–3276.
(17) Fischer, D.; Bieber, T.; Li, Y.; Elsässer, H.-P.; Kissel, T. A. Novel non-viral vector for DNA delivery based on low molecular weight, branched polyethylenimine: effect of molecular weight on transfection efficiency and cytotoxicity. *Pharm. Res.* **1999**, *16*, 1273–1279.
(18) Tømmeraas, K.; Vårum, K. M.; Christensen, B. E.; Smidsrød, O. Preparation and characterisation of oligosaccharides produced by nitrous acid depolymerisation of chitosans. *Carbohydr. Res.* **2001**, *333*, 137–144.
(19) Tømmeraas, K.; Strand, S. P.; Christensen, B. E.; Smidsrød, O.; Vårum, K. M. Preparation and characterization of branched chitosans. *Carbohydr. Polym.* **2011**, *83*, 1558–1564.
(20) Tømmeraas, K.; Köping-Höggård, M.; Vårum, K. M.; Christensen, B. E.; Artursson, P.; Smidsrød, O. Preparation and characterisation of chitosans with oligosaccharide branches. *Carbohydr. Res.* **2002**, *337*, 2455–2462.
(21) Ma, Z.; Lim, L.-Y. Uptake of chitosan and associated insulin in Caco-2 Cell monolayers: a comparison between chitosan molecules and chitosan nanoparticles. *Pharm. Res.* **2003**, *20*, 1812–1819.
(22) Köping-Höggard, M.; Tubulekas, I.; Guan, H.; Edwards, K.; Nilsson, M.; Vårum, K.; Artursson, P. Chitosan as a nonviral gene delivery system. Structure-property relationships and characteristics compared with polyethyleneimine in vitro and after lung administration in vivo. *Gene Ther.* **2001**, *8*, 1108–1121.
(23) Reitan, N. K.; Maurstad, G.; de Lange Davies, C.; Strand, S. P. Characterizing DNA condensation by structurally different chitosans of variable gene transfer efficacy. *Biomacromolecules.* **2009**, *10*, 1508–1515.
(24) von Gersdorff, K.; Sanders, N. N.; Vandenbroucke, R.; De Smedt, S. C.; Wagner, E.; Ogris, M. The internalization route resulting in successful gene expression depends on both cell line and polyethylenimine polyplex type. *Mol. Ther.* **2006**, *14*, 745–753.
(25) Cohen, R. N.; van der Aa, M. A. E. M.; Macaraeg, N.; Lee, A. P.; Szoka, F. C., Jr. Quantification of plasmid DNA copies in the nucleus after lipoplex and polyplex transfection. *J. Controlled Release* **2009**, *135*, 166–174.
(26) Hama, S.; Akita, H.; Ito, R.; Mizuguchi, H.; Hayakawa, T.; Harashima, H. Quantitative comparison of intracellular trafficking and nuclear transcription between adenoviral and lipoplex systems. *Mol. Ther.* **2006**, *13*, 786–794.
(27) Chen, H. H.; Ho, Y.-P.; Jiang, X.; Mao, H.-Q.; Wang, T.-H.; Leong, K. W. Quantitative comparison of intracellular unpacking kinetics of polyplexes by a model constructed from quantum Dot-FRET. *Mol. Ther.* **2008**, *16*, 324–332.
(28) Jiang, X.; Dai, H.; Leong, K. W.; Goh, S. H.; Mao, H. Q.; Yang, Y. Y. Chitosan-g-PEG/DNA complexes deliver gene to the rat liver via intrabiliary and intraportal infusions. *J. Gene Med.* **2006**, *8*, 477–487.
(29) Oupicky, D.; Ogris, M.; Howard, K. A.; Dash, P. R.; Ulbrich, K.; Seymour, L. W. Importance of lateral and steric stabilization of polyelectrolyte gene delivery vectors for extended systemic circulation. *Mol. Ther.* **2002**, *5*, 463–472.
(30) Nimesh, S.; Thibault, M.; Lavertu, M.; Buschmann, M. Enhanced gene delivery mediated by low molecular weight chitosan/DNA complexes: effect of pH and serum. *Mol. Biotechnol.* **2010**, *46*, 182–196.
(31) Lee, M.; Nah, J.-W.; Kwon, Y.; Koh, J. J.; Ko, K. S.; Kim, S. W. Water-soluble and low molecular weight chitosan-based plasmid DNA delivery. *Pharm. Res.* **2001**, *18*, 427–431.
(32) Jiang, H.-L.; Kwon, J.-T.; Kim, E.-M.; Kim, Y.-K.; Arote, R.; Jere, D.; Jeong, H.-J.; Jang, M.-K.; Nah, J.-W.; Xu, C.-X.; Park, I.-K.; Cho, M.-H.; Cho, C.-S. Galactosylated poly(ethylene glycol)-chitosan-*graft*-polyethylenimine as a gene carrier for hepatocyte-targeting. *J. Controlled Release* **2008**, *131*, 150–157.

Supporting Information

Table 2. Z-average hydrodynamic diameter of different chitosan-based polyplexes with M_w 10, 30 or 70 kDa and N/P ratio 3-30. The data represent mean values ± s.d., n = 3.

Chitosan	**LIN10**		**SB30**		**TCO30**		**SBTCO30**		**SB70**		**SBTCO70**	
N/P	**3**	**10**	**3**	**10**	**5**	**30**	**5**	**30**	**3**	**10**	**5**	**30**
Z-avg. ± s.d. (nm)	82±2	78±3	86±3	93±4	82±1	90±4	99±1	95±2	80±1	92±1	79±3	95±2

Paper II

Journal of Controlled Release 158 (2012) 261–268

Contents lists available at SciVerse ScienceDirect

Journal of Controlled Release

journal homepage: www.elsevier.com/locate/jconrel

siRNA delivery with chitosan nanoparticles: Molecular properties favoring efficient gene silencing

Jostein Malmo, Hanne Sørgård, Kjell M. Vårum, Sabina P. Strand *

Norwegian Biopolymer Laboratory (NOBIPOL), Department of Biotechnology, Norwegian University of Science and Technology (NTNU), N-7491 Trondheim, Norway

ARTICLE INFO

Article history:
Received 7 September 2011
Accepted 6 November 2011
Available online 17 November 2011

Keywords:
Chitosan
siRNA
Nanoparticles
Chain length
Chain architecture

ABSTRACT

Chitosan has gained increasing interest for siRNA delivery. Although chitosan covers a family of structurally different polysaccharides, most siRNA delivery studies have been performed with conventional partially *N*-acetylated chitosans. Herein, the purpose was to identify fundamental chitosan molecular properties favoring siRNA delivery and efficient gene silencing in mammalian cells. Nanoparticles were prepared from well-defined chitosans of various chemical compositions, degrees of polymerization (DP_n) and chain architectures. Structure-activity relationships were determined by the cellular uptake of siRNA and the knockdown efficiency at mRNA and protein levels. Additionally, the nanoparticle cytotoxicity was evaluated on the basis of cellular metabolic activity and membrane integrity. Our results show that the most efficient gene silencing was achieved using fully de-*N*-acetylated chitosans with intermediate chain lengths (DP_n 100–300). These chitosans mediated efficient siRNA delivery at low siRNA concentrations and, in several cell lines, potent long-term silencing of both exogenous and endogenous target genes, with minimal cytotoxicity.

1. Introduction

RNA-interference (RNAi) represents a new and potent strategy for post-transcriptional gene silencing that can be mediated by delivery of synthetic double-stranded small interfering RNA (siRNA). This process results in the degradation of homologous mRNA and thereby causes knockdown of the specific target-gene. RNAi is well established as a tool for studying gene function [1] and has shown promising therapeutic possibilities for the treatment of cancer [2], viral infections [3], and inflammatory diseases [4]. Despite its many promises, the intracellular delivery of siRNA has proved difficult because these macromolecules (~13 kDa) are easily degraded by nucleases and cannot cross cell membranes. Consequently, siRNA cannot be efficiently transported into cells without the aid and protection of suitable carriers.

One of the candidates for nucleic acid delivery that has gained considerable attention during the last decade is chitosan. Chitosan is a family of biopolymers derived from chitin, composed of β-1,4 linked *N*-acetylated D-glucosamine (GlcNAc; A-unit) and D-glucosamine (GlcN; D-unit). Chitosans can be prepared with widely varying content of GlcNAc and chain lengths [5]. One of the main advantages of chitosans in biomedical applications is their excellent biocompatibility and safety profile, in addition to being biodegradable in humans [6,7]. Chitosan has repeatedly been shown to possess low toxicity both *in vitro* [8–10] and *in vivo* [11] without causing any deleterious immunologic responses [11].

Chitosan is a weak polybase with a pKa that is close to 6.6 [12], and its charge density, thus, strongly depends on the pH. The high degree of protonization of amino groups at pH values below the pKa strongly favors electrostatic interactions with polyanionic molecules such as DNA or siRNA, leading to the formation of nanosized particles with different shapes and properties [13,14]. A low-charge density at physiological conditions contributes to low cytotoxicity and may facilitate intracellular release of siRNA from the nanoparticles, but may also lead to premature dissociation of the nanoparticles. To circumvent premature dissociation, the nanoparticles are often stabilized by ionic crosslinkers such as tripolyphosphate, or, alternatively, chitosan is quarternized by the trimethylation of amino groups [15–17]. However, these approaches may lead to excessive stability of the nanoparticles and increased cytotoxicity.

The chitosan family offers enormous structural and functional versatility. It has been clearly demonstrated in studies on plasmid DNA delivery that tailoring of the degree of polymerization (DP_n), the fraction of *N*-acetylated units (F_A) and the chain architecture is essential to optimizing the delivery efficiency of the nanoparticles [8,9,18-20]. Compared to DNA delivery, relatively little is known about the effect of the chitosan carrier on siRNA delivery efficiency. Most studies employing chitosan for siRNA delivery have been performed using conventional partially de-*N*-acetylated chitosans with $F_A > 0.15$ and high N/P ratios. There are a few reports showing that chitosans with higher charge densities and higher molecular weights mediate more efficient siRNA delivery than those with high F_A and low DP_n

* Corresponding author.
E-mail address: sabina.strand@biotech.ntnu.no (S.P. Strand).

0168-3659/$ – see front matter © 2011 Elsevier B.V. All rights reserved.
doi:10.1016/j.jconrel.2011.11.012

[13,16,17,21]. However, no systematic investigation that includes a broader range of less conventional chitosans has yet been performed.

The overall goal of this study was to identify the molecular properties of chitosans that favor the cellular uptake of siRNA and an efficient knockdown of genes. By using well-defined and characterized chitosans prepared in our laboratory to formulate the nanoparticles, the efficiency of siRNA delivery was determined both on endogenously expressed and stably transfected target genes. In addition, off-target effects as well as nanoparticle-mediated toxicity were evaluated. We show that fully de-*N*-acetylated linear chitosans of $DP_n > 50$ efficiently mediate gene silencing at low doses and in different cell lines, including primary cells, with minimal toxic effects.

2. Materials and methods

2.1. siRNA

The following siRNAs used in this study were predesigned and supplied by Ambion: anti-EGFP (Silencer), anti-GAPDH (Silencer) in addition to a non-targeting (NT) siRNA sequence (Silencer, Negative Control #1). For flow cytometry, a NT Alexa-647 conjugated siRNA duplex (AllStars Negative Control, Qiagen) was used.

2.2. Transfection reagents

The chitosans used in this study are described and characterized in Table 1.

All of the fully de-*N*-acetylated chitosans used in this study were prepared in our laboratory from shrimp chitin. Chitosans with degrees of polymerization (DP_n) ranging from approximately 50 to 300 monomers were prepared by nitrous acid depolymerization and $NaBH_4$ reduction of a fully de-*N*-acetylated chitosan ($F_A < 0.002$), as previously described [22]. The self-branched chitosan was prepared by omitting the reduction step and incubating the chitosan solution under selective reduction conditions ($NaCNBH_3$) for 48 h [23]. Glycosylation of the self-branched chitosan using the trimer 2-acetamido-2-deoxy-D-glucopyranosyl-β-(1–4)-2-acetamido-2-deoxy-D-glucopyranosyl-β-(1–4)-2,5-anhydro-D-mannofuranose (AAM) was performed as previously described [24]. The partially *N*-acetylated chitosan (F_A 0.15) was provided by Pronova Biopolymers (Drammen, Norway).

To determine the F_A and the degree of substitution (d.s.), the chitosan samples were characterized by ^1H NMR (Avance DPX 400, Bruker). The weight and number averages of the molecular weight and the polydispersity distributions were determined by size-exclusion chromatography (SEC) with a refractive index detector (RI, Dawn Optilab 903, Wyatt Technology) and a multiangle laser light scattering detector (MALLS, Dawn DSP, Wyatt Technology). All samples were dissolved in Milli-Q (MQ) deionized water (5–7 mg/mL) and filtered through a 0.22 μm syringe filter (Millipore). A TSK 3000 PWXL column (Tosoh Bioscience) was used, and the sample was eluted with 0.2 M ammonium acetate (pH 4.5) at a low flow rate of 0.5 mL/min.

The four different structure types of chitosan oligomers are denoted as linear (LIN), self-branched (SB), self-branched trisaccharide-substituted (SBTCO), and *N*-acetylated (F_A). The number used in the notation is the measured DP_n, while the *N*-acetylated chitosan is denoted by its fraction of *N*-acetylated units.

The lipid-based transfection reagent Lipofectamine RNAiMAX (RiM) was purchased from Invitrogen, and lipoplexes were prepared, as described in the manufacturer's protocol at 13.3 μl RiM/μg siRNA.

Table 1
Characterization of the chitosans included in the study. The chitosans are denoted according to their chemical composition or molecular architecture: linear (LIN), *N*-acetylated (F_A), self-branched (SB), and self-branched trisaccharide substituted (SBTCO). The weight and number averages of the molecular weight (M_w, M_n) and the polydispersity index (PDI) were analyzed by SEC-MALLS. The degree of AAM-substitution (d.s.) and the fraction of *N*-acetylated units (F_A) were determined by ^1H NMR.

Notation	DP_n	M_n	M_w	PDI	Chain architecture	F_A	d.s.
		kDa	kDa				% AAM
LIN50	54	10.8	16.4	1.52	Linear	<0.002	0
LIN100	105	20.9	34.8	1.67	Linear	<0.002	0
LIN150	156	31.3	54.6	1.74	Linear	<0.002	0
LIN200	199	39.8	74.5	1.87	Linear	<0.002	0
LIN250	247	49.5	100.3	2.03	Linear	<0.002	0
LIN300	320	64.1	141.6	2.21	Linear	<0.002	0
F_A0.15	320	63.8	188.7	2.96	Linear	0.15	0
SB150	167	33.4	67.4	2.02	Self-branched	<0.002	0
SBTCO150	170	33.9	71	2.09	Self-branched AAM substituted	<0.002	8.3

2.3. Preparation of siRNA-chitosan nanoparticles

Formulations with different amino/phosphate (N/P) ratios were prepared by a self-assembly method while keeping the amount of siRNA constant (1.2 μg/mL). A solution of siRNA (5 μM, 6.65 μg/mL) was diluted with the necessary amount of sterile nuclease free water (5 Prime). Subsequently, the required amount of chitosan was added from a sterile filtered solution (0.1 mg/mL) during vortex mixing (1200 rpm). The assembled nanoparticles were incubated for 30 min at room temperature before transfection. When assembling the nanoparticles for transfection at different doses, the particles were first made at the highest concentration and incubated for 30 min before serial dilution.

2.4. Size determination of nanoparticles

The sizes of the nanoparticles were determined using dynamic light scattering (DLS) on a Zetasizer Nano ZS (Malvern Instruments). Measurements were performed in MQ water at a 173° angle and a temperature of 25 °C. The size is expressed as the z-average hydrodynamic diameter obtained by a cumulative analysis of the correlation function using the viscosity and refractive index of water in the calculations.

2.5. Cell culture

The transduced H1299 cell line (human lung carcinoma) stably expressing destabilized EGFP (Enhanced Green Fluorescent Protein) was a gift from Prof. Jørgen Kjems (Dept. of Molecular Biology, Aarhus University, Denmark). The cells were grown in RPMI 1640 medium (Sigma) supplemented with 1 mM non-essential amino acids (Gibco, Invitrogen), 10% FBS (Gibco, Invitrogen) and 500 μg/mL G418 selection antibiotic (Sigma). MCF-7 (human breast cancer) cells were provided by Kristin G. Sæterbø (Dept. Physics, NTNU) and HUVEC (human umbilical vein endothelial) cells were supplied by Lonza. MCF-7 cells were grown in MEM (Gibco, Invitrogen) with 1 mM non-essential amino acids, 1 mM sodium pyruvate (Gibco, Invitrogen) and 10% FBS. The HUVEC cells were grown in EBM-2 (Lonza) with full supplements (EGM-2 BulletKit, Lonza). When seeding cells for experiments, growth media supplemented with 100 U/mL of penicillin and streptomycin (PEST, Sigma) was used. The cells were cultivated at 37 °C in a humidified atmosphere with 5% CO_2.

2.6. In vitro transfection

Cells were seeded in tissue culture wells 24 h prior to experiments in densities with approximately 50–75% confluency on the day of transfection. For example, 7500 cells in 100 μl growth medium were seeded in 96-well plates (Corning CellBIND). The nanoparticles assembled in water were diluted with an equal volume of Opti-MEM

(Gibco, Invitrogen), supplemented with 270 mM mannitol (Sigma) and 20 mM HEPES (Sigma) for adjustment of the osmolarity to 300 mOsm/kg and pH to 7.2. The formulations were not supplemented with FBS or antibiotics. Prior to adding the nanoparticles, the cells were washed and briefly incubated with 100 μL/well of Hanks balanced salt solution (HBSS, Gibco, Invitrogen) at 37 °C and 5% CO_2. Next, HBSS solution was removed and 50 μl aliquots of nanoparticle formulation containing typically 0.03 μg (45 nM) siRNA were added to each well in 96-well plates. The formulations were removed after 5 h of incubation and replaced by 200 μl of growth media supplemented with PEST.

2.7. Flow cytometry

EGFP knockdown and cellular uptake of siRNA were measured using a Gallios flow cytometer (Beckman Coulter) and data were analyzed and visualized using the Kaluza software package (Kaluza Flow Cytometry Analysis v1.1, Beckman Coulter). Knockdown was measured 48 h after transfection with anti-EGFP siRNA. The cells were washed in PBS (Gibco/Invitrogen), trypsinized, resuspended in ice-cold PBS supplemented with 5% FBS, filtered through 40 μm nylon mesh (BD) and kept on ice until the time of analysis. The cellular uptake of siRNA was determined by transfection with Alexa-647 conjugated siRNA (Qiagen). After incubating with polyplexes for 4 h, the cells were washed with PBS and further incubated with RPMI for 30 min. Afterwards, the cells were incubated with heparin supplemented RPMI (1 mg/mL, Sigma) for 30 min before they were harvested and analyzed.

For each sample, 10,000 gated events were counted and a dot plot of forward scatter versus side scatter established a collection gate for cells to exclude cellular debris, dead and aggregated cells. The EGFP or Alexa-647 positive cells were excited using a 488 nm or 633 nm laser line, respectively. Emitted light was collected at FL1 or FL6 using a 525/40 nm or 660/20 nm band pass filter, respectively. Untreated cells were analyzed to determine the normal level of EGFP fluorescence intensity. The knockdown of EGFP in transfected cells was calculated from the number of EGFP positive cells or median fluorescence intensity (FI) relative to the untreated cells. To define the Alexa-647 positive cells, untreated cells were analyzed as negative controls, to set a threshold for the fluorescence intensity above the level of autofluorescence. The relative amount of internalized Alexa-647 was estimated from the median FI of the Alexa-647 positive population.

2.8. GAPDH knockdown

Knockdown of the ubiquitously expressed endogenous gene GAPDH (glyceraldehyde-3-phospate dehydrogenase) was measured at mRNA level using the ABI 7500 real-time PCR system (Applied biosystems). The mRNA was harvested, and cDNA was synthesized and amplified using the Cells-to-C_T kit (Applied Biosystems) as described in the manufacturer's protocol. Reverse transcription was performed at 37 °C for 60 min. Quantitative Real-Time PCR (qRT-PCR) was performed using the following cycle conditions: 95 °C for 10 min, 40 cycles at 95 °C for 15 s, and 60 °C for 1 min. The following primers (Eurofins MWG Operon) were used: GAPDH forward 5′-TGGGCTACACTGAGCACACG-3', GAPDH reverse 5′-CAGCGTCAAAGGTGGAGAG-3′, β-actin forward 5′-TCCACCTTCCAGCAGATGTG-3′, and β-actin reverse 5′-GCATTTGCGGTGGACGAT-3′. The primer efficiencies were determined using standard curves. The percentage of mRNA expression relative to untreated cells or cells treated with NT siRNA was calculated using the comparative C_t method, where the target sample was normalized to endogenous β-actin.

The effect of the knockdown on the GAPDH protein activity was measured using the KDalert GAPDH assay kit (Ambion) according to the manufacturer's protocol, where the amounts of lysate and assay reagents were halved, and measurements were performed in half-area 96-well plates (Corning) at 615 nm using a spectrophotometer (Molecular Devices).

2.9. CLSM

H1299 cells were seeded onto 8-chamber microscopic slides (Ibidi) and transfected with anti-EGFP siRNA, as described previously. After 48 h, the cells were treated with 5 μg/mL of CellMask plasma membrane stain (Invitrogen). Live cells were examined using an LSM 510 (Carl Zeiss) confocal laser scanning microscope (CLSM) equipped with a c-Apochromat 40×/1.2 NA W corr objective. EGFP and CellMask were excited using 488 nm argon and 633 nm HeNe laser lines, respectively. The emitted light was collected using a 500/30 nm band pass and 650 nm long pass filters. The acquired images had resolutions of 512×512 pixels.

2.10. Toxicity

The effect of transfection on the metabolic activity was measured using an Alamar blue assay (Invitrogen). Cells were seeded in wells and transfected with anti-EGFP siRNA, as previously described. A volume of 10 μl of the Alamar blue assay reagent that was diluted in 100 μl of growth medium was added to the cells at 4- and 48-h post-transfection. The sample absorbances were measured 4 h after adding the assay reagent using a spectrophotometer at 570- and 600-nm. The metabolic activity of the cells was evaluated as a percentage reduction of the Alamar blue reagent relative to the untreated cells (that received only growth medium and assay reagent).

Possible deleterious effects on the cellular membrane as a consequence of transfection were evaluated using the LDH cytotoxicity assay (Cayman), which measured levels of cellular cytoplasmic LDH leakage. This assay was performed at conditions similar to the Alamar blue assay. Measurements of absorbance were performed 48 h post-transfection in serum-free medium as suggested in the manufacturer's protocol. The amounts of cell suspension and assay reagents were halved, and measurements were performed in half-area 96-well plates at 490-nm using a spectrophotometer.

2.11. Statistical analysis

The measured values were collected and expressed as mean values ± standard deviation (s.d.). Statistical differences between raw data were investigated using the SigmaPlot 11.0 software package with one-way ANOVA, in conjunction with a multiple comparison test (Holm-Sidak).

3. Results

3.1. siRNA uptake and silencing of EGFP in H1299 cells

Four structurally different chitosans, including completely de-*N*-acetylated linear (LIN150), self-branched (SB150), self-branched trisaccharide-substituted (SBTCO150), and a partially *N*-acetylated linear chitosan (F_A0.15) were compared for their ability to deliver siRNA and to mediate knockdown. Structure-activity relationships for nanoparticles prepared from these chitosans were evaluated by measuring the uptake of siRNA and silencing the stably expressed EGFP in H1299 cells using flow cytometry.

As illustrated in Fig. 1A and B, which show the median cellular fluorescence intensities (FI) of Alexa-647 conjugated siRNA, the siRNA was typically internalized by almost all of the cells (Fig. 1B) but the amounts varied with the type of chitosan carrier (Fig. 1A). The partially *N*-acetylated (F_A0.15) and substituted (SBTCO150) chitosans mediated higher uptakes compared to the linear chitosan (LIN150), the self-branched chitosan (SB150), and the commercial

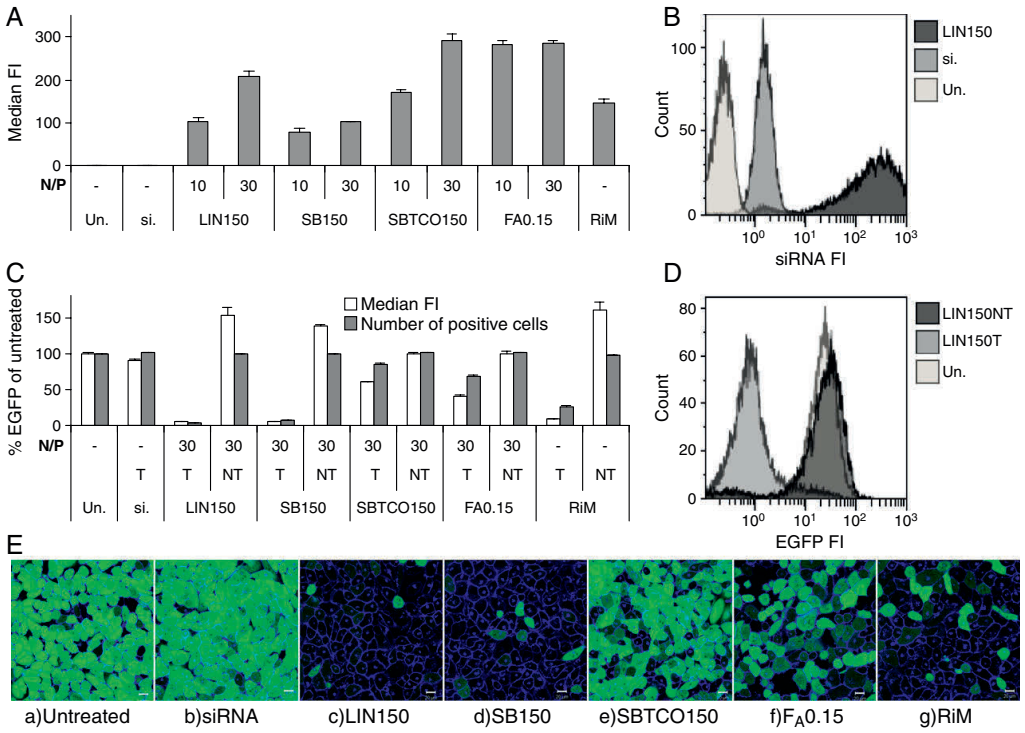

Fig. 1. Effect of chitosan chain architecture and *N*-acetylation on siRNA delivery and knockdown of EGFP in H1299 cells. A) Relative amount of internalized Alexa-647 conjugated siRNA expressed as median fluorescence intensity (FI) of the Alexa-647 positive cells. The cells were analyzed 4 h after transfection. B) Representative histogram from flow cytometry of H1299 cells showing fluorescence distribution of untreated cells, from internalized naked siRNA (si.) or siRNA delivered by LIN150 at N/P 30. C) Knockdown of EGFP measured as the median FI or the number of EGFP positive cells relative to untreated cells (Un.) 48 h after transfection with anti-EGFP (targeting, T) or non-targeting (NT) siRNA. Data represent mean values ± s.d., n = 3. D) Representative histogram from flow cytometry of H1299 cells showing EGFP fluorescence of untreated cells or after delivery of T/NT siRNA by LIN150 at N/P 30. E) Representative CLSM images of untreated H1299 cells (a), 48 h after adding naked siRNA (b) or transfection with LIN150 (c), SB150 (d), SBTCO150 (e), F_A0.15 (f) at N/P 30 or RiM (g). The cellular plasma membrane was stained with CellMask (blue) and EGFP is indicated with the green color. The bar size is 20 μm. The siRNA was delivered at a concentration of 90 nM.

lipid based vector RNAiMAX (RiM). Although, most of the cells appeared to internalize even the naked siRNA as shown in Fig. 1B, the relative amounts of siRNA taken up by the cells were insignificant (Fig. 1A).

Following the uptake confirmation, we examined the degree of EGFP knockdown in H1299 cells using anti-EGFP (targeting, T) siRNA or non-targeting (NT) negative control siRNA. Fig. 1C and D show that nanoparticles based on the fully de-*N*-acetylated LIN150 and SB150 mediated the most efficient knockdown, giving ~5% of both the median FI and number of EGFP positive cells compared to the untreated cells. In contrast, when using the partially *N*-acetylated chitosan F_A0.15 or the substituted SBTCO150 as delivery vehicles, 68% and 85% of the cells still expressed EGFP, respectively. However, the FI was reduced to 41% and 61% of the FI in untreated cells, respectively. Interestingly, cells transfected with NT siRNA using SB150, LIN150 and RiM showed increased EGFP expression compared to untreated cells; an increase in FI of approximately 50% was typically recorded (Fig. 1C). Such an increase in the EGFP expression was not observed when NT siRNA was delivered by F_A0.15 and SBTCO150. The knockdown of EGFP in the H1299 cells was qualitatively confirmed by CLSM, as shown in Fig. 1E.

Based on the results in Fig. 1, which show promising delivery of siRNA with fully de-*N*-acetylated linear chitosan, this type of chitosan was selected to elucidate the effect of the chain length (expressed as DP_n) on siRNA uptake and knockdown efficiency in H1299 cells. Again, almost 100% of the gated cells internalized siRNA independent of the formulation (naked siRNA 92%), even when delivered at a concentration of 45 nM (data not shown). However, the median FI of Alexa-647 conjugated siRNA was dependent on both the N/P ratio and the chain length. As illustrated in Fig. 2A, the uptake of siRNA increased when the N/P ratios were increased from 10 to 60. The siRNA uptake also increased with the chain length of the chitosans, however, only for chitosans with a DP_n below 200. As shown in Fig. 2B, all chitosans with chain lengths in the range of DP_n 150–300 mediated efficient knockdown at N/P ratios of 10, 30 and 60. Only the chitosan with DP_n 50 (LIN50) required an N/P ratio of 60 to obtain comparable knockdown efficiency. To demonstrate that the decrease in EGFP expression was not related to toxic or non-specific effects of the chitosan itself, we performed mock transfections with naked chitosan (M) and transfections using NT siRNA. As shown in Fig. 2C, the mock transfections resulted in only a small decrease in EGFP expression, reaching a minimum of 87% when using LIN100. In contrast and as noted earlier, the delivery of NT siRNA mediated an increased EGFP expression for some chitosans. One example is shown from the samples of cells transfected with LIN250, which showed up to 140% EGFP expression compared to the untreated cells.

Selected nanoparticles based on the fully de-*N*-acetylated linear chitosans were further characterized by measuring their z-average hydrodynamic diameters in MQ water. As shown in Table 2, the size of the nanoparticles ranged from approximately 30 to 100 nm. The

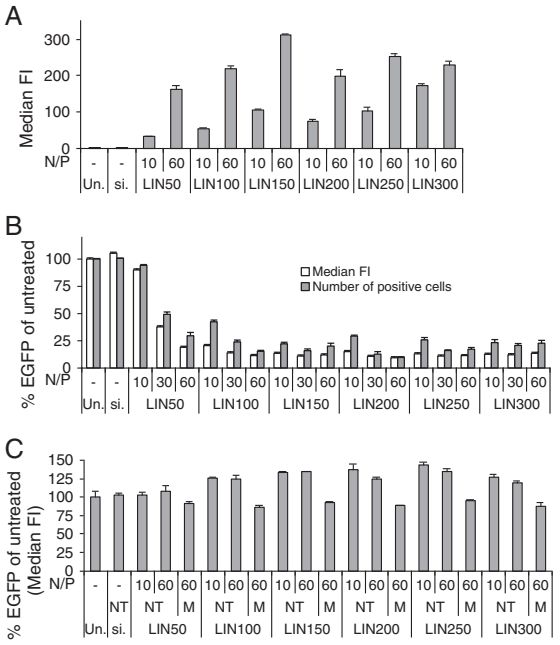

Fig. 2. Effect of chain length and N/P ratio on siRNA uptake and EGFP knockdown efficiency in H1299 cells, using fully de-*N*-acetylated linear chitosans. A) Relative amount of internalized Alexa-647 conjugated siRNA expressed as median FI of the Alexa-647 positive cells. The cells were analyzed 4 h after transfection. B) Knockdown of EGFP measured as the median FI or the number of EGFP positive cells relative to untreated cells (Un.) 48 h after transfection with anti-EGFP siRNA. C) EGFP expression relative to untreated cells 48 h after mock transfection (M) or transfection with non-targeting (NT) siRNA. siRNA was delivered at a concentration of 45 nM. Data represent mean values ± s.d., n = 3.

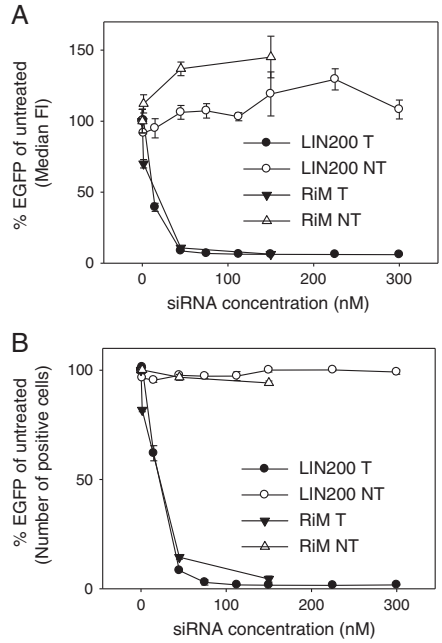

Fig. 3. Dose-dependent EGFP knockdown in H1299 cells transfected using RiM or nanoparticles formed with LIN200 and anti-EGFP (T) or non-targeting (NT) siRNA at N/P 30. The knockdown was measured as A) the median FI and B) the number of EGFP positive cells relative to untreated cells 48 h after transfection. Data represent mean values ± s.d., n = 3.

particles of low DP_n and N/P ratios were in general smaller compared to those of increasing DP_n and N/P.

The minimum effective dose for the knockdown of EGFP in H1299 cells was determined using LIN200 to deliver different concentrations of anti-EGFP siRNA at N/P 30, and its efficiency was compared to that of RiM. Fig. 3A shows that both carriers resulted in a more than 90% reduction in EGFP expression at siRNA concentrations of 45 nM. Additional increase of the concentration mediated only a marginal increase in gene silencing but there was a further 5% decline in the number of EGFP positive cells as it increased from 45 to 75 nM. LIN200 and RiM showed similar knockdown efficiencies in the selected range of concentrations. However, a higher increase in the EGFP expression was observed when the commercial transfection reagent delivered NT siRNA as compared to the chitosan.

Table 2
Z-average hydrodynamic diameter of nanoparticles based on fully de-*N*-acetylated linear chitosans with DP_n 50-300 at N/P 10–60. Data represent mean values ± s.d., n = 3.

	Hydrodynamic diameter (z-average ± s.d., nm)		
N/P	10	30	60
LIN50	34.0 ± 0.5	51.7 ± 1.2	63.6 ± 1.1
LIN100	45.3 ± 7.1	48.1 ± 1.6	61.9 ± 1.2
LIN200	51.3 ± 1.1	55.7 ± 1.2	95.4 ± 3.0
LIN300	57.9 ± 5.7	58.4 ± 4.2	89.3 ± 8.6

3.2. Knockdown kinetics and the silencing of GAPDH in selected cell lines

In addition to EGFP, we also examined the knockdown of GAPDH, an ubiquitously expressed endogenous gene chosen as a model for a random target. GAPDH was targeted by anti-GAPDH siRNA using the chitosan LIN200, and the knockdown efficiency was determined from levels of GAPDH mRNA and protein activity 48 h after transfection. The results presented in Fig. 4A show that anti-GAPDH siRNA delivered by LIN200 reduced the mRNA amount and the protein activity to 18 and 55%, respectively, as compared to the untreated cells. The delivery efficiency of chitosan was comparable to that of RiM, showing mRNA levels and protein activity of 15 and 40% compared to the untreated cells, respectively. Neither the delivery of NT siRNA nor the mock transfection with chitosan showed any significant effect on the levels of GAPDH mRNA or protein activity.

The kinetics of GAPDH knockdown presented in Fig. 4B shows mRNA levels of 10% already one day after transfection compared to cells transfected with NT siRNA. The mRNA levels remained very low and increased to only 20% five days after transfection. The protein activity of GAPDH in transfected cells decreased from 50% one day after transfection to 15% at day five, compared to cells treated with NT siRNA. Cells transfected with NT siRNA were used as a negative control rather than untreated cells because of observed differences in the confluencies between nanoparticle treated and untreated cells. The cell density can affect the expression of GAPDH relative to β-actin [25], and, consequently, samples of similar density were compared.

Based on the encouraging results that show efficient gene silencing in H1299 cells with e.g. LIN200 and LIN300, these chitosans were applied to deliver siRNA in other cell lines. In this experiment, the chitosans delivered anti-GAPDH siRNA and silenced the GAPDH gene in MCF-7 cells and the primary cell line HUVEC. As shown in

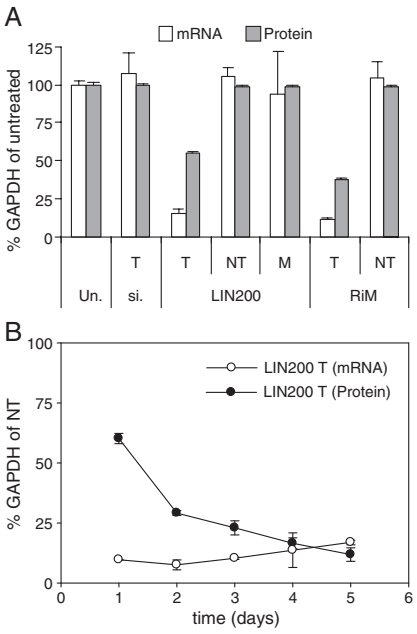

Fig. 4. Knockdown of GAPDH in H1299 cells. A) Levels of GAPDH mRNA (white bars) and protein activity (grey bars) 48 h after transfection with RiM or LIN200 and anti-GAPDH (targeting, T), non-targeting (NT) siRNA or mock transfection (M) at N/P 30. B) Time course of GAPDH mRNA and protein activity after transfection with LIN200 and T/NT siRNA at N/P 30. siRNA was delivered at a concentration of 45 nM. Data represent mean values ± s.d., n = 3.

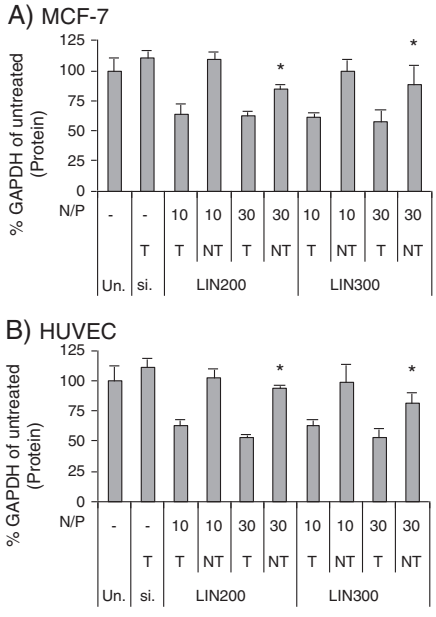

Fig. 5. Knockdown of GAPDH using nanoparticles of LIN200 or LIN300 and anti-GAPDH (targeting, T) or non-targeting (NT) siRNA at N/P 10 or 30. The siRNA was delivered at a concentration of 45 nM in A) MCF-7 and B) HUVEC cells. Data represent mean values ± s.d., n = 3. Formulations with NT siRNA that yielded significantly reduced ($p<0.05$) GAPDH activity compared to untreated cells are indicated with asterisks ("*").

Fig. 5A and B, the nanoparticles successfully reduced GAPDH protein activity in these cell lines, resulting in knockdown efficiencies of ~50–60% activity compared to the untreated cells 48 h after transfection, which is comparable to the results achieved in the H1299 cells. Off-target or toxic effects were generally insignificant when NT siRNA was delivered, but some reduction in GAPDH activity was observed at N/P 30.

3.3. Toxicity

To determine the safety of the chitosan based nanoparticles used in this study for delivering siRNA, the relative metabolic activity of transfected cells was measured using the Alamar blue assay 4- and 48-h after transfection. As shown in Fig. 6A, a low but significant decrease in metabolic activity was recorded in cells treated with a variety of formulations, both 4- and 48-h after transfection, compared to the untreated cells. In general, the decrease was low, typically 5–10%. Whereas only RiM and LIN300 at N/P 10 and 60 showed a significant decrease at 4 h, most chitosan nanoparticles with N/P 60 and RiM were shown to decrease the metabolic activity 48 h after transfection.

In addition to the metabolic activity, cellular membrane integrity was measured using the LDH cytotoxicity assay. Fig. 6B shows that only cells treated with RiM suffered a significant increase in leakage of cytoplasmic LDH 48 h after transfection.

4. Discussion

This study demonstrates that fully de-*N*-acetylated chitosans with moderate chain lengths are highly efficient as siRNA carriers. The maximum charge density obtained by complete de-*N*-acetylation appears crucial to obtaining high knockdown efficiencies (Fig. 1C). Partially *N*-acetylated chitosan (F_A0.15) and the AAM-substituted SBTCO150 that contains uncharged *N*-acetylated glucosamine units (GlcNAc) show significantly lower knockdown compared to their fully de-*N*-acetylated counterparts represented by LIN150 and

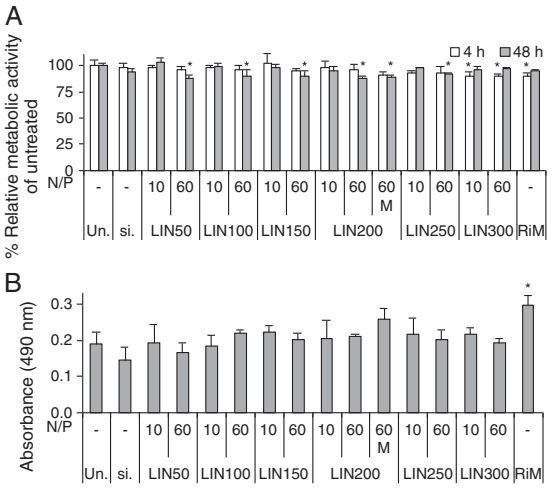

Fig. 6. Evaluation of toxicity in H1299 cells treated with chitosan based nanoparticles. A) Metabolic activity relative to untreated cells measured by the Alamar blue assay. Activity was measured 4- (white bars) and 48-h (grey bars) after transfection. B) Leakage of cytoplasmic LDH relative to untreated cells measured by the LDH assay. LDH was measured 48 h after transfection. The cells were mock transfected (M) or transfected using anti-EGFP siRNA formulated with fully de-*N*-acetylated linear chitosans of different DP_n and N/P ratios. The siRNA was delivered at a concentration of 45 nM. Data represent mean values ± s.d., n = 4. Formulations that yielded significantly reduced ($p<0.05$) metabolic activity or increased LDH leakage compared to untreated cells are indicated with asterisks ("*").

SB150. The complete de-*N*-acetylation of chitosan thus eliminates the need for ionic crosslinking of the nanoparticles and for trimethylation of the amino groups.

Surprisingly, despite lower knockdown efficiencies, SBTCO150 and F_A0.15 show higher cellular uptake of siRNA (Fig. 1A). This observation indicates that these chitosans are able to form stable nanoparticles with siRNA that are internalized, but their cellular processing seems less efficient than that for the linear or self-branched chitosans. It is not clear why the increased uptake does not correlate with high knockdown efficiency. Possibly, the acetylated chitosans release siRNA in the endo-lysosomal compartments, as reported for chitosan-mediated pDNA delivery by Thibault et al. [26], which results in rapid degradation. The lower charge density of these chitosans may also render them to be less efficient in escaping the endocytotic vesicles. The relationship between charge density, nanoparticle stability and silencing efficiency has previously been shown to be positively correlated when assembling nanoparticles of chitosan and siRNA at different DP_n, F_A or N/P ratios [13,17,21,27]. However, the correlation between the uptake of nanoparticles and knockdown was not investigated in these previous studies.

The siRNA delivery appears relatively unaffected by the chitosan chain length, particularly for chitosans equal to and above DP_n 100 (Fig. 2). This observation is in contrast to previous work on chitosan mediated pDNA delivery, where the efficiency of gene transfer has shown a critical dependency on chitosan chain length. It has been shown that there is a balance between the nanoparticle stability and its ability to undergo intracellular dissociation; the kinetics of the intracellular dissociation can be optimized by selecting the proper chain lengths [19]. Since the length of pDNA (typically several kbp) largely exceeds that of siRNA, pDNA molecules are able to form multiple inter-chain bridges with chitosan molecules, and the electrostatic interactions between pDNA and chitosan are thus much stronger. Therefore, by using short chitosan chains (low DP_n), the interaction strength between pDNA and chitosan may be reduced, promoting intracellular dissociation. Short siRNA duplexes, on the other hand, will have substantially weaker interaction with chitosan, and this limits the stability of the nanoparticles. Therefore, above a certain DP_n, the stability of the nanoparticles will not depend on the chitosan chain length. This is in agreement with our data, showing that chitosans below DP_n 100 mediate weak siRNA uptake and knockdown, probably due to insufficient stability of the nanoparticles. This is also in agreement with results reported by Liu et al. [13], where a chitosan of approximately DP_n 50 and F_A 0.05 has been shown to form unstable nanoparticles at N/P 50 and to mediate poor knockdown [13]. However, as all chitosan preparations in this study are polydisperse with respect to chain length, it is not possible to identify what would be a minimum chain length for efficient delivery.

When compared to other studies [13,17,21,28], our chitosan nanoparticles reach maximum knockdown efficiency at relatively low N/P ratios such as an N/P of 10. Only the knockdown efficiency of LIN50, and partially LIN100, increased with the N/P ratio (Fig. 2), suggesting that a part of the chains in the polydisperse sample with average DP_n 50 is able to form stable complexes with siRNA. The possibility of compensating for the lower DP_n of chitosans by increasing their N/P ratios is generally not considered an optimal strategy, as higher N/P ratios imply a large excess of free chitosans that bind to the cell surface [8] and increase the potential for unspecific interactions. Therefore, chitosan nanoparticles with low N/P ratios are highly beneficial. A plausible explanation for the low N/P ratios needed is that the fully de-*N*-acetylated chitosans are able to bind siRNA more tightly, thereby reducing the need for excess chitosan.

A significant knockdown of the target gene was achieved at a siRNA concentration as low as 15 nM, and the maximum gene knockdown was reached at 45 nM (Fig. 3). Compared to other studies on polycation-mediated siRNA delivery, concentrations in the range of 50–200 nM have been typically used to obtain efficient gene silencing, with the majority of studies in the upper concentration range of 100–200 nM [17,21,28-31].

The siRNA-chitosan nanoparticles are also able to silence endogenously expressed genes such as GAPDH. Despite low levels of GAPDH mRNA that were already present at 24 h post-transfection and for up to the five days measured (Fig. 4), the protein activity measured at 48 h remained between 30–55% of the control (Fig. 4A and B). This range is significantly higher than that observed when silencing the EGFP gene and can be explained by the longer half-life of the GAPDH (>35 h [32]) compared to the destabilized EGFP (2 h [33]) protein. Indeed, the GAPDH activity decreased further, reaching below 20% at day 4–5, similar to the knockdown of EGFP at day 2 (Fig. 4B). Also, the EGFP knockdown kinetics was found to be similar to the kinetics for the GAPDH mRNA ($t_{1/2,\ GAPDH\ mRNA} = 8$ h [34]), indicating that the differences were caused by the different protein turn-overs (data not shown).

It is well established that the ability of different carriers to deliver siRNA is highly cell line dependent. After the successful delivery of siRNA into HEK293, HeLa and H1299 (data shown only for H1299), we also investigated delivery to primary cells (HUVEC) and MCF-7 cells that have previously proved difficult to transfect. The knockdown efficiencies obtained in these cell lines were similar to the H1299 cells, further demonstrating that the chitosans used in this study could be used as efficient delivery vehicles for siRNA in a broad range of cell lines.

The off-target effects of siRNA, the toxicity of the carrier and other non-specific effects have repeatedly been lifted as serious concerns in the field of siRNA delivery [35–37]. Therefore, in all of our experiments, appropriate non-targeting siRNA have been used as a negative control to distinguish non-sequence specific effects. We also performed mock transfection with chitosan only. As shown in Figs. 1C, 2C, and 3A, the delivery of NT siRNA in some cases increased the cellular levels of EGFP whereas the naked chitosan in mock transfections mediated only a moderate decrease in EGFP of ~10%. In contrast to EGFP, the levels of GAPDH mRNA or protein activity do not seem to be affected by the delivery of NT siRNA or the mock transfection (Figs. 4A and 5), suggesting that the off-target effects influence random genes and not the global gene expression in treated cells. The extent of increased EGFP seems to be more pronounced for chitosans of mid-range DP_n (Fig. 2C). Interestingly, mock transfections performed at increased chitosan concentrations of 3.5, 35 and 70 μg/mL (corresponding to N/P 10, 100, and 200) in a time course of 1–3 days show 75–100% EGFP compared to the untreated cells. However, the decrease seems to be random with respect to the chain length, the time point and the chitosan concentration (data not shown).

The chitosan nanoparticles used in our study showed minimal cytotoxicity, as assessed by the analysis of metabolic activity and membrane integrity (Fig. 6). Our results also emphasize the need to evaluate several cellular parameters to determine the potential cytotoxicity of a compound [38]. Whereas RiM appeared to disrupt the cellular membrane, hence causing leakage of cytoplasmic LDH, only a low reduction of metabolic activity was observed. The low toxicity of chitosan is in agreement with previous studies that recognize different types of siRNA- or pDNA-chitosan nanoparticles as safe delivery reagents [8–10,28,29,39]. However, Liu et al. [13] have shown significantly reduced metabolic activity when treating H1299 cells with siRNA-chitosan nanoparticles, likely caused by the high siRNA concentration and the N/P ratio in the formulation used. This result highlights the importance of using tailored chitosans that are able to deliver small doses of siRNA at low N/P ratios.

5. Conclusions

This study demonstrates that the choice of chitosan molecular structure has a large impact on siRNA delivery and knockdown efficiency. Fully de-*N*-acetylated chitosans are superior siRNA carriers

compared to conventional partially *N*-acetylated chitosans. These chitosans demonstrate highly efficient siRNA delivery in several cell lines, potent long-term silencing of both exogenous and endogenous target genes, low cytotoxicity, and few non-specific effects.

Acknowledgements

This work was supported by a Ph.D. grant from NTNU (J. M.) and by the Norwegian Research Council (grant 182695/40). We wish to thank Ann-Sissel Ulset (Dept. of Biotechnology, NTNU) for performing the SEC-MALLS analysis, Kristin G. Sæterbø (Dept. of Physics, NTNU) for assistance with cell culture and flow cytometry, and Morten J. Dille (Dept. of Biotechnology, NTNU) for nanoparticle size characterization. The authors would also like to thank Rahmi Lale (Dept. of Biotechnology, NTNU) for help with the RT-PCR experiments.

References

[1] P.J. Paddison, A.A. Caudy, G.J. Hannon, Stable suppression of gene expression by RNAi in mammalian cells, Proc. Natl. Acad. Sci. U. S. A. 99 (2002) 1443–1448.
[2] H.D. Han, L.S. Mangala, J.W. Lee, M.M.K. Shahzad, H.S. Kim, D. Shen, E.J. Nam, E.M. Mora, R.L. Stone, C. Lu, S.J. Lee, J.W. Roh, A.M. Nick, G. Lopez-Berestein, A.K. Sood, Targeted gene silencing using RGD-labeled chitosan nanoparticles, Clin. Cancer Res. 16 (2010) 3910–3922.
[3] D.V. Morrissey, J.A. Lockridge, L. Shaw, K. Blanchard, K. Jensen, W. Breen, K. Hartsough, L. Machemer, S. Radka, V. Jadhav, N. Vaish, S. Zinnen, C. Vargeese, K. Bowman, C.S. Shaffer, L.B. Jeffs, A. Judge, I. MacLachlan, B. Polisky, Potent and persistent in vivo anti-HBV activity of chemically modified siRNAs, Nat. Biotechnol. 23 (2005) 1002–1007.
[4] K.A. Howard, S.R. Paludan, M.A. Behlke, F. Besenbacher, B. Deleuran, J. Kjems, Chitosan/siRNA nanoparticle-mediated TNF-α knockdown in peritoneal macrophages for anti-inflammatory treatment in a murine arthritis model, Mol. Ther. 17 (2008) 162–168.
[5] K. Vårum, O. Smidsrød, Structure–property relationship in chitosans, in: S. Dumitriu (Ed.), Polysaccharides: Structural diversity and functional versatility, 2nd ed., CRC Press, New York, 2004, pp. 625–643.
[6] R.J. Nordtveit, K.M. Vårum, O. Smidsrød, Degradation of partially N-acetylated chitosans with hen egg white and human lysozyme, Carbohydr. Polym. 29 (1996) 163–167.
[7] K.M. Vårum, M.M. Myhr, R.J.N. Hjerde, O. Smidsrød, In vitro degradation rates of partially N-acetylated chitosans in human serum, Carbohydr. Res. 299 (1997) 99–101.
[8] J. Malmo, K.M. Vårum, S.P. Strand, Effect of chitosan chain architecture on gene delivery: comparison of self-branched and linear chitosans, Biomacromolecules 12 (2011) 721–729.
[9] S.P. Strand, M.M. Issa, B.E. Christensen, K.M. Vårum, P. Artursson, Tailoring of chitosans for gene delivery: novel self-branched glycosylated chitosan oligomers with improved functional properties, Biomacromolecules 9 (2008) 3268–3276.
[10] O. Germershaus, S. Mao, J. Sitterberg, U. Bakowsky, T. Kissel, Gene delivery using chitosan, trimethyl chitosan or polyethylenglycol-graft-trimethyl chitosan block copolymers: establishment of structure-activity relationships in vitro, J. Control. Release 125 (2008) 145–154.
[11] P. Baldrick, The safety of chitosan as a pharmaceutical excipient, Regul. Toxicol. Pharmacol. 56 (2010) 290–299.
[12] S.P. Strand, K. Tømmeraas, K.M. Vårum, K. Østgaard, Electrophoretic light scattering studies of chitosans with different degrees of N-acetylation, Biomacromolecules 2 (2001) 1310–1314.
[13] X. Liu, K.A. Howard, M. Dong, M.Ø. Andersen, U.L. Rahbek, M.G. Johnsen, O.C. Hansen, F. Besenbacher, J. Kjems, The influence of polymeric properties on chitosan/-siRNA nanoparticle formulation and gene silencing, Biomaterials 28 (2007) 1280–1288.
[14] N.K. Reitan, G. Maurstad, C. de Lange Davies, S.P. Strand, Characterizing DNA condensation by structurally different chitosans of variable gene transfer efficacy, Biomacromolecules 10 (2009) 1508–1515.
[15] V. Dehousse, N. Garbacki, S. Jaspart, D. Castagne, G. Piel, A. Colige, B. Evrard, Comparison of chitosan/siRNA and trimethylchitosan/siRNA complexes behaviour in vitro, Int. J. Biol. Macromol. 46 (2010) 342–349.
[16] H. Katas, A.H. Oya, Develpment and characterisation of chitosan nanoparticles for siRNA delivery, J. Control. Release 115 (2006) 216–225.
[17] T. Rojanarata, P. Opanasopit, S. Techaarpornkul, T. Ngawhirunpat, U. Ruktanonchai, Chitosan–thiamine pyrophosphate as a novel carrier for siRNA delivery, Pharm. Res. 25 (2008) 2807–2814.
[18] M.M. Issa, M. Köping-Höggård, K. Tømmeraas, K.M. Vårum, B.E. Christensen, S.P. Strand, P. Artursson, Targeted gene delivery with trisaccharide-substituted chitosan oligomers in vitro and after lung administration in vivo, J. Control. Release 115 (2006) 103–112.
[19] S.P. Strand, S. Lelu, N.K. Reitan, C. de Lange Davies, P. Artursson, K.M. Vårum, Molecular design of chitosan gene delivery systems with an optimized balance between polyplex stability and polyplex unpacking, Biomaterials 31 (2009) 975–987.
[20] M. Lavertu, S. Méthot, N. Tran-Khanh, M.D. Buschmann, High efficiency gene transfer using chitosan/DNA nanoparticles with specific combinations of molecular weight and degree of deacetylation, Biomaterials 27 (2006) 4815–4824.
[21] S. Techaarpornkul, S. Wongkupasert, P. Opanasopit, A. Apirakaramwong, J. Nunthanid, U. Ruktanonchai, Chitosan-mediated siRNA delivery in vitro: effect of polymer molecular weight, concentration and salt forms, AAPS PharmSciTech 11 (2010) 64–72.
[22] K. Tømmeraas, K.M. Vårum, B.E. Christensen, O. Smidsrød, Preparation and characterisation of oligosaccharides produced by nitrous acid depolymerisation of chitosans, Carbohydr. Res. 333 (2001) 137–144.
[23] K. Tømmeraas, S.P. Strand, B.E. Christensen, O. Smidsrød, K.M. Vårum, Preparation and characterization of branched chitosans, Carbohydr. Polym. 83 (2011) 1558–1564.
[24] K. Tømmeraas, M. Köping-Höggård, K.M. Vårum, B.E. Christensen, P. Artursson, O. Smidsrød, Preparation and characterisation of chitosans with oligosaccharide branches, Carbohydr. Res. 337 (2002) 2455–2462.
[25] S. Greer, R. Honeywell, M. Geletu, R. Arulanandam, L. Raptis, Housekeeping genes; expression levels may change with density of cultured cells, J. Immunol. Methods 355 (2010) 76–79.
[26] M. Thibault, S. Nimesh, M. Lavertu, M.D. Buschmann, Intracellular trafficking and decondensation kinetics of chitosan–pDNA polyplexes, Mol. Ther. 18 (2010) 1787–1795.
[27] X. Yuan, B. Shah, N. Kotadia, J. Li, H. Gu, Z. Wu, The development and mechanism studies of cationic chitosan-modified biodegradable PLGA nanoparticles for efficient siRNA drug delivery, Pharm. Res. 27 (2010) 1285–1295.
[28] K.A. Howard, U.L. Rahbek, X. Liu, C.K. Damgaard, S.Z. Glud, M.O. Andersen, M.B. Hovgaard, A. Schmitz, J.R. Nyengaard, F. Besenbacher, J. Kjems, RNA interference in vitro and in vivo using a chitosan/sirna nanoparticle system, Mol. Ther. 14 (2006) 476–484.
[29] U. Mittnacht, H. Hartmann, S. Hein, H. Oliveira, M. Dong, A.P. Pego, J. Kjems, K.A. Howard, B. Schlosshauer, Chitosan/siRNA nanoparticles biofunctionalize nerve implants and enable neurite outgrowth, Nano Lett. 10 (2010) 3933–3939.
[30] O. Veiseh, F.M. Kievit, C. Fang, N. Mu, S. Jana, M.C. Leung, H. Mok, R.G. Ellenbogen, J.O. Park, M. Zhang, Chlorotoxin bound magnetic nanovector tailored for cancer cell targeting, imaging, and siRNA delivery, Biomaterials 31 (2009) 8032–8042.
[31] A.R. Grayson, A. Doody, D. Putnam, Biophysical and structural characterization of polyethylenimine-mediated siRNA delivery in vitro, Pharm. Res. 23 (2006) 1868–1876.
[32] H.A. Franch, S. Sooparb, J. Du, N.S. Brown, A mechanism regulating proteolysis of specific proteins during renal tubular cell growth, J. Biol. Chem. 276 (2001) 19126–19131.
[33] X. Li, X. Zhao, Y. Fang, X. Jiang, T. Duong, C. Fan, C.-C. Huang, S.R. Kain, Generation of destabilized green fluorescent protein as a transcription reporter, J. Biol. Chem. 273 (1998) 34970–34975.
[34] C. Dani, M. Piechaczyk, Y. Audigier, S. El Sabouty, G. Cathala, L. Marty, P. Fort, J.-M. Blanchard, P. Jeanteur, Characterization of the transcription products of glyceraldehyde 3-phosphate-dehydrogenase gene in HeLa cells, Eur. J. Biochem. 145 (1984) 299–304.
[35] S. Akhtar, I. Benter, Toxicogenomics of non-viral drug delivery systems for RNAi: potential impact on siRNA-mediated gene silencing activity and specificity, Adv. Drug Delivery Rev. 59 (2007) 164–182.
[36] C. Tschuch, A. Schulz, A. Pscherer, W. Werft, A. Benner, A. Hotz-Wagenblatt, L. Barrionuevo, P. Lichter, D. Mertens, Off-target effects of siRNA specific for GFP, BMC Mol. Biol. 9 (2008) 60.
[37] A.L. Jackson, P.S. Linsley, Recognizing and avoiding siRNA off-target effects for target identification and therapeutic application, Nat. Rev. Drug Discovery 9 (2010) 57–67.
[38] H. Lv, S. Zhang, B. Wang, S. Cui, J. Yan, Toxicity of cationic lipids and cationic polymers in gene delivery, J. Control. Release 114 (2006) 100–109.
[39] D.W. Lee, K.-S. Yun, H.-S. Ban, W. Choe, S.K. Lee, K.Y. Lee, Preparation and characterization of chitosan/polyguluronate nanoparticles for siRNA delivery, J. Control. Release 139 (2009) 146–152.

Paper III

Is not included due to copyright